DEVELOPMENT AND ANALYSIS OF ACTIVE REAR AXLE STEERING FOR 8X8 COMBAT VEHICLE

By

Brett Russell

A Thesis Presented in Partial Fulfillment
of the Requirements for the Degree of

Master of Applied Science

In

Automotive Engineering

Faculty of Engineering and Applied Science
University of Ontario Institute of Technology
Oshawa, Ontario, Canada

AUGUST 2018

This page is left blank intentionally for the placement of the Certificate of Approval.
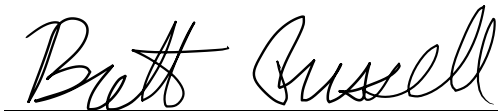
ABSTRACT

This thesis proposes and compares multiple vehicle dynamics controllers using rear axle steering of an 8x8 combat vehicle. The controllers are assessed on ability to increase maneuverability at low speed, increase stability at higher speeds, avoiding rollover and ability to dampen the effects of external disturbances. The two controllers that are proposed to improve the lateral vehicle dynamics include a feed-forward Zero Side Slip (ZSS) controller which steers the rear axle based on the vehicle speed, and a Linear Quadratic Regulator (LQR) controller that monitors the steering angle and compares the vehicle yaw rate and sideslip angle to the desired values calculated at steady state. These controllers are evaluated by performing simulations using a previously validated 8x8 combat vehicle as a TruckSim© full vehicle model. The controllers are developed in MATLAB/Simulink and are applied in co-simulation with TruckSim©. The simulation events to evaluate the controller performance include a 15-meter constant step slalom, modified J-turn, FMVSS 126 ESC and NATO double lane-change. These simulations are performed in between 20 km/h and 80 km/h over low friction (μ =0.35) and high friction (μ=0.85) surfaces. The rollover prevention capabilities of the controllers are evaluated using a fishhook maneuver over a high friction surface and damping of external disturbances will be tested using a crosswind simulation. The ZSS controller is a very responsive controller that increases the maneuverability at low speed and increases the stability at higher speeds. The responsiveness results in oversteering at mid range speeds and low lateral displacement during FMVSS 126 ESC. The LQR controller, as designed, is not applicable to improve low speed maneuverability but improves the lateral stability at high speed while achieving a respectable lateral displacement during the FMVSS 126 ESC maneuver. Both the ZSS and LQR controllers reduce the lateral accelerations at high speeds. The LQR controller also dampens the external disturbances applied during a cross wind simulation.

AUTHOR'S DECLARATION

I hereby declare that this thesis consists of original work of which I have authored. This is a true copy of the thesis, including any required final revisions, as accepted by my examiners.

I authorize the University of Ontario Institute of Technology to lend this thesis to other institutions or individuals for the purpose of scholarly research. I further authorize University of Ontario Institute of Technology to reproduce this thesis by photocopying or by other means, in total or in part, at the request of other institutions or individuals for the purpose of scholarly research. I understand that my thesis will be made electronically available to the public.

Brett Russell

STATEMENT OF CONTRIBUTIONS

Part of the work described in Chapters 3, 4 and 5 have been submitted to be published as:

Russell, B., El-Gindy, M., "Development of Control System for Active Rear Axle Steering of an 8x8 Combat Vehicle", International Journal of Automation and Control (IJAAC), 2018 (Submitted)

I am the primary author of the submitted paper.

ACKNOWLEDGEMENTS

I would like to express my appreciation to my thesis supervisor, Dr. Moustafa El- Gindy, for supporting me throughout this process. This thesis would not have been possible without his guidance and the opportunity to research under his supervision.

I would like to thank General Dynamics Land Systems-Canada for their technical guidance and financial support.

Most importantly I would like to express my gratitude to my family and friends who have faith in me and push me to believe in myself. Your constant support has given me the courage to continue to best myself even when I feel I am at my limits.

DISCLAIMER

Some numerical values used in this thesis cannot be published due to the confidential nature of this work. The confidential, proprietary, and privileged vehicle data was released to the author to complete this work.

TABLE OF CONTENTS

LIST OF FIGURES

LIST OF TABLES

GENERAL ABBREVIATIONS

ABS	Anti-lock Braking System
AVTP	Allied Vehicle Testing Publication
ESC	Electronic Stability Control
FMVSS	Federal Motor Vehicle Safety Standard
FRA	Fixed rear axle (Conventional Vehicle)
LAV	Light Armoured Vehicle
LQR	Linear Quadratic Regulator
MLS	Multi-link Suspension
NATO	North Atlantic Treaty Organization
RAS	Rear Axle Steering
ROM	Roll Over Mitigation
S-RAS	Simplified rear axle steering (GDLS-C)
UOIT	University of Ontario Institute of Technology
ZSS	Zero Side-slip

CONTROL SYSTEM REPRESENTATIONS

m	Vehicle mass
I_{zz}	Vehicle vertical mass moment of inertia about COG
$k_{i \to j}$	Steering angle ratio between two given axles i and j
a_i	Absolute distance from COG to axle i
x_n	Forward distance from COG to axle n (rear axles are negative)
U	Longitudinal speed
V	Lateral speed
F_x	Longitudinal tire force
F_y	Lateral tire force
δ_i	Ground wheel steer angle (Average for axle i)
α_i	Tire slip angle

$C_{\alpha i}$	Tire cornering stiffness (assumes double value of single tire for bicycle model for axle i)
β	Vehicle side slip angle
r	Yaw rate about the centre of gravity
β_{ss}	Side-slip angle at steady state
r_{ss}	Yaw rate at steady state
M_z	Yaw moment about the centre of gravity, external yaw moment
μ	Road friction coefficient
g	Acceleration due to gravity, 9.81 m/^{2}

CONTROL MATRIX ABBREVIATIONS

$[A]$	State matrix
$[B]$	Input matrix
$[C]$	Output matrix
$[D]$	Feed-forward matrix
$[J]$	LQR cost function performance index
$[K]$	Control gain matrix (LQR control gain)
$[Q]$	state weighting matrix
$[R]$	Output weighting matrix
$[x]$	State variable vector
$[y]$	Output variable vector
$[u]$	Input variable vector

CHAPTER 1
INTRODUCTION TO THESIS AND REVIEW OF HELPFUL MATERIAL

1.1 MOTIVATION

Combat vehicles with wheels rather than tracks are becoming increasingly popular for use in militaries due to the maneuverability and modularity. These vehicles can be used as infantry section carrier, command post, reconnaissance, ambulance, and many other configurations [1]. Multi-axle wheeled combat vehicles, such as Infantry Fighting Vehicles (IFV), were first introduced in the 1970's with the South African Military presenting the 'Ratel' 6x6 in 1976, and the Swiss company MOWAG presenting the Light Armoured Vehicle (LAV) platform in 1977 [2]. These multi-wheeled vehicles were designed primarily to decrease exposure time by being extremely mobile and mechanically dependent as compared to tracked vehicles. Comparing to a regular 2 axle vehicle, the added axles allow for added payload capacity as well as mobility advantages in soft soils with better load distribution.

Despite the success of multi-axle combat vehicles, there are disadvantages attributed to the large carrying capacity and a higher suspension. This results in a higher center of gravity causing reduced lateral stability and maneuverability. Rollovers during training exercises and in missions have been blamed on the high center of gravity as well as human error and lack of training [3]. The influence of the driver input is unpredictable, therefore, no matter how stable or predictable the vehicle is designed to be, the driver can still input commands to contribute to a vehicle reaching the limits of it's dynamic capabilities.

The knowledge of unpredictable driver behaviour as well as unpredictable terrain has lead to the widespread application of active safety control systems in vehicles. These control systems, including Anti-lock Braking Systems (ABS), Traction Control Systems (TCS) and Electronic Stability Control (ESC) systems have decreased the likelihood of a single vehicle crash by up to 40% [4].

Rear Axle Steering (RAS) has been implemented into many passenger vehicles to improve turning performance at low speeds as well as improve the lateral stability of the vehicle at high speeds. Companies producing multi-axle combat vehicles have began implementing RAS using actuator systems to decrease the turning radius at low speeds. By using the available hardware, an active control system used to improve dynamic lateral stability can be implemented using the rear axle steering.

Ultimately, since the wheeled combat vehicle is used as a reconnaissance and troop-carrying vehicle, improving the vehicles maneuverability and stability will improve the usefulness of the vehicle. The respective military member has a greater chance of surviving a mission with a more maneuverable and stable vehicle.

1.2 SCOPE AND OBJECTIVE

1.2.1 Scope

This research is focused on the application of control systems to rear axle steering on an 8 wheeled armoured vehicle. The application of rear axle steering aimed at improving the stability and maneuverability of the vehicle will be explored. In this thesis, only the use of rear axle steering is to be analyzed as a function of increasing the stability and maneuverability while intuitively reducing the risk of rollover. A rollover mitigation controller is to be developed and tested against the other controllers.

1.2.2 Objectives

The final objective of this thesis is to provide insight into the application of rear axle steering on an 8x8 heavy vehicle as well as the benefits of introducing a comprehensive control system for the rear axle steering. The overall control system should be designed with the objective of implementing the system on a combat vehicle, meaning the control system should remain simple and intuitive. The effects of introducing this system will be analyzed using a validated multi-wheel combat vehicle within TruckSim with the control system developed in co-simulation in MATLAB/Simulink.

2

The objectives include:

- Design a feed-back, closed-loop control system using optimal control theory with the rear axle steering angle as the output
- Design a feed-forward controller to minimize the turning radius of the vehicle and increase the maneuverability at low speeds using only the rear axle as a control parameter
- Perform simulations to analyze the controller in different dynamic maneuvers at low speeds and high speeds using the validated non-linear TruckSim model
- Compare the difference between the designed feed-forward controller and the proposed feed-back, closed loop controller for low, mid-range and high speeds
- Assess the performance of each controller for best maneuverability at low speed and best stability at high speed and offer conclusions towards future development

1.3 OUTLINE OF THESIS

Chapter 1 consists of the motivation, scope, outline, and objectives of this thesis. The working fundamentals of vehicle dynamics are included in this chapter as an introduction to the literature review. The use of rear axle steering in Multi-Axle Combat vehicles is presented.

Chapter 2 outlines a literature review for vehicle stability control systems including torque differential distribution and rear axle steering. Theory behind multi-axle vehicles is introduced.

Chapter 3 presents the vehicle models necessary for developing the control systems introduced in Chapter 4. Co-Simulation with TruckSim© and Simulink is explained along side the full vehicle model in TruckSim©. The linear bicycle models are derived for the use in the control systems. The state space equations are derived to support the linear quadratic regulator (LQR) control system and the reference model. The linear bicycle model is solved for steady state to derive the zero-sideslip equation for the feed-forward controller.

Chapter 4 specifics how the control system is implemented in Simulink. The design of the LQR controller and parameters for the LQR controller are discussed and defined. The theory behind the LQR control system is presented and the final control systems are implemented.

Chapter 5 presents the simulation results for the ZSS and LQR controlled vehicles against the conventional vehicle. The maneuvers include low, mid-range, and high speed comparisons over low friction and high friction surfaces.

Chapter 6 presents the results of the controlled vehicles compared to the conventional vehicle when the steering input causes rollover on the conventional vehicle. The two developed controllers will be simulated to demonstrate the effectiveness during crosswind as an external disturbance.

Chapter 7 concludes the results and offers further recommendations. The next steps to develop this controller and implement onto a physical vehicle are presented.

1.4   WORKING FUNDAMENTALS

This chapter will present supporting information based on common theories in vehicle dynamics and control systems.

1.4.1   Vehicle Dynamics Theory

Vehicle dynamics is a theory that follows the rules of physics. As Newton's Fist law states: An object will remain at rest or in uniform motion unless acted on by an external force. Vehicle dynamics describes how a vehicle reacts to the environment through isolation and control [5]. The vehicle isolates the driver from the impact of externally generated disturbances such as the road surface and aerodynamics (crosswind) by use of aerodynamic devices and shock absorbers etc. Vehicle control, which is the main focus of this work, can be used to improve vehicle stability and performance based on the driver's input. The driver is able to demand the vehicle trajectory by using the throttle and brakes to adjust the longitudinal properties and the steering wheel to adjust the lateral performance of the vehicle. The vehicle's performance is highly dependent on the tire and suspension

characteristics. At low speeds the vehicle behaviour can be approximated by finding the instantaneous turning center, however at high speeds this assumption cannot be followed due to the lateral slip provided by higher lateral accelerations, demonstrated in Figure 1-1. Vehicle dynamics at higher speeds can be more accurately explained by referencing pneumatic tire mechanics [5].
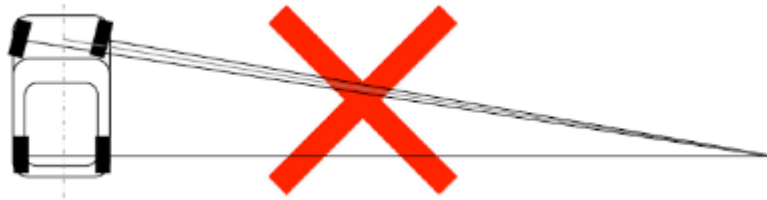
Figure 1-1 Improper Assumptions of vehicle trajectory at high speeds [5]

The Society of Automotive Engineers (SAE) vehicle coordinate system is universally used when analyzing vehicle dynamics results. Analyzing the SAE coordinates for a full vehicle in Figure 1-2, it can be seen that the Y-axis is in the lateral direction of the vehicle, the X-axis is the longitudinal direction and the Z-axis is the vertical direction. The pitch of the vehicle describes the angle about the Y-axis and affects the load transfer from the front to rear of the vehicle. The roll of the vehicle is the angle about the X-axis of the vehicle and can be used to determine if the vehicle is in a rollover condition. The yaw of the vehicle describes the angle around the Z-axis and is often used to describe the handling performance of the vehicle.
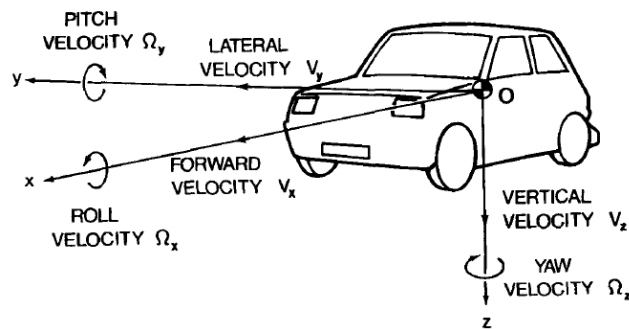
Figure 1-2 SAE vehicle coordinate system [6]

5

1.4.1.1 Pneumatic Tire Dynamics

The pneumatic tire in automotive engineering has its own SAE coordinate system as seen in Figure 1-3. It follows similar coordinate system as a full vehicle model. However, the tire axis system is always aligned with the tire, not in the direction of the vehicle travel.
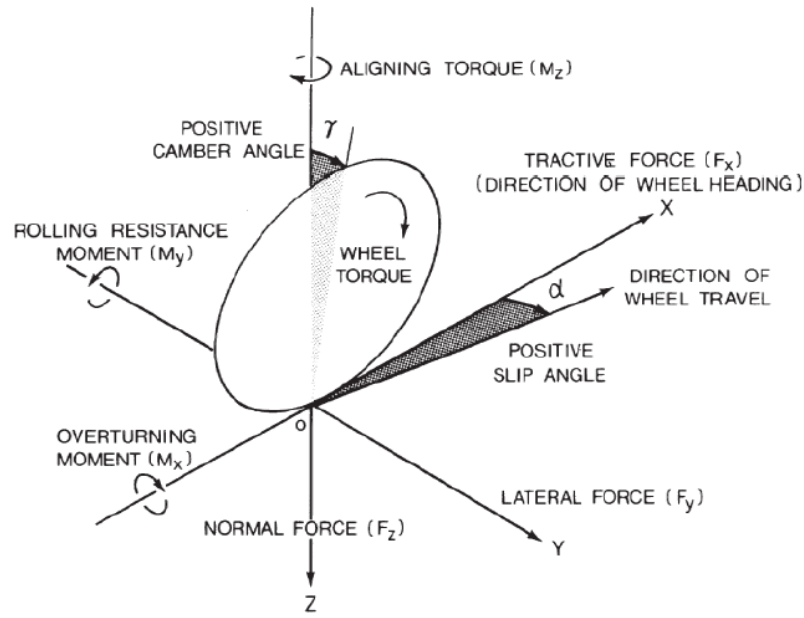
Figure 1-3 Tire Axis System as Defined by SAE [6]

The origin of the tire axis is at the center of the contact patch with the Z-axis normal to the ground surface, even if it is not inline with the camber of the tire. The normal force F_z is the force from the weight of the vehicle. The axis that the traction of the tire is developed in (F_x) is defined as the X-axis. The tire produces a cornering force (F_y) in the lateral (Y-axis) direction which is perpendicular to the X-axis on the surface plane. The moments around each of these axes can be described as the aligning torque (M_z), the rolling resistance (M_y) and the overturning moment (M_x). Throughout this work, the theory is based on the lateral and longitudinal forces as these are the forces which can be controlled by the driver.

Longitudinal and Lateral forces

The longitudinal forces from the tire generate the acceleration or braking forces in line with the X-axis. The amount of force which is provided by the tire is dependent on the percentage of slip (i) between the tire and the surface as illustrated in Figure 1-4 .

$$Longitudinal\ slip = i = \left(1 - \frac{V_t}{r_{effective}\,\omega_{tire}}\right) \cdot 100\% \qquad \qquad 1\text{-}1$$
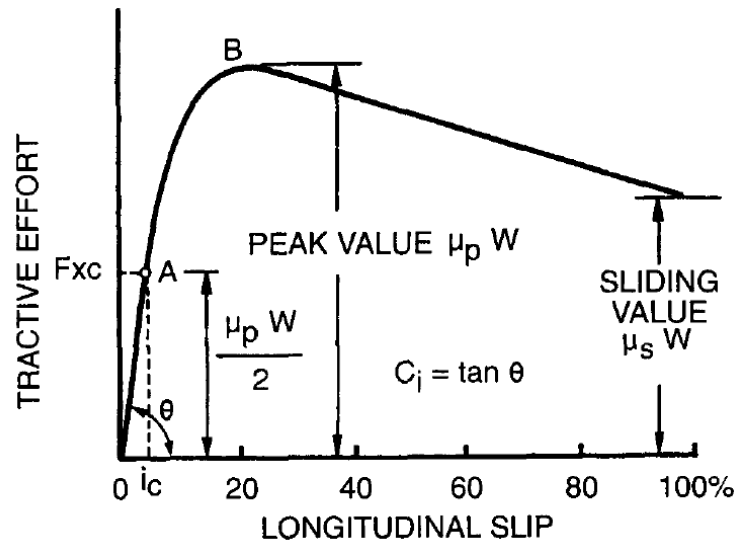
Figure 1-4 Variation of tractive effort with longitudinal slip of a tire [6]

The pneumatic tire is required to slip in order to produce tractive or braking forces due to the elastic properties of the tire material [7]. The tractive or braking effort is also dependent on the surface friction properties. The tractive and braking forces increase as the slip percentage increases. The peak tractive forces are produced in the range of 20-25% slip for most tire types [6].

Similarly, for lateral forces, slip is required to produce lateral forces due to the elastic properties of the tire. When a tire is steered, the tire deforms deflecting the tire contact patch as seen in the grey area of Figure 1-5. The slip angle, α, is the direction of travel in reference to the heading angle of the tire. The lateral, or cornering, force is the reaction force to the tire resisting the deformation, otherwise known as the aligning moment.

7
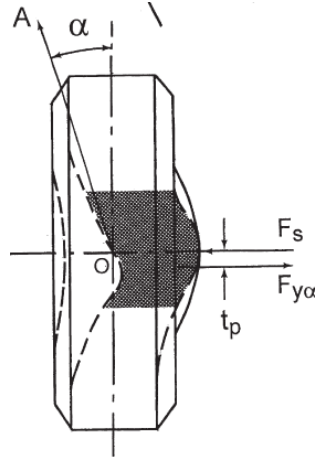
Figure 1-5 Cornering behaviour of tire patch (top view of tire) [6]

The pneumatic tire is not a linear system. The elastic properties of the tire have limits which are reached at higher slip angles. The cornering force at lower slip angles can be mathematically explained in Equation 1-2 as a function of the cornering stiffness, C_α, and the slip angle.

$$C_\alpha = \frac{\partial F_{y\alpha}}{\partial \alpha}\bigg|_{\alpha = 0}$$

1-2

At higher slip angles the cornering force saturates (Figure 1-6) and when the cornering force from the tire surpasses the road adhesion limit, the tire will slide.
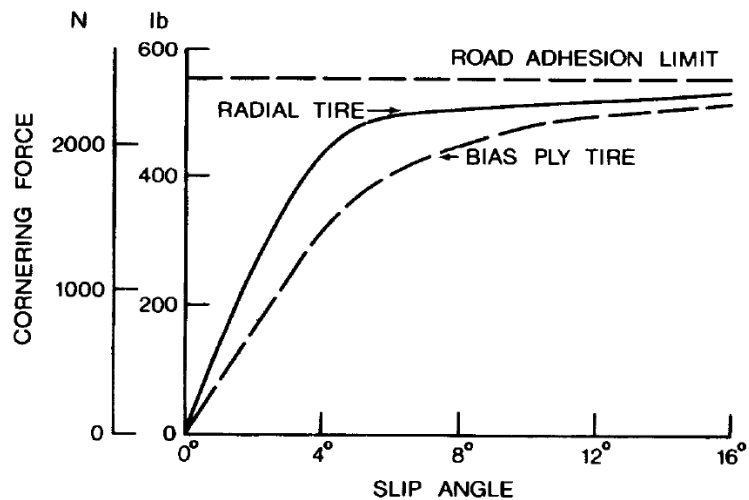
Figure 1-6 Cornering force relationship with slip angle for bias-ply and radial tire [6]

A tire has limits for how much combined lateral and longitudinal forces can be generated. A common method for representing this graphically is with the use of the friction ellipse.

8
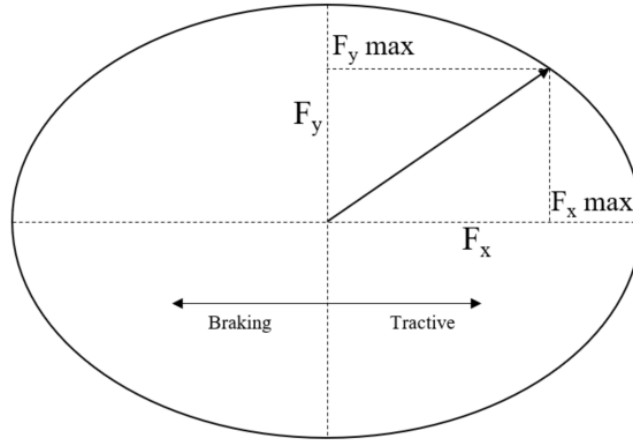
Figure 1-7 Tire friction ellipse

The effective tire traction and braking forces can be determined from the tire friction circle. This ellipse is a function of normal load, tire slip angle, and tire characteristics. With the horizontal axis representing the longitudinal, braking and tractive forces and the vertical axis representing the magnitude of the lateral cornering forces, the perimeter of the ellipse represents the limit of force to be produced by a tire. The equation for the tire friction circle is:

$$\frac{F_{y\alpha^2}}{F_{y\alpha max}} + \frac{F_{x^2}}{F_{xmax}} = 1 \qquad \qquad 1\text{-}3$$

Where $F_{y\alpha\,max}$ and F_{xmax} are determined by the lateral and longitudinal properties of the tire and the normal force.

1.4.2   Control Systems Theory

The purpose of a control system is to do just that, control a system, by manipulating the input to obtain the desired output [8]. This system is governed by a set of equations that is defined as the plant in control systems theory. The mathematical representation of the control system can be denoted at the state space representation, which will have a fundamental role in the control theory in this work. In control systems there are three widely accepted measures of performance; the response delay (transient response), the inevitable error between the input and output signals (steady state error), and the stability of the system. Control systems are useful in many applications to improve precision and speed

9

compared to human adjustments by analyzing inputs at a quickly and calculating error response precisely.
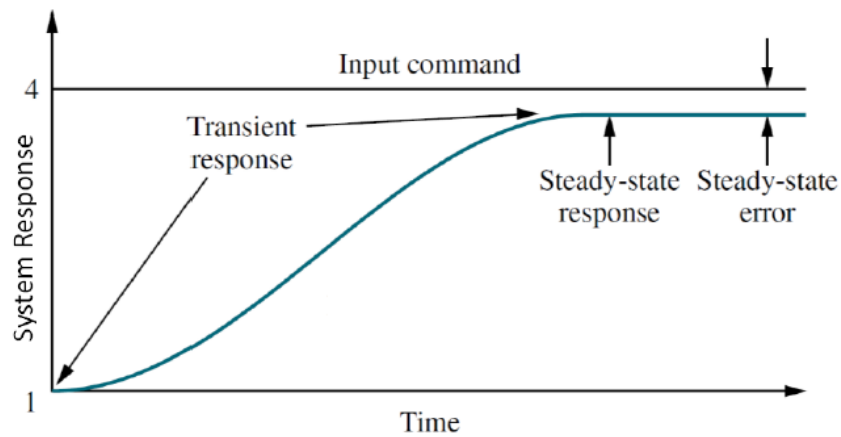
Figure 1-8 Step input response [9]

System Configurations

The internal architecture of a total control system relies on two main configurations of control systems: open loop (feed-forward) and closed loop (feed-back).
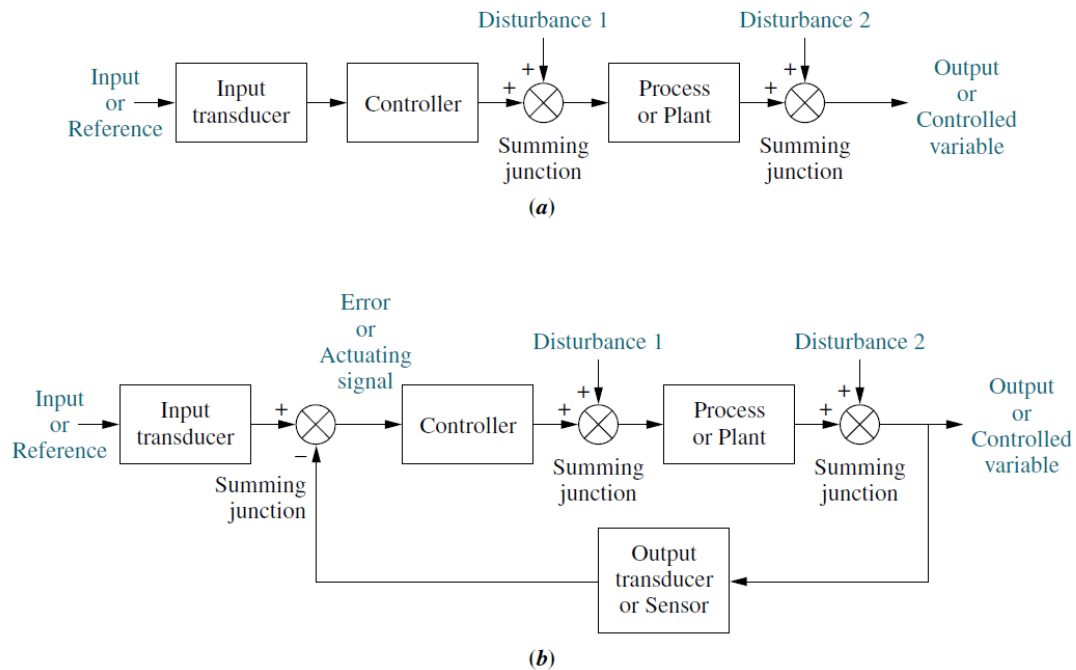
Figure 1-9 Control system block diagrams: (a) open- loop system; (b) closed loop system [9]

An open loop controller is a system that uses the input, or reference signal to produce a control signal that is sent to the plant as shown in Figure 1-9 (a). These controllers are functional and cost effective, however they are unable to compensate for external disturbances from the controller or the environment [9] (as illustrated by disturbance 1 and disturbance 2 in Figure 1-9 (a)).

The closed loop controller is similar, except it allows for these disturbances to be detected by the output response and the error signal is considered prior to the controller. This encourages increased accuracy, decreased sensitivity to noise and external disturbances and increased control over transient response and steady state error [9].

In vehicle dynamics controls, the steady state can be determined from the speed of the vehicle and the steering input from the driver based on the vehicle parameters.

1.5   COMBAT VEHICLE TECHNOLOGY

Wheeled combat vehicles have become extremely popular for military use by offering maneuverable, portable and fuel-efficient qualities when compared to a tracked vehicle. Wheeled combat vehicles are capable of maximum speeds of 100-110 km/h [10] with light armour and modular configurations for troop and/or infantry transportation. They are designed to withstand typical combat threats such as ballistic, mines improvised explosive devices and rocket propelled grenades. They are also extremely maneuverable on various terrains due to the multi-axle configurations that offer more efficient weight distribution. The added axles also allow for a higher maximum Gross Vehicle Weight Rating (GVWR) than smaller vehicles.

With three or four axles, the wheelbase of these wheeled combat vehicles is long resulting in a vehicle with a large turning radius. Many manufacturers of these vehicles have introduced rear axle steering to reduce the turning radius.

The MOWAG Piranah (Figure 1-10 (a)) reduces its turning radius by steering the rear axle [11]. The FNSS PARS III 8x8 (Figure 1-10 (b)) steers all axles with a gradual decrease of steer by wire output and locking over a certain speed [12]. The Patria AMV (Figure 1-10 (c)) offers rear axle steering as an optional method for decreasing the turning radius

[13]. The Hagglunds SEP (Figure 1-10 (d)) was a proposed electric combat vehicle including rear axle steering. This project was cancelled due to lack of international support [14]. *Other companies producing vehicles with rear active steering cannot be properly cited.*

(a) MOWAG Piranha V (gdels.com)	**(b)** FNSS PARS III 8x8 (fnss.com.tr)
(c) Patria AMV (patria.fi)	**(d)** Hagglunds SEP (Military-today.com)

Figure 1-10 Production and pre-production RAS combat vehicles

Most of these vehicles offer only rear axle steering as this provides significant improvement on the turning radius, which is the initial intention of adding this feature. This thesis will use solely active rear axle steering as a constraint to analyze the most popular configuration of actuated rear axle steering seen on multi-axle wheeled combat vehicles.

CHAPTER 2
LITERATURE REVIEW

2.1 CHAPTER INTRODUCTION

This chapter will provide a review of past studies involving yaw moment control methods and more specifically, using rear axle steering. This review will provide a guideline on how to implement rear steering into a future 8x8 combat vehicle. The majority of previous rear axle steering and control research has been completed on a four-wheel, two-axle vehicle, however the research methods can be interpreted into a four-axle 8x8 vehicle.

2.2 VEHICLE STABILITY CONTROL SYSTEMS

In the automotive industry today, it is extremely unlikely to find a consumer vehicle to be offered without a driver aid control system. Since the introduction of these systems, the focus has expanded to include vehicle performance instead of vehicle safety. The development of stability control systems originates from Anti-lock Braking Systems (ABS) and Traction Control Systems (TCS) which aided in maintaining directional stability of the vehicle during emergency situations. These systems limit the longitudinal wheel slip and lock up through active manipulation of the throttle and braking. When the tires are operating at the slip of maximum adhesion, the shortest braking distances and most efficient accelerating times can be achieved [15]. Further developments aimed towards regaining stability during the event of the vehicle heading in an undesired direction by using Electronic Stability Control (ESC). When the vehicle trajectory is different from the intended direction of the driver input, the ESC system strategically activates the brakes in order to regain directional stability of the vehicle. A study completed by the Swedish Road Administration in 2006 [16] concluded that ESC has decreased the amount of crashes with personal injury by 13% for all types of crashes and by 35% for crashes on wet or icy road surfaces.

Transport Canada, which follows Federal Motor Vehicle Safety Standards (FMVSS), is starting to enforce a new standard in 2019. FMVSS 136 requires heavy vehicles with a

gross vehicle weight rating of 11 793 kg or more and manufactured after August 1, 2019 to include ESC [17]. During a cost-benefit analysis performed by Transport Canada, ESC was ruled to be more beneficial than Rollover Stability Control (RSC) because of the extended benefits from controlling directional stability rather than only rollover. RSC would not include the required hardware to detect yaw motion which determines understeer or oversteer conditions. Prevention of rollover would benefit primarily the single heavy vehicle, while retaining directional stability with ESC decreases the risk of multi-vehicle accidents.

The progression of vehicle control using computers has advanced from aiding in an emergency situation to enhancing vehicle performance. One of the concentrations for aiding the vehicles directional performance has been on controlling the yaw motion of the vehicle. Many methods in consumer vehicles have been used including differential braking, torque vectoring, as well as active front and rear axle steering. All of these methods focus on increasing or decreasing the yaw moment on the vehicle to increase performance and stability of the vehicle. It is also beneficial to reduce the vehicle sideslip angle in order to maintain controllability over low friction surface as well as maintaining the tires within their steering range of operation for generating lateral forces [18].

Liebmann et al. [19] studies the effectiveness of the Bosch Electric Stability Control Program (ESP). Bosch introduced ESC to the automotive manufacturing world as a supplier, subsequently supplying more than ten-million systems in various vehicle configurations worldwide. ESP can be adapted to control the yaw as well as limit the sideslip angle of the vehicle for different configurations of vehicles by using active braking control. The ESP system has been adapted to include rollover mitigation for higher center of gravity vehicles.

2.3 BASIC PRINCIPLES OF YAW CONTROL
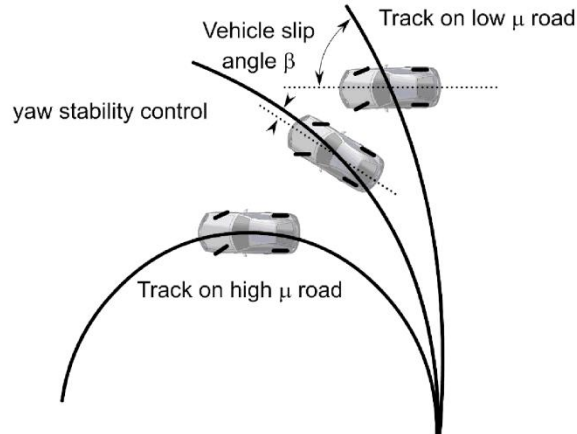
Figure 2-1 Functioning Yaw Stability Control [20]

Vehicle yaw describes the rotational behaviour of the vehicle around it's vertical axis. In terms of vehicle performance, the vehicle's yaw behaviour can be used to interpret the vehicles expected trajectory against the intended trajectory. By applying a system to control the vehicle yaw, the directional stability can be maintained. The theory behind controlling the yaw motion of the vehicle is to control the moment produced through the manipulation of the tire-road contact. Controlling the yaw rate of the vehicle strengthens the stability of the vehicle while also allowing the vehicle to follow the intended path more closely than just correcting the high yaw rate.

There are many different methods for controlling the yaw of a vehicle. All approaches use the same theory which is increasing the moment around the center of gravity by actively controlling the lateral or longitudinal forces distributed by the tires. The lateral dynamics of the vehicle can be controlled effectively by introducing a slip angle to a tire or by varying the distribution of the driving or braking torque.

Stability control systems that focus on yaw rate feed-back are being widely commercialized by automotive manufacturers [19, 21-24]. Monitoring yaw is an effective method of retaining control of a vehicle without compromising drivability of the vehicle. Desired yaw rate is interpreted from the steering wheel input and the vehicle speed and is being utilized in commercial vehicles as a safety measure and to allow the driver to operate closer to the vehicle's handling limits without losing control.

15

2.4 BASIC PRINCIPLES OF SIDESLIP CONTROL

Vehicle sideslip (β) is used to describe the heading angle of the vehicle versus the direction of travel for the vehicle. Limiting the vehicle sideslip angle allows for better control as consequently the tires slip angles are limited from reaching saturation [25].

Though vehicle sideslip is not easy to measure accurately, there are increasing methods for acquiring the exact sideslip angle of a dynamic vehicle. Reasonable approximations of vehicle sideslip can be estimated with vehicle speed and lateral acceleration. More accurate estimation can be acquired through the integration of GPS based vehicle speed vector with the vector of vehicle speed from the Inertial Measurement Unit (IMU). Daily et al. [26] define the main source of error resulting from the error of GPS measurement and can be corrected using a speed error function. The main issue with GPS based measurement is the unreliability in environments where there are tall objects.

Piyabongkarn et al. [18] determine other methods of observing the vehicle sideslip angle include the use of optical sensors and dynamic model-based estimations. Also discussed within this article is a new slip angle estimation method which uses a model-based estimation combined with a kinematics-based estimation. Through experimental implementation, the vehicle sideslip was effectively calculated and provides robust estimation of vehicle sideslip angle through extreme maneuvers.

2.5 TORQUE VECTORING

Torque vectoring is a term for the distribution of the engine torque to the drive wheels. If a vehicle is turning, the outside wheel travels a percentage more than the inside wheel. By applying more torque to the outside wheels during a turn, the vehicle is more likely to complete the maneuver with more confidence.

Early development of torque vectoring by Mitsubishi Motors was to create "a vehicle that anyone can drive safely". To avoid the brake assisted steering which would reduce the vehicle speed and conflict with the driver's input, Mitsubishi developed the Active Yaw Control system (AYC) using a "torque transfer mechanism" along-side their already developed Active Stability Control (ASC). The result was a torque transfer differential

which was applied to only the rear axle of the 4WD vehicle. The system used a feed-forward control system to improve the responsiveness of the vehicle by analyzing the driver input steering wheel angle and throttle position. It was coupled with feed-back control to monitor the lateral wheel speed difference. Additional systems could maintain control during a drift maneuver and would adjust the gain of the controller by estimating the surface friction coefficient, μ. The system allowed for higher lateral accelerations to be achieved through the use of left/right torque control while improving the control of the vehicle. When in use with the ASC system, the vehicle becomes easier to control, and if the control limits are reached the vehicle is able to recover [27].

2.6   ACTIVE BRAKING ASSIST

The use of braking is an effective method of applying a yaw torque in order to either regain stability or increase the yaw rate performance of a vehicle. Many car companies are able to implement an active braking assist with ease because it uses the same hardware as ABS and ESC, which is standard in all vehicles sold in North America [28].

Using braking torque to control the yaw motion of the vehicle is different than a braking-based ESC as it is not required to be braking to activate. Ghike et al. [29] state that varying the torque by using the brakes is less intrusive and more effective at controlling lateral vehicle dynamics than the ESC while also causing less of a decrease in speed. By braking the inside wheel of a slip-differential based axle, more engine torque is sent to the outside wheel, completing the desired torque distribution. As seen in Figure 2-2 the yaw moment can be applied by braking the inside wheel.
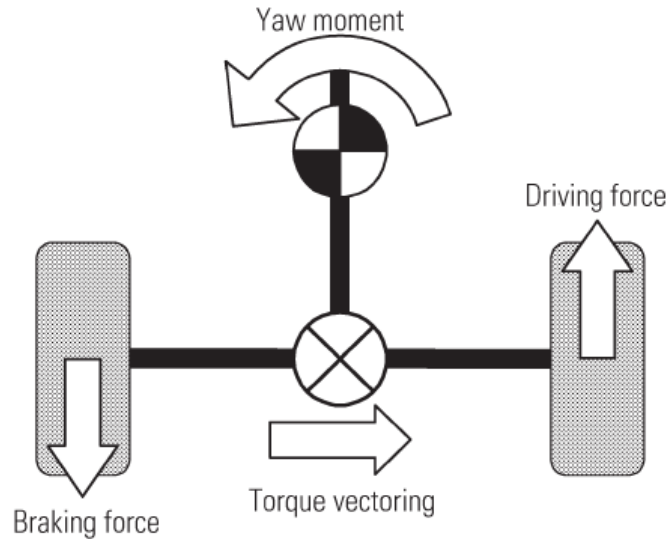
Figure 2-2: Lateral Braking Control [21]

2.7 ACTIVE STEERING ASSIST

Active steering assist describes a system which allows the steering angle to be manipulated to adjust for the lateral dynamics of a vehicle. This system also allows for the addition of semi-autonomous systems such as lane assist and emergency steering assist which is useful as control systems have quicker and more precise reactions than the human driver [30]. Active steering assist allows the driver determine the direction of the vehicle while the disturbance adjustments are handled by the control system [31]. Active steering also presents some advantages in terms of vehicle performance as continuous operation steering control can correct the driver when a mistake is made, allowing the limits of the vehicles stability capabilities to be tested with more confidence.
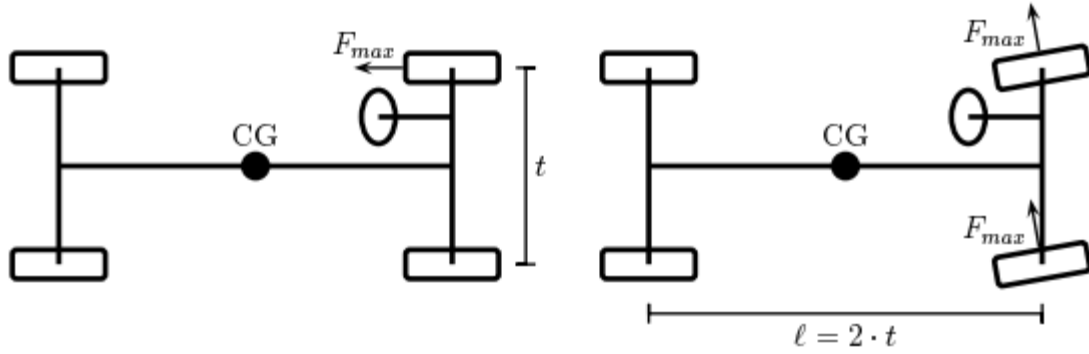
Figure 2-3: Vehicle Torque while braking front wheel (left) and front wheel steering (right) [30]
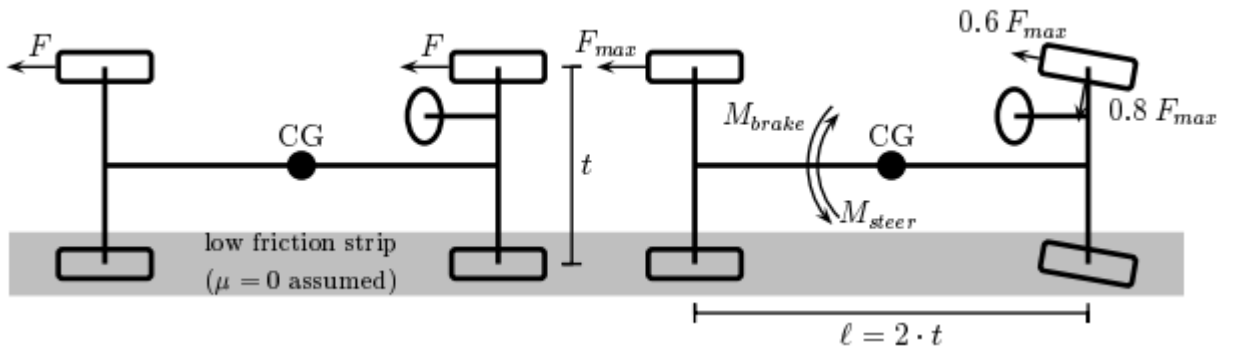
Figure 2-4: Split-µ braking - Balance of torques with active steer [30]

Ackermann et al. [30] demonstrate in Figure 2-3 that during a yaw corrective procedure, two tires steering require around a quarter of the tire force when compared to one wheel selectively braking. Figure 2-4 demonstrates that active steering applied with selective braking can balance the yaw torque caused by asymmetric braking over a split-µ surface, offering a more stable braking condition than solely braking.

2.8 REAR AXLE STEERING (RAS)

Rear axle steering has been used in many vehicles as a method of improving the dynamic performance of the vehicle. RAS is commonly used to reduce the turning radius of a vehicle at low speeds by automotive companies on larger vehicles. Rear axle steering can also be used to compensate for the oversteering or understeering characteristics of a production vehicle under varying conditions [32].

19

Rear axle steering is an effective method of controlling the lateral forces generated by the rear tires. The use of RAS is commonly used for decreasing the turning radius of a vehicle at low speeds while reducing tire wear and is found in all types of vehicles including heavy haul trucks, pickup trucks and even sports cars. Rear axle steering can be used at high speeds to reduce the vehicle sideslip as well as offtracking and improve the stability by controlling the yaw rate of the vehicle. With "steer-by-wire" used for RAS, there are increased possibilities for improving the vehicles dynamic stability. Much like active steering assist, an active rear steering system can improve the lateral dynamics of the vehicle, only separate from the front steering angles. Advanced dynamic stability becomes very useful in heavy vehicles with a high center of gravity as a rollover prevention measure and to increase lateral vehicle performance. Many large trucks already include RAS in order to improve maneuverability at low speed, however Kharrazi et al. [33] suggest existing RAS can be used to improve split-μ braking, and enhance safety as well as driver comfort.

There are several methods used for controlling the steer angles of the rear axles. Passive rear steering can be implemented into a vehicle by mechanical means, or in methods which the driver does not have any control on. Porsche introduced rear steering using a mechanical linkage, called the Weissach axle, that would reduce the oversteering behaviour by inducing toe-in on the rear axle [34]. Though passive steering is not in the scope of this work, it is necessary to appreciate the methods of increasing performance through mechanical approaches. Feed-forward control methods generally use the input of the driver to determine the steering of the rear axle. Feed-back control methods use the vehicle performance measures to tune the rear steer angle to satisfy the ideal vehicle driving model. In practice, feed-forward control aids performance of the vehicle while feed-back controllers aid the external disturbances [35]. These disturbances could be introduced as side wind, roughness in terrain, split-μ surfaces, road crowning, etc.

2.8.1 Feed-forward Rear Axle Steering Control Methods

Feed-forward control methods are an effective means for benefiting from active rear steering by outputting a rear steer angle with reference to the steering input. Knowledge of the vehicle layout and dynamic performance of a vehicle can lead to the optimal tuning of

a feed-forward controller. Low speed maneuverability can be easily increased using a feed-forward controller and the stability of the vehicle is not as crucial to safety at low speeds. A study by Furukawa et al. [36] highlights two methods for feed-forward control methods.

First is the Zero Side Slip (ZSS) control method. ZSS considers the speed of the vehicle and the steering input. These inputs are used in a transfer function which was derived by analyzing the two degree of freedom bicycle model of the vehicle with front and rear steer angles. To satisfy the zero-sideslip portion of the controller, the sideslip angle in the transfer function is set to zero and the yaw rate portion is eliminated, thus producing a speed dependent ratio gain for the steering angle of the rear axle compared to the front axle.

$$k = \frac{-b - \frac{ma}{C_r l} U^2}{a + \frac{mb}{C_f l} U^2} \qquad\qquad 2\text{-}1$$

Where a and b represent the distance of the front and rear axles to the center of gravity, respectively, l is the wheelbase of the vehicle, C_f and C_r are the cornering stiffness of the front and rear tires respectively, and U is the vehicle speed. This produces a relationship presented in Figure 2-5.
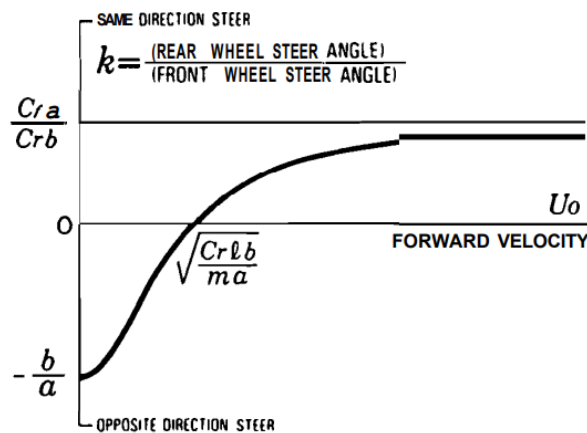
Figure 2-5 Zero Side Slip (ZSS) Speed Dependent Front to Rear Ratio

Zero Sideslip rear steering controllers have been used in several production applications. Most notably Nissan used this method in their High Capacity Actively-controlled Steering system (HICAS) [37] as well as Mazda in Speed-Sensing Four Wheel Steering (SS-4WS) [38]. This method effectively reduced the turning radius of these production vehicles as well as aids with stability of the vehicle at higher speeds.

The second method reviewed by Furukawa et al. [36] is a purely steering angle dependent relationship. For small input steering angles, the rear wheels steer in the same direction as the front wheels. For larger steering angles, which are more likely to occur at low speed, steer the rear wheels opposite of the front wheels for increased maneuverability. This system enables the low speed and high-speed steering to be improved without the need to update vehicle speed in the controller. This method was developed further and used in OshKosh heavy vehicles [39]. The improved controller includes a transition zone which allows for a smoother transition from the rear wheels being steered with the front wheels to the rear wheels being steered opposite of the front wheels [39]. This decreases the sudden change in steering mode for the rear wheels allowing for intuitive vehicle response to the driver.
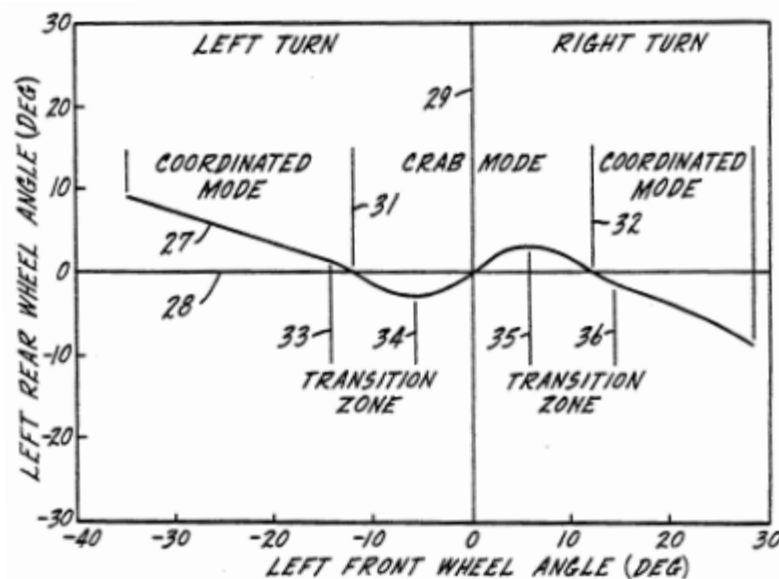
Figure 2-6 Steer Angle Dependent RAS found in OshKosh vehicles [39]

Lin [40] defines rear steering control methods as proportional control, first order lead control, first order delay control, zero sideslip control, and ideal/advanced four wheel

steering control where all wheels are actively controlled. Zero sideslip steering control was defined by the author to be the best control for the rear axle steering with the downfall of excessive understeer characteristics at high speed. The author suggested including a closed loop system for the front axle steering to allow extra control with the similar driving feel of the conventional vehicle.

2.8.2 Feed-back Steering Control Systems

Many different control systems are able to solve the active steering control problem. The control problem in this scenario is determining the desired behaviour of the vehicle and applying a steering angle to achieve a satisfactory response. The ideal vehicle behaviour defines the steady state model and is tracked by the controller despite possible external disturbances or sensor errors. A good controller will also track the reference if the dynamics of the plant system are changed during operation [41]. Sato et al. [42] studied an all wheel steering system using yaw speed feed-back rear steering and determined this method improves tracking, steering properties and response to external disturbances. Yamamoto et al. [43] indicate that while the previously stated improvements as well as optimized steering response can result from a yaw speed feed-back controller, the lateral tire adhesion limits are reached easily, and other control systems should be adopted when these limits are reached.

The previously mentioned ZSS controller was improved by Whitehead [44] to monitor the rate of change of the sideslip angle. This closed loop approach allowed the vehicle sideslip angle to remain closer to zero during transient motion as opposed to the open-loop approach which is directly responding to the steering wheel angle and gain set by the vehicle speed. Inoue et al. introduced a system that includes both a feed-forward and feed-back control system that allows the vehicle to follow the reference yaw rate with the responsiveness of a feed-forward controller.

Kharrazi et al. [33] observed the effectiveness of rear axle steering on the yaw stability and responsiveness of a heavy truck using MATLAB-Simulink and on a full-scale Volvo truck. The control system focused on split-μ braking and high-speed maneuvers as measures for analyzing vehicle control. The controller steers the rear axle in order to satisfy the driver's

23

input, or the reference yaw rate. The high-speed steering controller consists of first-order feed-forward and a proportional feed-back:

$$\delta_3 = (K_{FF} - T_{FF}s)\delta_1 + K_{FB}(r_{ref} - r) \qquad 2\text{-}2$$

The split-μ braking controller uses a proportional gain feed-forward controller to steer the rear axle to compensate for uneven braking forces on the left and right. This decreases the stopping distance by allowing the ABS to perform at its capacity without forcing the driver to counter steer. The controller can be described as:

$$\delta_3 = K_p M_{brake} \qquad 2\text{-}3$$

The simulations and full vehicle tests conclude the yaw rate error can be reduced by 64% while decreasing the effort needed by the driver. The split-μ braking controller using RAS could reduce braking distance by at least 10% by using a more aggressive ABS system and RAS to maintain the same level of driver input needed as a stock vehicle.

Nagai et al. [45] used a Model Matching Controller (MMC) which applies the state feed-back of both the yaw rate and the side slip angle of the vehicle to aid the vehicle in following the ideal dynamic path. MMC method uses linear control theory but proved to be effective at improving the vehicle handling and stability even when the vehicle parameters change. The robustness of a controller is extremely important in a combat vehicle as the vehicle mass and cornering stiffness changes depending on terrain, tire pressure, and vehicle configuration.

Other control systems use both feed-forward and feed-back methods to decrease the response time and increase the disturbance rejection. Hiaoka et al. [46] use a model following sliding mode control, which uses the feed-forward zero side slip model as the reference model. It proved to be robust against system uncertainties.

Optimum controller theory is a good place to start when designing complex systems. For most vehicles there is more than one dynamic property that needs to be controlled. Optimal controllers, such as linear quadratic regulator, are ideal solutions for multi-input multi-output systems as well as systems that are not technically controllable [47].

2.8.3 Rollover Mitigation (ROM)

Vehicles with higher center of gravity and softer suspensions are generally more susceptible to rollover. Rollover can be caused by large lateral accelerations which occur when a vehicle enters a curve too fast or by what is known as a 'tripped rollover' which occurs when a vehicle is skidding and hits an obstacle. ESC in many instances is sufficient to reduce the risk of rollover by decreasing the lateral acceleration of the vehicle, however with an additional rollover mitigation system in use, the risk of rollover can be further reduced [48]. The prediction of a rollover will result in the application of a ROM method.

Typical systems predict rollover by analyzing the steering angle as well as the lateral acceleration of the vehicle, other systems may use a roll speed sensor to measure the rotational speed about the longitudinal axis. Odenthal et al. [49] estimate critical rollover with a rollover coefficient defined as:

$$R = \frac{F_{z,R} - F_{z,L}}{F_{z,R} + F_{z,L}} \approx \frac{2(h_{COG})}{T_{trackwidth}} \cdot \frac{a_{y_{COG}}}{g} \qquad \textit{2-4}$$

When the left or right side of the vehicle lifts, the value of R will be equal to ± 1 which determines rollover condition. Rollover condition can also be predicted using lateral acceleration (a_y) at the height of the COG (h_{COG}) of the vehicle as well as the trackwidth of the vehicle.

Many ROM systems use the application of ABS hardware to selectively brake a wheel based on providing the corrective lateral accelerations. Coordinating the ROM with a yaw stability system will allow the vehicle to follow the yaw rate reference provided by the steering wheel while preventing rollover [50]. Using active steering along side active braking allows for increased reduction of rollover risk which is caused by steering input from the driver [49, 51]. Steering is a more effective method than braking for immediately decreasing the risk for rollover by effecting the yaw rate immediately. Systems using multiple feed-back loops allow for the damping of the roll rate during regular operation of the vehicle while minimizing the risk of rollover during the event of a "tripped rollover" or harsh steering input.

Using similar theory [49-51], Zhang et al. [52] applied an emergency rollover mitigation system using individual rear wheel steering to steer the outside rear wheel of the vehicle during the condition of the rollover coefficient magnitude in Equation 2-4 being more than 0.8. When the rollover condition is met, a sinusoidal pulse signal is sent to the rear, outside wheel to correct the lateral dynamics of the vehicle. The system is called the pulsed active rear steering (PARS) which uses the same pulse theory as ABS for regaining the stability of the vehicle. The two design factors of this controller are the steering amplitude of the pulse signal and the frequency. This system successfully decreased the yaw rate and lateral acceleration of the vehicle when applied on the outside wheel during a steady state steering manoeuvre (Figure 2-7). During application on a physical road vehicle, the results were similar.
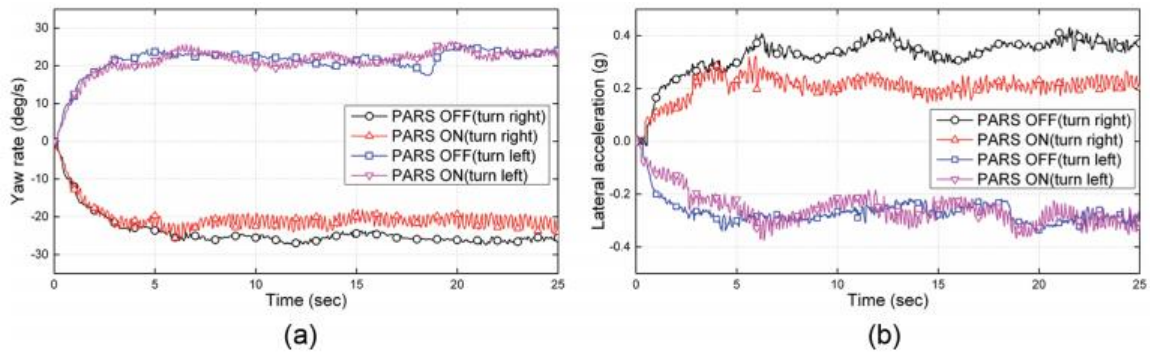
Figure 2-7 Yaw rate (a) and lateral acceleration (b) of vehicle during steady state cornering maneuver [52]

2.9 MULTI-WHEEL VEHICLE CONTROL

Vehicles with multiple axles are believed to have increased performance over 2 axle vehicles in terms of off-road performance, steering capability, obstacle maneuvering as well as fail-safe performance in case of emergency. Many studies have been completed on actively controlling 2 axle vehicles, most of which can be directly applied to multi axle vehicles, but lateral dynamics due to the extra axle(s) need to be respected.

One of the problems with long vehicles, as well as multi-axle vehicles, is the offtracking, otherwise known as the increased lateral displacement from the front axle to the rear axle. When this is present in soil, there is increase in rolling resistance. Harnisch [53] describes how steering control for multi-axle vehicles can be used to control the multi-pass of tires

in loose terrain to avoid high rolling resistance while turning over loose terrain. It is determined that an 8x8 vehicle with a static 3rd axle will have negligible effect on the rolling resistance, while symmetric steering decreases the rolling resistance when compared to the traditional vehicle. Multi-axle steering is determined to increase the rolling resistance when initiating a turn but could be improved with intelligent steering system design for the initiation of a turn. A publicly available vehicle built by a Russian company, Avtoros [54], is a 8x8 vehicle with individually steered wheels, allowing for various steering configurations such as normal Ackermann front wheel steer, contra-steer for tight maneuvering and the ability to "crab" or steer all wheels equally in the same direction to avoid multi-pass, otherwise promoting offtracking.

Watanabe et al. [55] discuss that a vehicle with differentials allows equal tractive forces on both the right and left side of the vehicle at steady state. Additionally, on an 8x8 vehicle with only the first two axles steered, the third axle has the largest lateral force in the direction of the outside of the turn Figure 2-8. Watanabe et al. also state that multi-axle vehicles with rear steering generally do not have identical steer centers, and concluded that the position of the steering center had negligible effect on turning radius when comparing non-symmetric steering to symmetric steering angles.
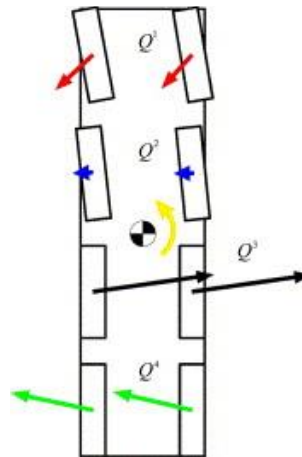
Figure 2-8 Lateral and longitudinal forces on a multi-axle vehicle [55]

Huh et al. [56] studied five different steering configurations for a 6x6 electric vehicle. It was concluded that the most effective method of steering has the second axle steering half of the front axle, with the last axle dependant on the yaw rate of the vehicle. This was most

effective as it provides the quickest yaw response as well as most decreased phase lag from the 4WS vehicle. The control law Equation 2-5 was derived from a bicycle model with the second wheel steered relative to the front wheel and the rear wheel steered to satisfy the desired yaw rate. The control law is based on the vehicle mass (M), speed (V_x), cornering stiffness of the tires on each axle (C_f, C_m, C_r) as well as the distance to the center of gravity (l_f, l_m, l_r).

$$\delta_r = \frac{-2C_f - C_m}{2C_r}\delta_f + \frac{MV_x^2 + 2\left(C_f l_f - C_m l_m - C_r l_r\right)}{2C_r V_x}r \qquad \textbf{2-5}$$

Linear Quadratic Regulator (LQR) control logic has been used very liberally throughout multi-axle vehicle control for controlling the steering angles of each axle individually as well as torque vectoring. Chen et al. [57] developed an LQR controller to actively control the last two axles on a 6x6 vehicle. An et al. [58] used LQR to control the front, middle and last axle of a six-wheeled vehicle referencing the desired yaw rate for a 4-wheeled vehicle. Improving on this study, An et al. [59] continued the work including the effect of the middle axle on the yaw rate control target. Both of these studies included the independent control of all six wheels which was then implemented and tested on a scale vehicle.

The LQR controller defines the dynamic system with state space equations which are derived from the vector-matrix differential equation. In the case of the dynamic vehicle model to monitor yaw rate and vehicle sideslip angle, the vector matrix differential equation is derived from a linear bicycle model [20]. Kiencke and DaiB [60] studied the difference between using a linear observer or a non-linear observer. Both observers were stable, however it was discussed that the stability of the linear observer could not be guaranteed over all driving conditions due to the nonlinear behaviour of the adhesion characteristics.

2.10 SUMMARY OF CHAPTER

Vehicle dynamic control systems have been introduced into production vehicles as electronic stability control. Using braking and engine torque control, companies have

successfully been able to reduce the risk of a vehicle losing control and traction reducing the risk of collision on roadways. FMVSS determined in a cost-analysis study that it is more effective to standardize ESC in heavy vehicles rather than a rollover mitigation control system as maintaining lateral stability is more effective at reducing multiple vehicle accidents, where a rollover mitigation system is more effective for only one vehicle. For this thesis, not only is the directional stability of this vehicle important, but protecting the single vehicle is also important, so rollover mitigation should be researched.

Many ESC systems use yaw control as well as sideslip control. By monitoring these two behaviours, a vehicle can maintain its directional stability. All control of the vehicle is accomplished by controlling the behaviour of the tires which are the only point of contact with the ground. Methods for controlling the tires include differential braking, torque vectoring, and active steering. Torque vectoring is one of the most effective methods as the longitudinal tire forces have a higher peak than the lateral forces achieved by steering. Additionally, torque vectoring does not apply braking forces causing the vehicle to decrease the speed. Torque vectoring will not be the direction of this thesis as the goal is to apply the control system to an active rear steering system. Active steering is effective for small corrections in yaw motion control and does not apply braking forces.

Active steering is also useful for rollover mitigation. Monitoring the lateral acceleration or the difference in vertical load from left to right side can effectively predict a near rollover condition. Alternatively, by applying a controller that decreases the lateral acceleration, rollover can be prevented intuitively by the system.

To reduce the turning radius, and increase low speed maneuverability, the ZSS feed-forward method will be introduced. The effectiveness of ZSS for high speed stability will be assessed against an active feed-back control method. Many active steering control systems use optimal control. LQR has been highly used for torque vectoring and differential braking. This method will be applied to control the yaw of the vehicle by steering the rear axle of the vehicle.

CHAPTER 3

SIMULATION ENVIRONMENT AND VEHICLE MODELS

3.1   INTRODUCTION

Validated vehicle models enable comprehensive virtual experimental testing through simulation avoiding the excessive cost of physical testing. To ensure strong and accurate conclusions from simulation, the tested vehicle needs to be validated [61].

Leblanc and El-Gindy [62] used a validated vehicle model to make recommendations to better the directional stability performance of self steering axles. El-Gindy and Mikulcik [63] investigated the yaw rate response sensitivity of a three-axle truck using frequency response and sensitivity analysis techniques to provide frequency domain information on the yaw rate sensitivity to the variation of basic vehicle parameters. Proper validation of a vehicle allows further proof of concept, sensitivity analysis, and control system design to be explored and fully concluded on before implementation into a physical prototype.

3.2   SIMULATION MODELLING TOOLS

The simulation software used is TruckSim© by Mechanical Simulation™. TruckSim© is a software developed by Mechanical Simulation™ to accurately simulate the performance of multi-axis vehicles. TruckSim© offers the opportunity to develop active controllers and analyze the results by calculating the vehicle's performance characteristics. By using Simulink, external controller models can use the desired vehicle data from the non-linear multi degree of freedom vehicle model in TruckSim©.

The validated vehicle model is a 25 Degree of Freedom (DOF) full vehicle model. The vehicle's steering system has one DOF, each individual wheel has two DOF for the rotation and vertical movement for a total of 16 DOF for the wheels, the front two steering axles

have one DOF each, and the sprung mass is assumed to be rigid with six DOF. Enabling the rear axle to be steered adds one extra DOF for a total of 26 DOF.

Figure 3-1 TruckSim© vehicle models; conventional vehicle (left), rear axle steering vehicle (right)

The two vehicle configurations are represented in TruckSim© in Figure 3-1. The vehicle configuration that is validated does not have a turret mounted and therefore is theoretically the most stable of the available configurations. The conventional vehicle has the front two axles steered and the rear two axles fixed, the rear axle steering vehicle has the fourth axle steered in addition to the front two axles steered.a

3.2.1 Vehicle Validation Method

The vehicle used in this thesis is an updated version of the Stryker 8x8 combat vehicle. The 8x8 combat vehicle model used in this thesis was validated by Ragheb [64] using measured data and published US Army validation criteria [65, 66].

Four standard maneuvers were used to compare the simulation model to physical, experimental results. These test events included double lane change, constant step slalom, J-turn maneuver, and a turning radius test. The test conditions shown in Table 3-1. were used in the experimental testing of the vehicle and the actual vehicle speed and steering wheel angle time history were recorded to be used as inputs into TruckSim©. The results from the speed and steering wheel angle time histories as input to TruckSim© was compared against the experimental results to validate the vehicle model.

Table 3-1 Experimental Test courses used for validation of 8x8 combat vehicle in [64]

Test Course	Vehicle Speed (km/h)	Additional Test Data
Double Lane Change (NATO AVTP-1 03-160W)	40, 52, 72, 81, maximum	-
J-Turn (75 ft radius)	30, 35,40, 45, 50	-
Constant Step Slalom (NATO AVTP-1 03-30)	40,53,60, maximum	30m cone spacing
Turning Circle (4x8 and 8x8)	Lowest Possible	-

3.2.2 TruckSim Full Vehicle Model

The vehicle model is governed by lookup tables and input values to define individual components of the vehicle. The complete powertrain is modelled in TruckSim© which includes the engine, torque converter, transmission, transfer case, and differentials (Figure 3-2). This simulated powertrain provides realistic torque distribution to the eight wheels through look-up tables for the engine torque vs engine speed and torque ratio output for the torque converter. Specific gear ratios, efficiency ratios, torsional stiffness and damping values, and spin inertias are determined for the transmission, transfer case, and each of the differentials. Airbrakes are responsible for slowing the vehicle down.
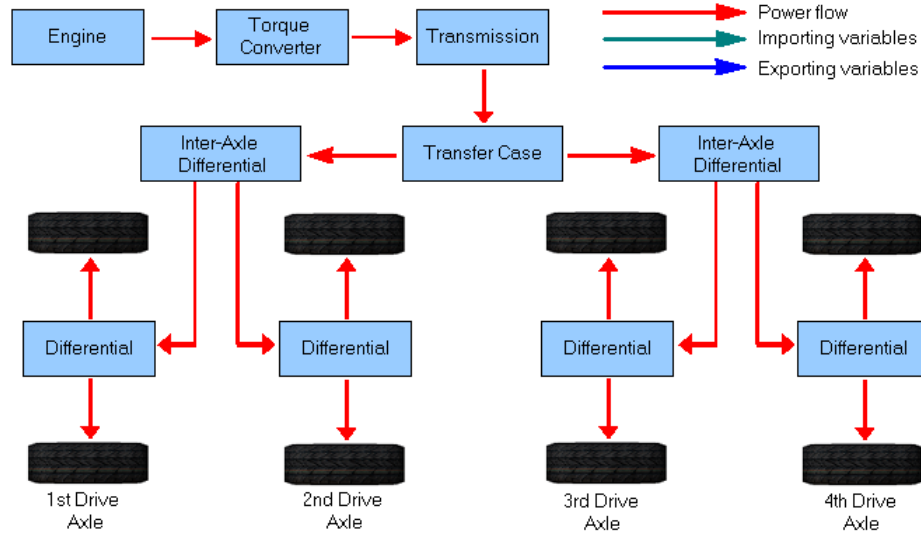
Figure 3-2 TruckSim© powertrain model

Within the TruckSim© environment the tires are modeled using lookup tables. The information was defined through modelling and validation of a Michelin 12.00R20 XML TL 149J off-road tire by Ragheb [64].

(a)   (b)
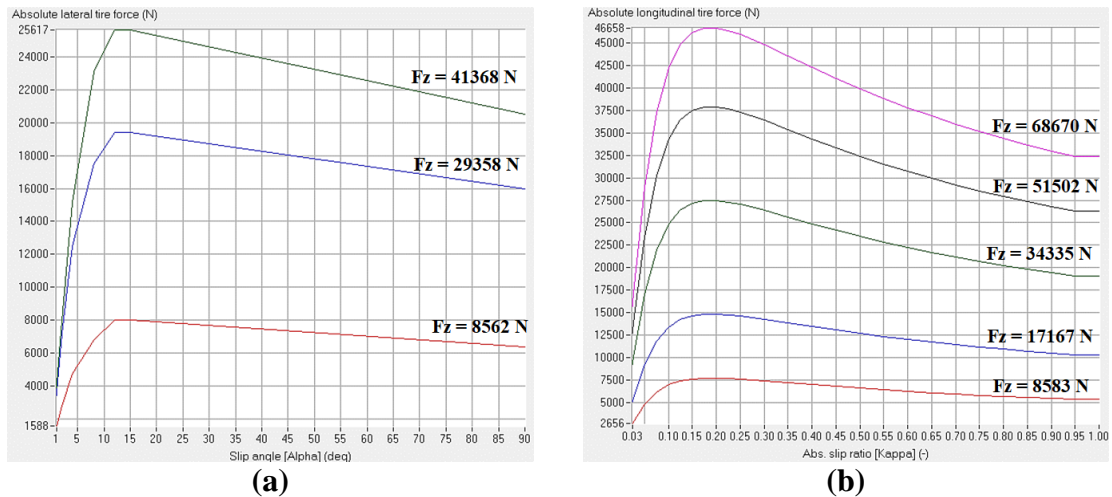
Figure 3-3 Tire characteristics lookup tables at different vertical loads: lateral tire force (a), longitudinal tire force (b)

Figure 3-3 shows the tire characteristics of the lateral tire force (a) and longitudinal tire force (b) as input into TruckSim©, additional lookup tables for the tires include the aligning moment, and camber thrust. Included are several sets of data for different vertical tire loads where the exact force is not available TruckSim© interpolates the value. The effective rolling radius, unloaded tire radius, spring rate and dynamic properties of the tire are input within TruckSim©.

33

The steering mechanism is also represented by lookup tables based on the steering rack ratio and steering wheel input. The steering lookup tables are available for the first and second axles of the vehicle within TruckSim©, however a separate set of lookup tables are used within the Simulink model for the rear axle steering, as the steering angle is determined individually from the steering input from the driver model. This vehicle model includes independent hydro-pneumatic suspension for each wheel. It is governed by a force-deflection curve.

The validated vehicle is a complex model that includes all considerations on the physical vehicle. The results from validation suggest the validated vehicle model is acceptable to predict vehicle behaviour with.

3.2.3   MATLAB and Simulink in Co-Simulation with TruckSim©

TruckSim© provides the vehicle and the maneuver with driver model which can interface with MATLAB/Simulink to provide interaction of a control system with the vehicle model. TruckSim© is implemented into Simulink as the S-function where the input and output variables are defined by the user (Figure 3-4 (b)). The outputs from TruckSim© are used as the inputs to the Simulink model at each time step. The control system process outputs the desired signals which are used in the TruckSim© S-function. All vehicle parameters, maneuver settings, and post-processing are all completed within TruckSim interface (Figure 3-4 (a)) after the Simulink calculations have been completed.
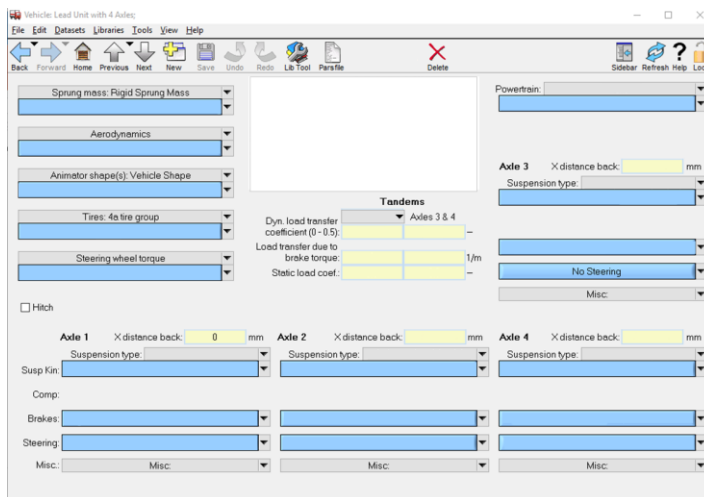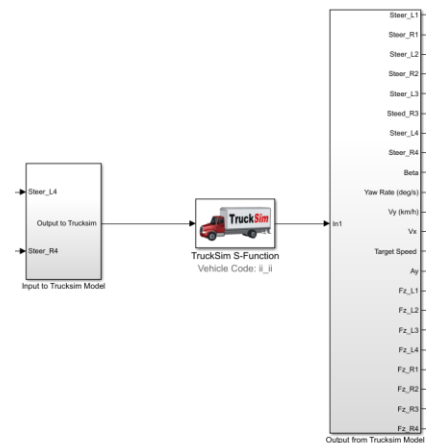
(a)   **(b)**

Figure 3-4 TruckSim© user interface (a), Simulink-TruckSim© interaction (b)

3.2.4   **Driver Model**

The driver model within TruckSim© determines the throttle and steering input. There are three options available in TruckSim©, which only open loop steering and closed loop path following are used.

Open loop steering allows the vehicle to be controlled by a time history steering wheel input. This makes the vehicle operate independent of the road which can input a specific steering input for standard tests or from measured steering inputs for validation. This is used in the FMVSS 126 ESC maneuver as well as the modified J-turn maneuver.

Closed loop path following imposes a steering function which is internally programmed within TruckSim© and is modified using a user-programmed PI controller. Using virtual sensors on the vehicle model, the lateral distance error and area error are collected, and the required corrective steering is output as the steering wheel angle. The driver preview time, lag time, low speed dynamic limit, and maximum steering wheel angle and rate are determined as a part or the maneuver. The closed loop path follower is used for maneuvers such as the slalom and double lane change.

3.3   DEVELOPMENT OF LINEAR VEHICLE MODELS

The mathematical vehicle model used to define the linearized plant for the control system is developed from the two degree-of-freedom (DOF) bicycle model as seen in Figure 3-5. The reference model is developed from the conventional vehicle with only the front two axles steering in order to reference to a familiar-driving vehicle. In the bicycle model, the tire forces from the left and right sides of the vehicle are combined into a single track; the resultant tire forces are added from both sides of the vehicle and the steering and resultant slip angles of the tires are averaged. The center of gravity is represented by the coloured circle in the center of the four wheels. The absolute distance of the axles from the center of gravity are represented as a_n for each axle, n. The forward vehicle speed, U, lateral vehicle speed, V, and yaw rate, r, act on the center of gravity. N is the external moment which can be related to any moment that is introduced separately from the steering input of the vehicle

and also acts on the center of gravity. The average axle steering angle is annotated by δ and the resultant tire slip angle is represented by α. The lateral forces produced by the tires, F_y, are directionally represented by the red arrows. The numerical subscripts note which axle, front being 1, rear being 4, δ, α and F_y represent. β is the sideslip angle of the vehicle at the center of gravity
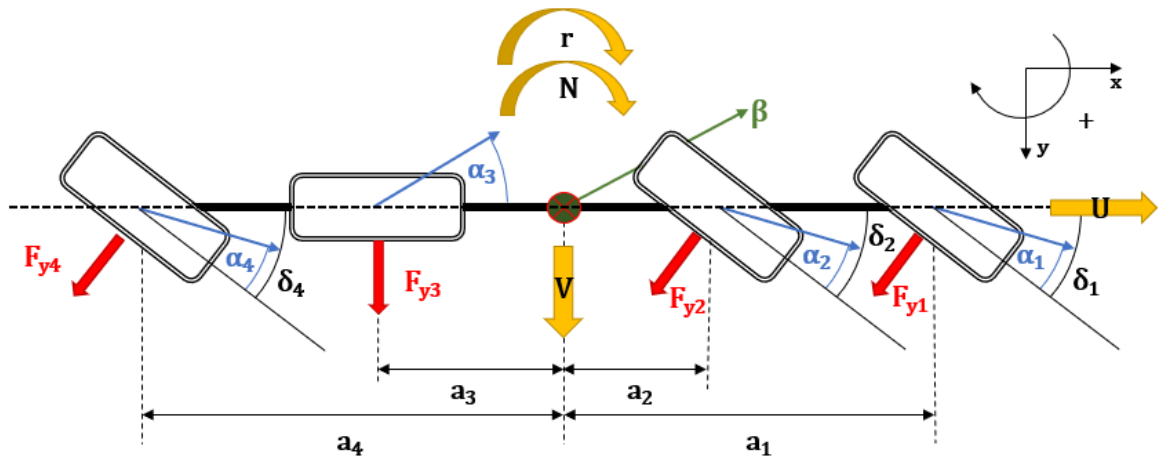
Figure 3-5 Rear Steered 8x8 Vehicle Bicycle Model

The state space equations for the vehicle are derived using the equations of motion from the bicycle model in Figure 3-5. The following assumptions will also be taken into consideration:

- Vehicle speed is constant in longitudinal and lateral directions.
- Small angle approximation is present for tire angles and slip angles.
- Tires operate within linear characteristics range. (limited to 0.4g for linear tire behaviour)
- Vehicle suspension characteristics (camber, toe and castor) are not considered.
- All external resistive forces are neglected. (aerodynamic, rolling resistance and grade)
- Lateral and longitudinal load transfers are neglected.
- Cornering stiffness of left and right sides are equal.
- Axle steer angles are average of left and right sides.

The equations of motion are:

$$\sum F_x = 0 \tag{3-1}$$

$$\sum F_y : \ m(\dot{V} + rU) = F_{y1} + F_{y2} + F_{y3} + F_{y4} \tag{3-2}$$

$$\sum M_z : \ I_{zz}\dot{r} = |a_1|F_{y1} + |a_2|F_{y2} - |a_3|F_{y3} - |a_4|F_{y4} \tag{3-3}$$

Where a_i is the distance of axle i to the center of gravity and Fy_i is the lateral force produced by axle i.

The lateral forces are calculated using the cornering stiffness of the two tires on the axle i ($C_{\alpha i}$) and the average slip angle of the tires on axle i (α_i)

$$F_y = \alpha_i C_{\alpha i} \tag{3-4}$$

Axles forward of COG: $\qquad\qquad \alpha_i = \delta_i - \left(\dfrac{V + a_i r}{U}\right)$ $\qquad$ 3-5

Axles rearward of COG: $\qquad\quad \alpha_i = \delta_i - \left(\dfrac{V - a_i r}{U}\right)$ $\qquad$ 3-6

3.3.1 Lateral Motion of Vehicle

Solving equation 3-2 by substituting in equations 3-4, 3-5, and 3-6 yields:

$$m(\dot{V} + rU) = C_{\alpha 1}\left[\delta_1 - \left(\frac{V + a_1 r}{U}\right)\right] + C_{\alpha 2}\left[\delta_2 - \left(\frac{V + a_2 r}{U}\right)\right] + C_{\alpha 3}\left[-\left(\frac{V - a_3 r}{U}\right)\right]$$
$$+ C_{\alpha 4}\left[\delta_4 - \left(\frac{V - a_4 r}{U}\right)\right] \tag{3-7}$$

$$\dot{V} = -\frac{(C_{\alpha 1} + C_{\alpha 2} + C_{\alpha 3} + C_{\alpha 4})}{mU}V + \left(-\frac{(a_1 C_{\alpha 1} + a_2 C_{\alpha 2} - a_3 C_{\alpha 3} - a_4 C_{\alpha 4})}{mU} - U\right)r$$
$$+ \left(\frac{C_{\alpha 1}\delta_1 + C_{\alpha 2}\delta_2 + C_{\alpha 4}\delta_4}{m}\right) \tag{3-8}$$

By using small angle approximation: $\dot{\beta} = \dot{V}/U \ and \ \beta = V/U$, and substituting into Equation 3-8, the system can be used in terms of sideslip angle.

$$\dot{\beta} = -\frac{(\ C_{\alpha 1} + C_{\alpha 2} + C_{\alpha 3} + C_{\alpha 4})}{mU}\beta + \left(-\frac{(a_1 C_{\alpha 1} + a_2 C_{\alpha 2} - a_3 C_{\alpha 3} - a_4 C_{\alpha 4})}{mU^2} - 1\right)r$$
$$+ \left(\frac{C_{\alpha 1}\delta_1 + C_{\alpha 2}\delta_2 + C_{\alpha 4}\delta_4}{mU}\right)$$

3-9

3.3.2   Yaw Motion of Vehicle

The yaw motion equation can be similarly derived by substituting Equations 3-4, 3-5, and 3-6 into Equation 3-3.

$$I_{zz}\dot{r} = |a_1|C_{\alpha 1}\left[\delta_1 - \left(\frac{V + x_1 r}{U}\right)\right] + |a_2|C_{\alpha 2}\left[\delta_2 - \left(\frac{V + a_2 r}{U}\right)\right]$$
$$- |a_3|C_{\alpha 3}\left[-\left(\frac{V - a_3 r}{U}\right)\right] - |a_4|C_{\alpha 4}\left[\delta_4 - \left(\frac{V - a_4 r}{U}\right)\right] + N$$

3-10

By rearranging and substituting $\beta = V/U$, the yaw motion can be described as:

$$\dot{r} = -\frac{(a_1 C_{\alpha 1} + a_2 C_{\alpha 2} - a_3 C_{\alpha 3} - a_4 C_{\alpha 4})}{I_{zz}}\beta - \frac{(a_1{}^2 C_{\alpha 1} + a_2{}^2 C_{\alpha 2} + a_3^2 C_{\alpha 3} + a_4{}^2 C_{\alpha 4})}{I_{zz}U}r$$
$$+ \frac{a_1 C_{\alpha 1}\delta_1 + a_2 C_{\alpha 2}\delta_2 - a_4 C_{\alpha 4}\delta_4 + N}{I_{zz}}$$

3-11

For this specific 8x8 vehicle x₃ and x₄ are negative, using the absolute value for all axles (a_{1-4}) yields the following equations which are used in the controller.

$$\dot{\beta} = -\frac{(C_{\alpha 1} + C_{\alpha 2} + C_{\alpha 3} + C_{\alpha 4})}{mU}\beta + \left(-\frac{(a_1 C_{\alpha 1} + a_2 C_{\alpha 2} - a_3 C_{\alpha 3} - a_4 C_{\alpha 4})}{mU^2} - 1\right)r$$
$$+ \frac{(C_{\alpha 1}\delta_1 + C_{\alpha 2}\delta_2 + C_{\alpha 4}\delta_4)}{mU}$$

3-12

$$\dot{r} = -\frac{(a_1 C_{\alpha 1} + a_2 C_{\alpha 2} + a_3 C_{\alpha 3} + a_4 C_{\alpha 4})}{I_{zz}}\beta$$
$$-\frac{(a_1{}^2 C_{\alpha 1} + a_2{}^2 C_{\alpha 2} + a_3{}^2 C_{\alpha 3} + a_4{}^2 C_{\alpha 4})}{I_{zz}U}r \qquad \textbf{3-13}$$
$$+\frac{a_1 C_{\alpha 1}\delta_1 + a_2 C_{\alpha 2}\delta_2 - a_4 C_{\alpha 4}\delta_4 + N}{I_{zz}}$$

The final vehicle model can be represented in state-space (Equations 3-14 and 3-15). The state variables of the system include the vehicle sideslip angle and yaw rate $\begin{bmatrix}\beta \\ r\end{bmatrix}$. The control variables for this system are the first and fourth steering angle, δ_1, and δ_4. It is important to note k_{12} is the ratio between the steering angles for the front axle to the second axle as they both steer with steering wheel input.

$$
\begin{bmatrix}\dot{\beta}\\ \dot{r}\end{bmatrix}
=
\begin{bmatrix}
\dfrac{-C_{\alpha 1} - C_{\alpha 2} - C_{\alpha 3} - C_{\alpha 4}}{mU} & \dfrac{-a_1 C_{\alpha 1} - a_2 C_{\alpha 2} + a_3 C_{\alpha 3} + a_4 C_{\alpha 4}}{mU^2} - 1 \\
\dfrac{-a_1 C_{\alpha 1} - a_2 C_{\alpha 2} + a_3 C_{\alpha 3} + a_4 C_{\alpha 4}}{I_{zz}} & \dfrac{-a_1{}^2 C_{\alpha 1} - a_2{}^2 C_{\alpha 2} + a_3{}^2 C_{\alpha 3} + a_4{}^2 C_{\alpha 4}}{I_{zz}U}
\end{bmatrix}
\begin{bmatrix}\beta\\ r\end{bmatrix}
$$
$$
+
\begin{bmatrix}
\dfrac{C_{\alpha 1} + k_{12}C_{\alpha 2}}{mU} & \dfrac{C_{\alpha 4}}{mU} \\
\dfrac{a_1 C_{\alpha 1} + k_{12}a_2 C_{\alpha 2}}{I_{zz}} & -\dfrac{a_4 C_{\alpha 4}}{I_{zz}}
\end{bmatrix}
\begin{bmatrix}\delta_1\\ \delta_4\end{bmatrix}
+
\begin{bmatrix}0 & 0 \\ 0 & \dfrac{1}{I_{zz}}\end{bmatrix}
\begin{bmatrix}0\\ N\end{bmatrix}
\qquad \textbf{3-14}
$$

$$y = [0 \quad 1]\begin{bmatrix}\beta\\ r\end{bmatrix} + [0 \quad 0 \quad 0]\begin{bmatrix}\delta_1\\ \delta_4\\ N\end{bmatrix} \qquad \textbf{3-15}$$

3.4 REFERENCE MODEL – LINEAR BICYCLE MODEL

To use a state feed-back controller, the error from the steady state model and actual vehicle performance states are required. The steady state yaw rate and sideslip angle are determined from the conventional vehicle bicycle model in Figure 3-6 in order to have the vehicle reference as a familiar vehicle.
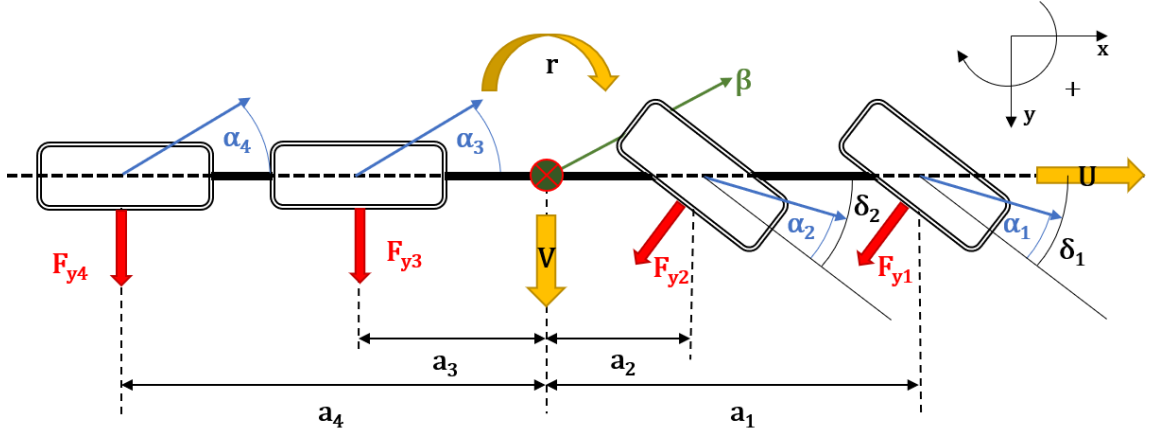
Figure 3-6 Conventional 8x8 combat vehicle bicycle model

Using the same method for determining the bicycle model for the RAS vehicle in Section 3.3, the bicycle model for the conventional fixed rear axle vehicle is as presented in Equation 3-16:

$$
\begin{bmatrix} \dot{\beta} \\ \dot{r} \end{bmatrix}
= \begin{bmatrix} \dfrac{-C_{\alpha 1} - C_{\alpha 2} - C_{\alpha 3} - C_{\alpha 4}}{mU} & \dfrac{-a_1 C_{\alpha 1} - a_2 C_{\alpha 2} + a_3 C_{\alpha 3} + a_4 C_{\alpha 4}}{mU^2} - 1 \\ \dfrac{-a_1 C_{\alpha 1} - a_2 C_{\alpha 2} + a_3 C_{\alpha 3} + a_4 C_{\alpha 4}}{I_{zz}} & \dfrac{-a_1{}^2 C_{\alpha 1} - a_2{}^2 C_{\alpha 2} + a_3{}^2 C_{\alpha 3} + a_4{}^2 C_{\alpha 4}}{I_{zz} U} \end{bmatrix} \begin{bmatrix} \beta \\ r \end{bmatrix}
$$

$$
+ \begin{bmatrix} \dfrac{C_{\alpha 1} + k_{12} C_{\alpha 2}}{mU} \\ \dfrac{a_1 C_{\alpha 1} + k_{12} a_2 C_{\alpha 2}}{I_{zz}} \end{bmatrix} [\delta_1] \qquad \textbf{3-16}
$$

The desired values for yaw rate is derived from the steady state analysis of the bicycle model as presented by Williams in [67]. A change of notation for the representation of axle distances from a_n to x_n will be included for the following equations to follow the notation followed in Williams' paper. The new representation means x_n is the axle distance **forward** from the COG, meaning x_3 and x_4 are negative. $(a_1 = x_1, a_2 = x_2, a_3 = -x_3, a_4 = -x_4)$

$$
\begin{bmatrix} \beta_{ss} \\ r_{ss} \end{bmatrix} = \dfrac{\begin{bmatrix} mU \sum_1^n x_n^2 C_n & -I(\sum_1^n x_n C_n + mu^2) \\ -mU^2 \sum_1^n x_n C_n & IU \sum_1^n C_n \end{bmatrix} \begin{bmatrix} \dfrac{C_1}{mU} & \cdots & \dfrac{C_n}{mU} \\ \dfrac{x_1 C_n}{I} & \cdots & \dfrac{x_n C_n}{I} \end{bmatrix} \begin{bmatrix} \delta_1 \\ \vdots \\ \delta_n \end{bmatrix}}{(\sum_1^n C_n)(\sum_1^n x_n^2 C_n) - (\sum_1^n x_n C_n)^2 - mu^2 \sum_1^n x_n C_n} \qquad \textbf{3-17}
$$

40

Deriving Equation 3-17 by isolating the steady state yaw rate yields:

$$\frac{r_{ss}}{\delta_1} = \frac{UC_1 \sum_1^n C_n(x_1 - x_n) + k_{12}UC_2 \sum_1^n C_n(x_2 - x_n)}{(\sum_1^n C_n)(\sum_1^n x_n^2 C_n) - (\sum_1^n x_n C_n)^2 - mU^2 \sum_1^n x_n C_n}$$

3-18

Which simplifies to:

$$\frac{r_{ss}}{\delta_1} = \frac{U(1 + k_{12})}{L_{eff} - U^2 K_{US}}$$

3-19

Where the understeer coefficient is;

$$K_{US} = \frac{m \sum_1^n x_n C_n}{C_1 \sum_1^n C_n(x_1 - x_n) + C_2 \sum_1^n C_n(x_2 - x_n)}$$

3-20

And the effective length is;

$$L_{eff} = \frac{(\sum_1^n C_n)(\sum_1^n x_n^2 C_n) - (\sum_1^n x_n C_n)^2}{C_1 \sum_1^n C_n(x_1 - x_n) + C_2 \sum_1^n C_n(x_2 - x_n)}$$

3-21

3.5 VEHICLE MODEL FOR ZERO SIDESLIP CONTROLLER

The ZSS control method is a feed-forward controller that decreases the turning radius at low speed and increases stability of the vehicle at higher speeds by steering the rear wheels opposite of the front at low speed and steering the rear wheels in the same direction as the front at higher speeds. This controller is dependent on the performance of the vehicle at steady state, which can be optimized by solving the rear steering angle to satisfy the vehicle performing with a zero-side slip angle as a function of vehicle speed.

The zero-sideslip condition can be determined using Equation 3-22 with reference to the RAS bicycle model in Figure 3-5 and solving for β_{ss} with the first axle being steered by the steering input and the second axle being related to the first axle with the parameters k_{12} and δ_4 representing the steering angle required to satisfy the zero-sideslip condition. The notation used in the denominator of Equation 3-22 is based off of the notation presented in

this thesis and does not represent the same in Williams paper [67] as was seen in the previous section.

$[\beta_{ss}]$

$$= \frac{[mU(-a_1^2 C_{\alpha 1} - a_2^2 C_{\alpha 2} + a_3^2 C_{\alpha 3} + a_4^2 C_{\alpha 4}) \quad -I((a_1 C_{\alpha 1} + a_2 C_{\alpha 2} - a_3 C_{\alpha 3} - a_4 C_{\alpha 4}) + mu^2)] \begin{bmatrix} \dfrac{C_1 + k_{12} C_2}{mU} & \dfrac{C_4}{mU} \\ \dfrac{a_1 C_1 + k_{12} a_2 C_2}{I_{zz}} & -\dfrac{a_4 C_4}{I_{zz}} \end{bmatrix} \begin{bmatrix} \delta_1 \\ \delta_4 \end{bmatrix}}{(\sum_1^n C_n)(\sum_1^n x_n^2 C_n) - (\sum_1^n x_n C_n)^2 - mu^2 \sum_1^n x_n C_n} \quad \textbf{3-22}$$

The required δ_4 to δ_1 relationship can be derived as a ratio and used as a feed-forward function by solving for $\beta_{ss} = 0$ and conducting matrix multiplication to isolate δ_4/δ_1:

$$\frac{\delta_4}{\delta_1} = \frac{\textbf{NUM}_{3\text{-}23}}{\textbf{DEN}_{3\text{-}23}}$$

$$\textbf{NUM}_{3\text{-}23} = \left\{ \left(\frac{a_1 C_{\alpha 1} + a_2 k_{12} C_{\alpha 2}}{I_{zz}} \right) \left(\frac{-a_1 C_{\alpha 1} - a_2 C_{\alpha 2} + a_3 C_{\alpha 3} + a_4 C_{\alpha 4} - U^2}{mU^2} \right) \right\}$$
$$- \left\{ \left(\frac{C_{\alpha 1} + k_{12} C_{\alpha 2}}{mU} \right) \left(\frac{-a_1^2 C_{\alpha 1} - a_2^2 C_{\alpha 2} + a_3^2 C_{\alpha 3} + a_4^2 C_{\alpha 4}}{I_{zz} U} \right) \right\} \quad \textbf{3-23}$$

$$\textbf{DEN}_{3\text{-}23} = \left\{ \left(\frac{C_{\alpha 4}}{mU} \right) \left(\frac{-a_1^2 C_{\alpha 1} - a_2^2 C_{\alpha 2} + a_3^2 C_{\alpha 3} + a_4^2 C_{\alpha 4}}{I_{zz} U} \right) \right\}$$
$$- \left\{ \left(\frac{a_4 C_{\alpha 4}}{I_{zz}} \right) \left(\frac{-a_1 C_{\alpha 1} - a_2 C_{\alpha 2} + a_3 C_{\alpha 3} + a_4 C_{\alpha 4} - U^2}{mU^2} \right) \right\}$$

And is simplified to:

$$\frac{\delta_4}{\delta_1} = \frac{\textbf{NUM}_{3\text{-}24}}{\textbf{DEN}_{3\text{-}24}}$$

$$\textbf{NUM}_{3\text{-}24} = \{(-a_1 C_{\alpha 1} - a_2 C_{\alpha 2} + a_3 C_{\alpha 3} + a_4 C_{\alpha 4})(C_{\alpha 1} + k_{12} C_{\alpha 2})\}$$
$$- \{(-a_1 C_{\alpha 1} - a_2 C_{\alpha 2} + a_3 C_{\alpha 3} + a_4 C_{\alpha 4})(a_1 C_{\alpha 1} + k_{12} a_2 C_{\alpha 2})\} \quad \textbf{3-24}$$
$$- \{mU^2(a_1 C_{\alpha 1} + k_{12} a_2 C_{\alpha 2})\}$$

$$\textbf{DEN}_{3\text{-}24} = \{(-a_1^2 C_{\alpha 1} - a_2^2 C_{\alpha 2} + a_3^2 C_{\alpha 3} + a_4^2 C_{\alpha 4})(C_{\alpha 4})\}$$
$$- \{(-a_1 C_{\alpha 1} - a_2 C_{\alpha 2} + a_3 C_{\alpha 3} + a_4 C_{\alpha 4})(a_4 C_{\alpha 4})\} - \{mU^2(a_4 C_{\alpha 4})\}$$

By plotting Equation 3-24 with vehicle speed, U, as the variable, the resultant ZSS ratio function is:
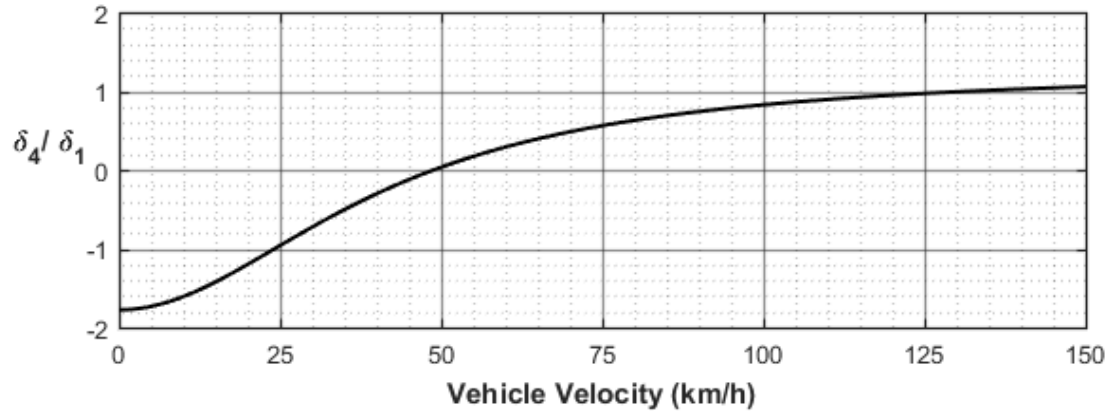
Figure 3-7 ZSS rear axle steering ratio as a function of vehicle forward speed

It is interesting to note in Figure 3-7 that the δ_4/δ_1 steering ratio reaches a ratio that is less than 1 at low speeds which indicated the rear axle is steered more than the front axle. This is due to the third axle being static and the fourth axle having to increase lateral force to satisfy a zero side-slip condition.

Multiplying this ratio by the front steer angle results in the steering angle for the rear axle.

$$\delta_4 = \frac{\delta_4}{\delta_1} \cdot \delta_1$$

3-25

3.6   SUMMARY OF CHAPTER

This chapter presented three separate vehicle models.

The 8x8 combat vehicle modelled in TruckSim© has been validated previously by Ragheb [64]. The vehicle includes 26 degrees of freedom to accurately model the vehicle motion and tire interaction with the ground. The vehicle includes the manufacturer powertrain data, hydropneumatics suspension, manufacturer tire data, and steering ratios for the two front axles. The unaltered TruckSim© model will provide the base test data and the control systems for the rear axle steering will be applied directly to this TruckSim© model in co-simulation with MATLAB/Simulink.

The second vehicle model developed in this chapter is the linear bicycle model required for the LQR controller synthesis. This model includes the rear axle steering. The external yaw moment was originally included to represent the rear axle steering, however, it was not needed and remains in the model for future use. The rear axle steering vehicle has been represented in state space in Equations 3-14 and 3-15 to satisfy the requirements for the LQR control input and output. The linear bicycle model for the conventional vehicle was developed as the reference model to provide the reference signal needed by the LQR controller. The conventional vehicle does not include the rear axle steering or the external yaw moment.

The third vehicle model presented in this chapter is the model required for the zero-sideslip controller. This controller uses a feed-forward signal to limit the slip of the tires during a turning maneuver. It is based on the steady state bicycle model that includes the rear axle steering. The steady state model is solved for a sideslip angle of zero resulting in a ratio from the rear axle to front axle steering angle with vehicle speed as the variable as presented in Equation 3-24. This controller is designed to reduce the turning radius at low speed and increase stability at high speeds.

CHAPTER 4
CONTROL SYSTEM DEVELOPMENT

4.1 INTRODUCTION

This chapter includes the development of the control systems within the MATLAB/Simulink software to be simulated within TruckSim©. The only output that can be controlled is the steering of the rear axle, which limits the effectiveness of the controller. However, the state equations have been modeled so that other outputs such as differential braking or torque vectoring can be implemented using an external torque.

The control system discussed in this chapter is the LQR optimal control system. The general form of the LQR control system is represented in Figure 4-1, where the feedback control gain is calculated separately from the normal control system.
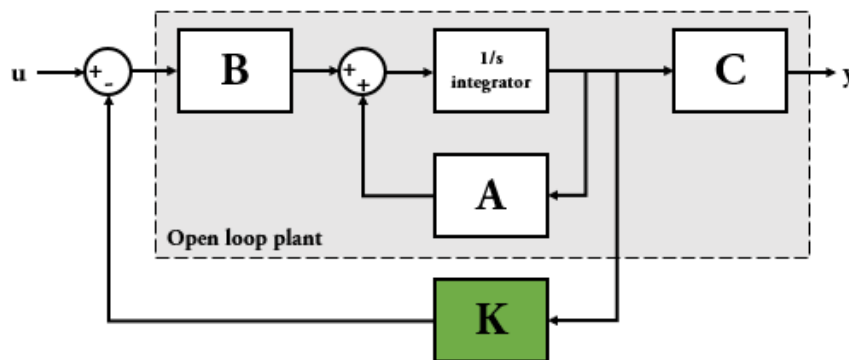

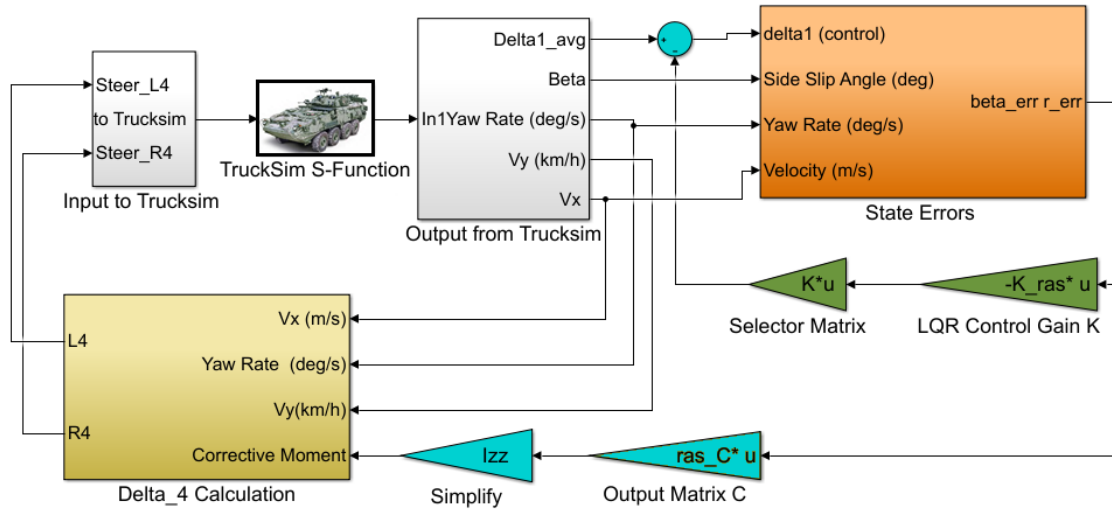**Figure 4-1 LQR Control Gain in open loop plant**

Figure 4-2 TruckSim / Simulink Software-in-the-Loop

The main components of the control system are the active yaw controller (orange block and green LQR feedback gains in Figure 4-2) and rear wheel steering controller (yellow block in Figure 4-2). The interaction between these controllers are illustrated in Figure 4-2.

TruckSim© provides the driver model and vehicle operation data as inputs to the control systems. The controllers within Simulink process the data and return a signal back to the TruckSim© environment to control the rear axle steering.

4.2 ACTIVE YAW CONTROLLER

The active yaw controller is modelled using the linear quadratic regulator. The control gains are developed within MATLAB and are input into the Simulink Model as the feed-back control gain.

The inputs required from TruckSim© for the active yaw controller are the vehicle speed and the steering input at the front axle. Within the orange block in Figure 4-2, state errors for the sideslip angle and yaw rate are calculated using the equations developed in Section 3.4 and are compared to actual vehicle states. The error signal is output and multiplied by the output matrix C to select the yaw rate error to be processed by the rear wheel steering controller. The state error signal is also processed through the closed-loop portion of the controller which applies the LQR control gain and selects the front steering angle as the feed-back signal.

46
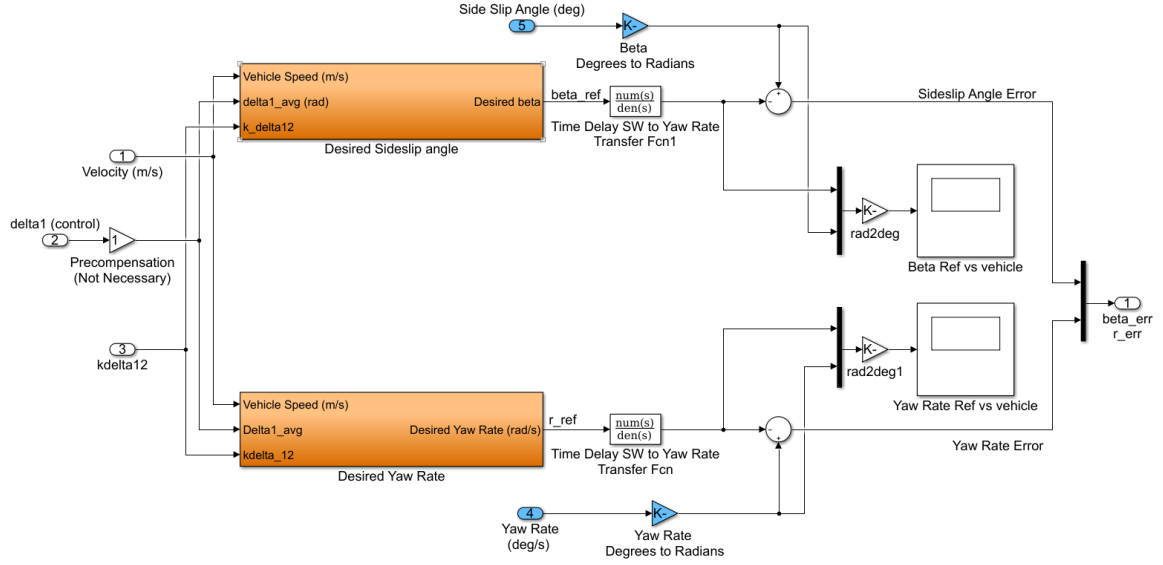
Figure 4-3 State Error Calculation in Simulink

The desired state signals are the linear two DOF model's steady state yaw and sideslip angle response in conjunction with a first order time delay. The first order time delay allows control over the vehicles state response time through the time delay, τ_{state}. The time delay is set to 0.3 seconds. The state error calculation is used within Figure 4-2 to determine the LQR feedback signal as well as the output yaw moment error.

4.2.1 LQR Control Gain

The control theory used for the active yaw controller has been influenced by multiple sources [68-70], all which use the vehicle sideslip angle and yaw rate as the controlled state variables. These sources use the LQR controller to control individual wheel torques of an electric powertrain to satisfy the required yaw moment. This controller uses the actuation of the rear axle to control the yaw moment.

To easily discuss this section, the state space model derived earlier will be represented in general form:

$$
\begin{aligned}
\dot{x} &= [A]x + [B]u \\
y &= [C]x + [D]u
\end{aligned}
$$

4-1

In this case the x is the state variable vector and includes the sideslip angle and yaw rate $[\beta, r]$. The input variable is represented by u and includes the inputs to the system. In this case u consists of the steering angles of the first and rear axles as well as the external yaw moment $[\delta_1, \delta_4, N]$. The state matrix [A] represents the 8x8 RAS vehicle as a whole, input matrix [B] applies the inputs to the mathematical system, the output matrix [C] controls the output for the control system and the feedthrough matrix [D] would be used for a feedthrough matrix, however is not used in this controller.

The LQR control system represented is presented in Figure 4-1 can be summarized into two parts: the open-loop plant enclosed in grey, and the LQR gain, K. In Simulink, the open-loop portion includes function blocks which calculate the steady state vehicle sideslip and yaw rate as well as their respective errors in order to determine the state variable vector, x. The feed-back signal, u, can be represented as Equation 4-2.

$$u = -Kx = -[K]\begin{bmatrix} \beta - \beta_{ss} \\ r - r_{ss} \end{bmatrix}$$
4-2

The LQR control gain K is calculated by minimizing the cost function, or performance index, J.

$$J = \int (x^T[Q]x + u^T[R]u)dt$$
4-3

In the cost function, J, [Q] is the state variable weighting matrix and [R] is the output variable weighting matrix. [Q] and [R] are positive symmetric square matrices with the dimensions of how many state variables there are in the system.

The control gain matrix [K] is generated within a black-box function in MATLAB that uses the [A] [B] [Q] and [R] matrices to generate the cost function J and optimize the feed-back gain based on minimizing the cost [71, 72].

4.2.2 Performance Index Tuning

The LQR controller is tuned using these matrices, with manual tuning regularly starting with an identity matrix. Previous works [71, 73, 74] have used a method defined as Bryson's rule [75] which defines the [Q] and [R] matrices based on the maximum desired values of the state variables and output control variables as represented by Equation 4-4:

$$Q = \begin{bmatrix} \dfrac{1}{x_{1max}^2} & 0 \\ 0 & \dfrac{1}{x_{2max}^2} \end{bmatrix} \quad R = \begin{bmatrix} \dfrac{1}{y_{1max}^2} & 0 \\ 0 & \dfrac{1}{y_{2max}^2} \end{bmatrix} \tag{4-4}$$

where x_i is the state variable and y_i is the output control variable. Using the state variables and output control variables defined in this work, the weighting matrices are defined as:

$$Q = \begin{bmatrix} \dfrac{1}{\beta_{max}^2} & 0 \\ 0 & \dfrac{1}{r_{max}^2} \end{bmatrix} \quad R = \begin{bmatrix} 1 & 0 \\ 0 & \dfrac{1}{N_{max}^2} \end{bmatrix} \tag{4-5}$$

The maximum for the sideslip angle and yaw rate are determined using methods in [20] where:

$$\beta_{max} = tan^{-1}(0.02\mu g) \quad r_{max} = (safety\ factor)\,\frac{\mu g}{U}$$
$$N_{max} = a_4(F_{y_{max}}) \tag{4-6}$$

In this thesis, to calculate the β_{max}, the surface friction coefficient, μ, was set to 0.3. This results in a β_{max} of 3 degrees as a value to minimize the drifting motion of the vehicle. The maximum output moment, N_{max}, is valued as the distance from the center of gravity to the rear steered axle multiplied by the peak lateral force of the tire at normal load distribution. This was calculated through interpolation of the tire model and the nominal vertical force over the rear axle.

4.2.3 Rear Wheel Steering Controller

The active yaw controller outputs the yaw rate error which is interpreted as the moment error by multiplying by the moment of inertia. This is shown as the yellow block in Figure 4-2. To satisfy the required moment for stabilization, the required moment signal is divided by the distance from the COG to the rear axle to calculate the required lateral force from the rear tires.

$$F_y = \frac{M_z}{a_4} \qquad \textbf{4-7}$$

Where the calculated lateral force of the fourth axle tire is:

$$F_y = C_{\alpha 4}\left[\delta_4 - \left(\frac{V - a_4 r}{U}\right)\right] \qquad \textbf{4-8}$$

By rearranging 4-8 and substituting in 4-7 the corrective steering angle becomes:

$$\delta_{4,corrective} = \frac{M_z}{a_4 C_4} + \left(\frac{V - a_4 r}{U}\right) \qquad \textbf{4-9}$$

4.3 SUMMARY OF CHAPTER

In this chapter the design of the active yaw controller using the rear axle steering was completed. The active yaw controller uses a linear quadratic regulator optimal controller to complete the closed loop system. The LQR controller design was completed referencing the two DOF vehicle models developed in Chapter 3. Proper design of the feed-back gain was discussed to complete the closed-loop system using proper tuning of the performance index and weighting functions. The output steering signal was determined using the lateral force of the rear tire on a turning vehicle and the required moment to satisfy the yaw rate error.

CHAPTER 5
ACTIVE REAR AXLE STEERING RESULTS AND DISCUSSION

5.1 CHAPTER INTRODUCTION

To evaluate the performance of the developed controllers, several standard test maneuvers have been simulated using TruckSim© and the full vehicle model. These results will be presented in this chapter. The two controllers for the rear axle steering to be tested are the ZSS feed-forward controller and the LQR optimal controller. These two controllers will be compared to the conventional fixed rear axle vehicle. The methods for analyzing the controllers is presented below.

1. The LQR controlled vehicle is evaluated at all speeds, despite low speed simulations suggesting the LQR controller is not suitable to improve maneuverability. This will help determine a speed which the LQR should be active.

2. The ZSS controller is evaluated for low speed performance as well as high speed performance. It is compared against the conventional vehicle as well as the LQR controlled vehicles at high speeds to determine if the feed-forward controller provides a reliable, simple solution to stability at high speeds.

The vehicle performance will be analyzed in terms of vehicle stability as well as maneuverability, where it is desired to have a maneuverable vehicle during low speed tests and increased stability during high speed tests. The steering input will be analyzed based on driver input where less driver input is more desirable.

To test the controllers, standard tests used in the industry for evaluating the performance of heavy vehicles will be selected. To compare the effectiveness of each controller for low speed maneuverability and high-speed stability, the test speeds have been selected accordingly. The different vehicle controller configurations will be tested over an high friction surface ($\mu=0.85$) and low friction surface ($\mu=0.35$) to test the robustness over different road friction surfaces. The validated vehicle model of the conventional vehicle,

described in Section 3.2, will serve as the baseline vehicle model. This vehicle does not have any control systems applied and the rear two axles are fixed. The LQR and ZSS will both be simulated in all test conditions to determine the most effective conditions for each controller. The LQR and ZSS controllers control only the rear axle of the vehicle.

For ease of discussion, the acronyms in Table 5-1 will be used throughout the remainder of the thesis.

Table 5-1 List of Vehicle Controller Acronyms

Vehicle Description	Acronym
Conventional vehicle, no control. -Fixed Rear Axle	FRA
Zero Sideslip – Feed-forward control	ZSS
Linear Quadratic Regulator – Feed-back control	LQR

To determine the maneuverability of the controlled vehicles compared to the conventional vehicle, several standard tests will be simulated including a constant step slalom with 15-meter cone spacing, J-turn maneuver and 100-ft radius constant acceleration. Generally, to increase the maneuverability of a vehicle, the controller is expected to steer the rear axle opposite to the front axle in order to generate a higher yaw rate. The high-speed stability will be compared using the FMVSS 126 ESC steering input as well as the NATO double lane change maneuver. The FMVSS 126 will be assessed not only for stability, but as well as the lateral displacement. To increase the lateral stability at high speeds it is expected the controller will steer the rear axle steering in the same direction as the front axle.

Table 5-2 outlines the simulations conducted for evaluating the vehicle performance.

Table 5-2 Simulation Events for Performance Evaluation

Simulation Event		Speed	Surface Friction
5.2Low Speed Maneuverability			
5.2.1.1	Constant Step Slalom (15-m cone spacing)	20 km/h	μ =0.85
5.2.1.2		Maximum	μ = 0.85
5.2.1.3			μ = 0.35
5.3Low-Medium Speed Transition			
5.3.1.1	Modified J-Turn Maneuver	40 km/h	μ = 0.85
5.3.1.2			μ = 0.35
5.3.2	Constant radius acceleration	Constant Acceleration 6 km/h per second	μ = 0.85
5.4High Speed Stability Testing			
5.4.1.3	FMVSS 126 ESC	60 km/h	μ = 0.35
5.4.1.1			μ = 0.85
5.4.1.4		80 km/h	μ = 0.35
5.4.1.2			μ = 0.85
5.4.2.1	Double Lane Change (NATO AVTP-1 03-30)	80 km/h	μ = 0.85
5.4.2.2		60 km/h	μ = 0.85

5.2 LOW SPEED MANEUVERABILITY

5.2.1 Constant step slalom (15-meter cone spacing)

The vehicle's transient response can be measured at low speed using a constant step slalom maneuver. One of the objectives is to measure the maneuverability of the rear axle steered vehicle compared to the conventional vehicle. The path used is described in Figure 5-1 where d_2 is 15m and the lateral offset, d_3, is 5m. This maneuver is performed at 20 km/h and near-maximum controllable speed to analyze the transient response of the vehicle with the different RAS steering ratios.
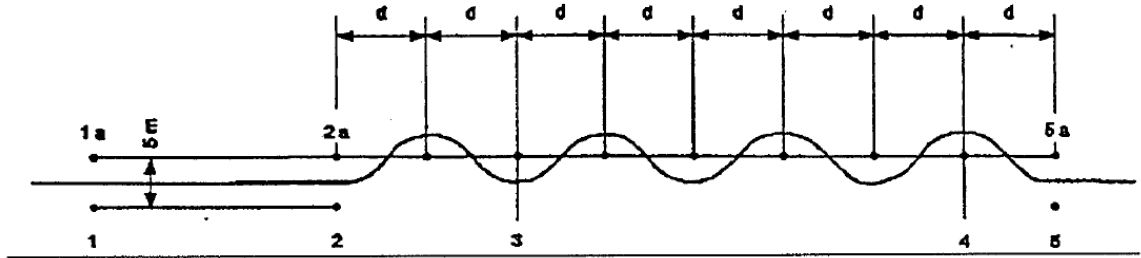
Figure 5-1: Constant step slalom test course [76]

5.2.1.1 20 km/h – μ=0.85

The first simulation will analyze each vehicle on the constant step slalom course at a speed of 20 km/h over a surface friction of μ=0.85. Every vehicle configuration successfully passes the test without interfering with a cone or losing control. Figure 5-2 illustrates each vehicle follows a similar path.
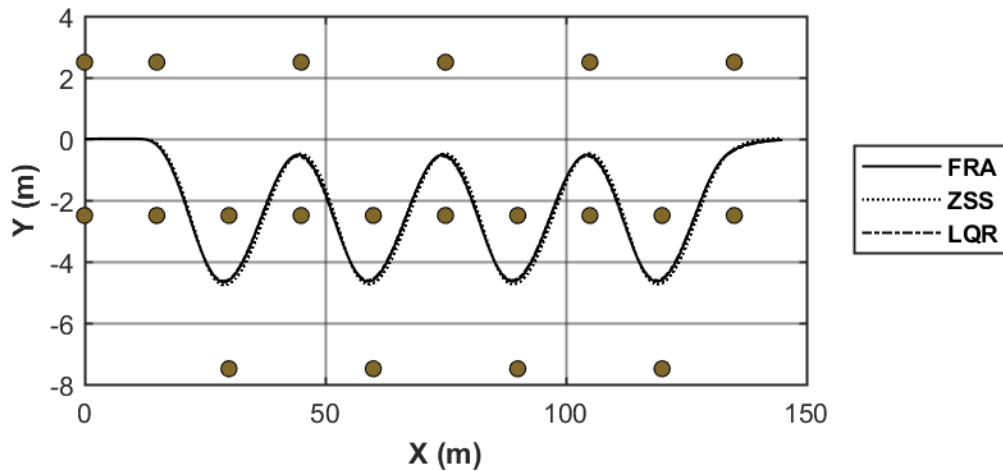

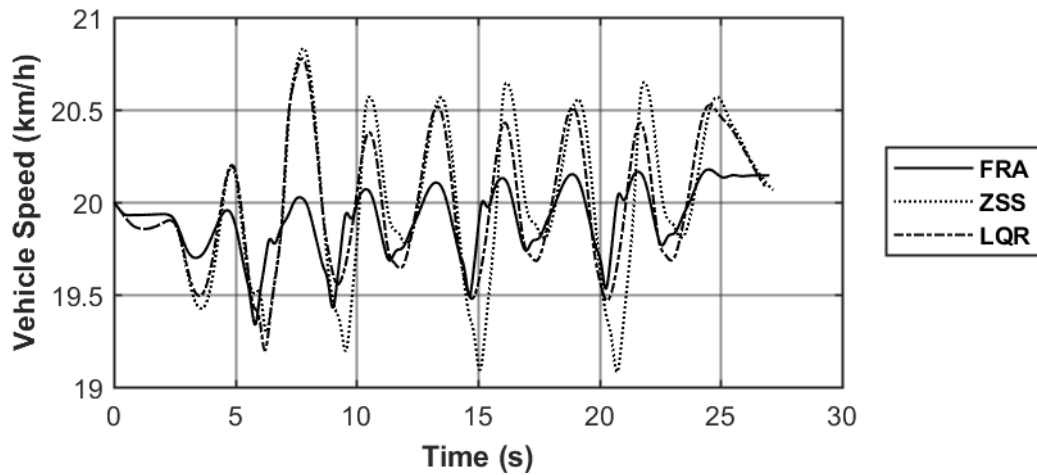**Figure 5-2 Vehicle Trajectory: 15m slalom at 20 km/h over μ=0.85**

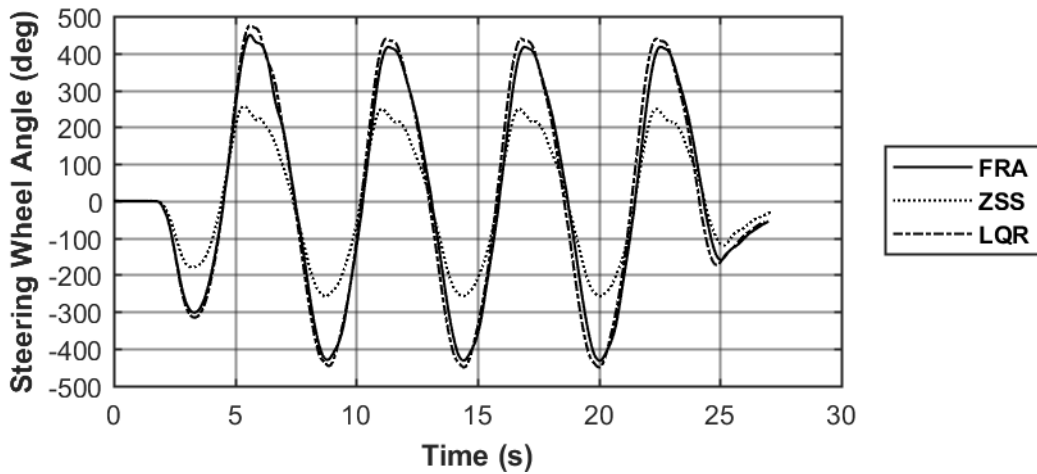**Figure 5-3 Vehicle Speed: 15m slalom at 20 km/h over μ=0.85**

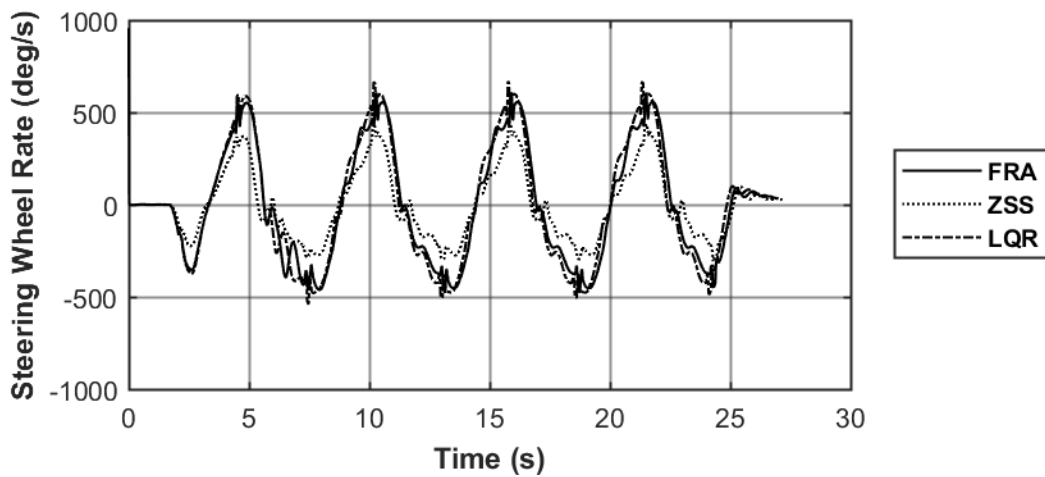**Figure 5-4 Steering Wheel Angle: 15m slalom at 20 km/h over μ=0.85**

Figure 5-5 Steering Wheel Rate: 15m slalom at 20 km/h over μ=0.85

To successfully complete the maneuver, each vehicle required different steering inputs as seen in Figure 5-4. The lowest steering input is seen in the ZSS controlled vehicle. This is also demonstrated in Figure 5-5 by the low amplitude of steering wheel rate required to maneuver the ZSS vehicle. The lower steering wheel input and steering wheel rate represent an easier vehicle to maneuver. During the simulation, the conventional vehicle remained at the most constant speed compared to the other vehicles, as seen in Figure 5-3, however the fluctuation of the speed seen in the ZSS and LQR vehicles is not a concern and would most likely not be noticed by the driver and would not have a major impact on the performance.
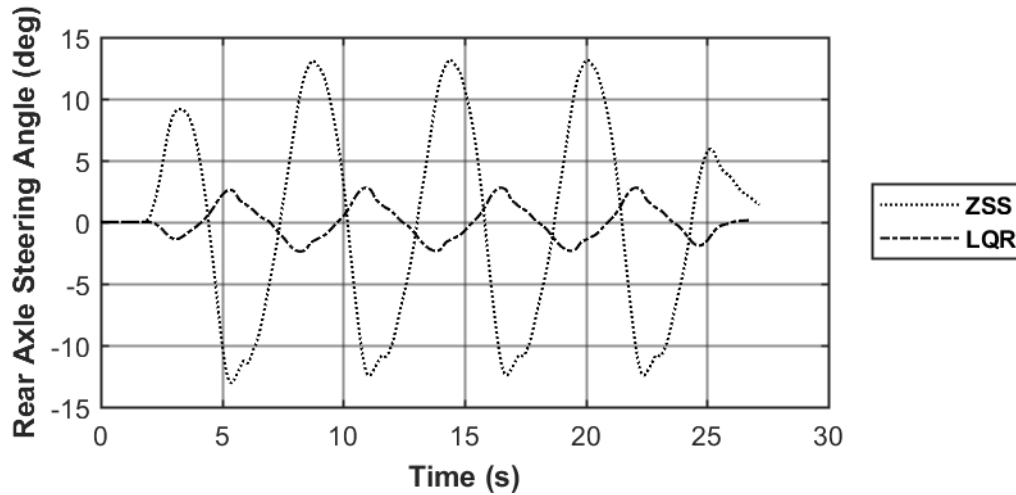

Figure 5-6 Rear Axle Steering Angle: 15m slalom at 20 km/h over μ=0.85

The lower steering effort seen in the ZSS vehicle is attributed to the contra-steer of the rear axle, which due to the low target speed of 20 km/h is a significant steering angle peaking at around 13 degrees (Figure 5-6). The LQR controller steers the rear axle opposite of the ZSS controller, which indicates the LQR controller is not suitable for increasing maneuverability of the vehicle. As seen in Figure 5-7 (b) the LQR controller steers the rear axle to the center of the turn, which decreases the maneuverability in tight spaces. The ZSS controller in Figure 5-7 (a) shows how steering the rear axle opposite of the front axles (contra-steer) results in better ability to navigate the course. Since the ability to change heading angle is increased with the ZSS, the vehicle is in better position for the next cone. The better maneuverability is also demonstrated by the abilty of the rear axle to follow the front axle when steered around an obstacle.
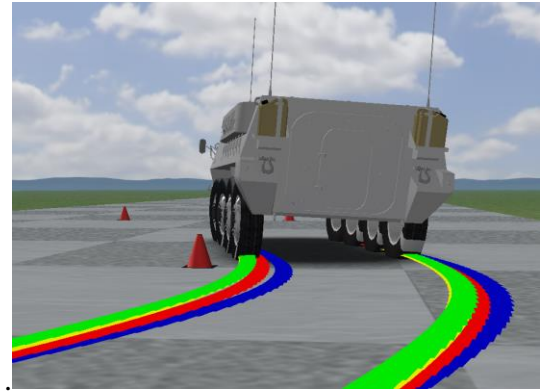
(a)   **(b)**

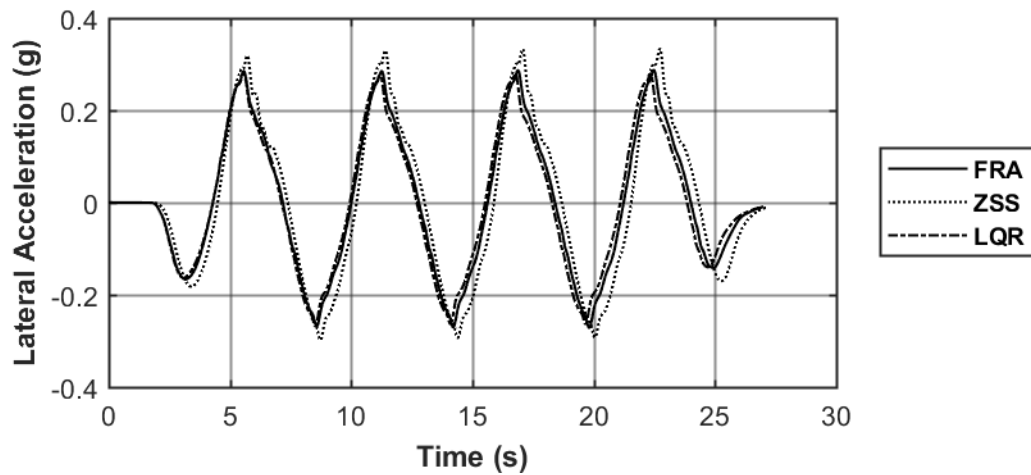**Figure 5-7 Vehicle behaviour during 15-m slalom ZSS vehicle (a) compared to LQR (b)**

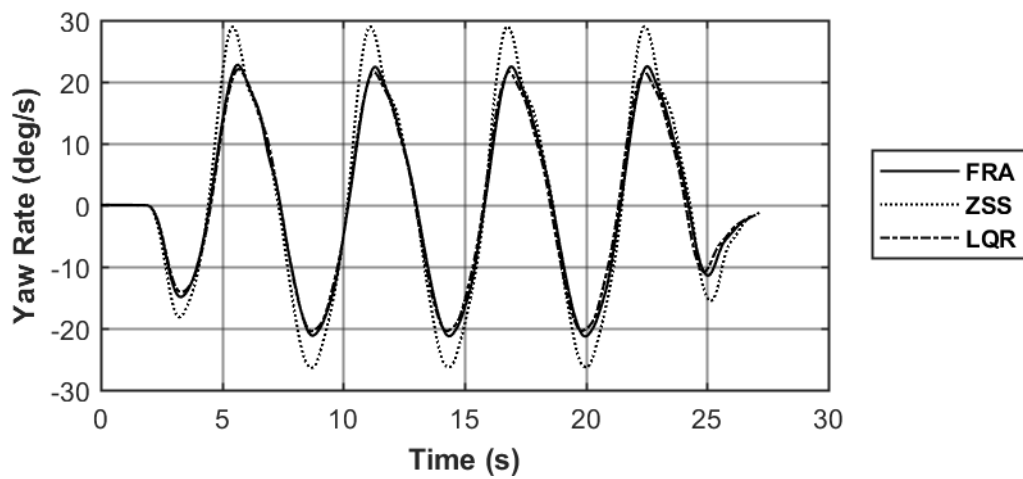**Figure 5-8 Lateral Acceleration: 15m slalom at 20 km/h over μ=0.85**

Figure 5-9 Yaw Rate: 15m slalom at 20 km/h over μ=0.85

The lateral acceleration results (Figure 5-8) and yaw rate results (Figure 5-9) indicate the previous statements are valid by demonstrating that the ZSS controller increases the lateral acceleration slightly and increases the yaw rate significantly. These plots also show the controller increases the yaw rate acceleration and rate of lateral acceleration which proves improved maneuverability. The peak lateral accelerations of the ZSS vehicle are not excessively large compared to the conventional vehicle and should not be interpreted as a decrease in performance at this speed. During a dynamic maneuver, this vehicle appears to be stable in this range of lateral accelerations. The LQR controller does not seem to change the resulting lateral acceleration and yaw rate, most likely due to the low speed and little performance difference from the reference model.
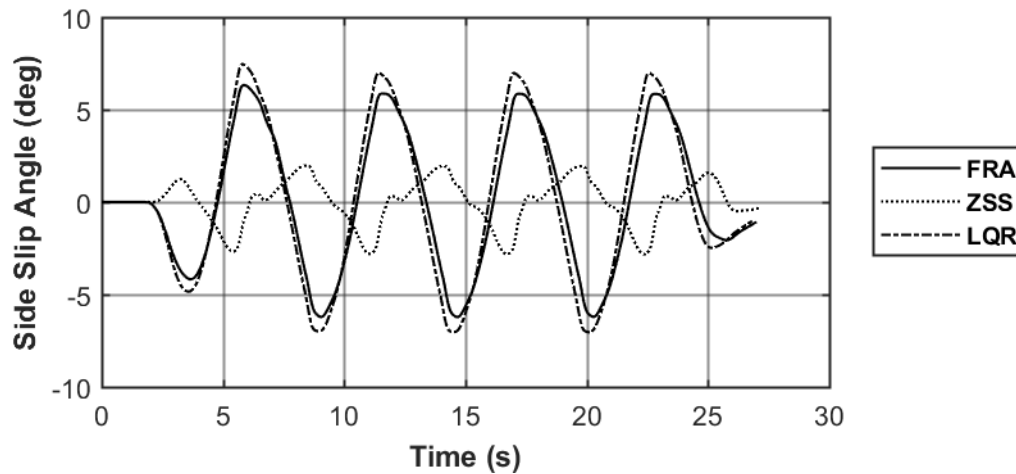

Figure 5-10 Side Slip Angle: 15m slalom at 20 km/h over μ=0.85

The sideslip angle of the ZSS vehicle is decreased and opposite of the conventional vehicle, shown in Figure 5-10. At 20 km/h, the ZSS controller minimizes the side slip angle of the vehicle which satisfies the design principle of the controller. Since this is not a steady state maneuver, which the ZSS was designed for, a minimized side slip angle is interpreted as successful implementation of the controller. Assuming the conventional vehicle is inherently understeer, opposite sideslip angle to this implies the ZSS vehicle has oversteer behaviour.

At low speeds the ZSS controller does not consider the stability of the vehicle as it is a feed-forward controller designed to reduce the sideslip of the vehicle and decrease the turning radius. At low speeds the stability of the vehicle is not an issue, considering it is

much easier for a driver to recover and there is less lateral acceleration due to the lower speed.

The LQR controlled vehicle uses the conventional vehicle at steady state as the reference model. The result is the LQR is inducing understeer by steering the rear axle in the same direction as the front axles (Figure 5-6), which suggests the vehicle is inducing understeer to provide less drift motion.

5.2.1.2   Maximum speed – µ=0.85

The maximum target speed for the ZSS and the conventional vehicle is 32 km/h while the LQR vehicle achieves 31 km/h as seen in Figure 5-12. In Figure 5-11, it is evident that the FRA and the LQR vehicle complete the maneuver, while the ZSS controlled vehicle ends up in a permanent oversteer loop on the last set of cones. This is caused by the corrections required to fix the oversteer produced by the rear axle steered opposite of the front wheels.
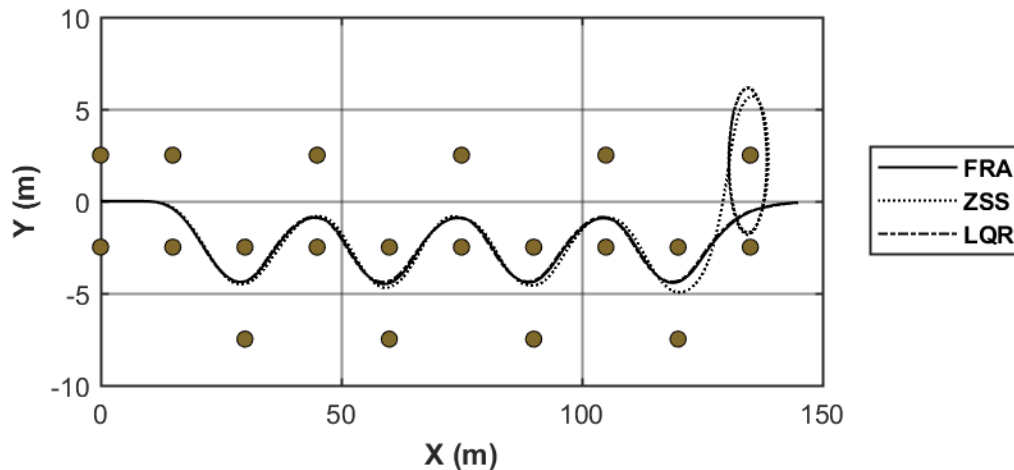

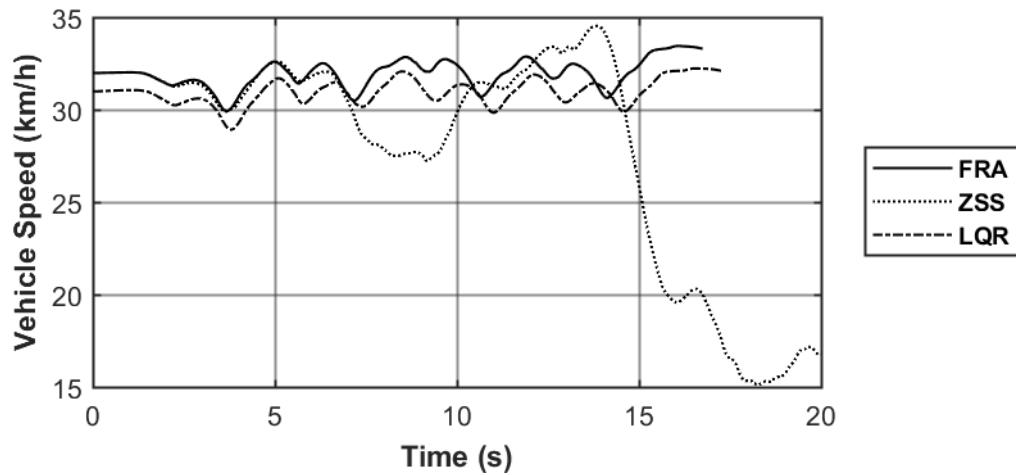**Figure 5-11 Vehicle Trajectory: 15m slalom at max speed over µ=0.85**

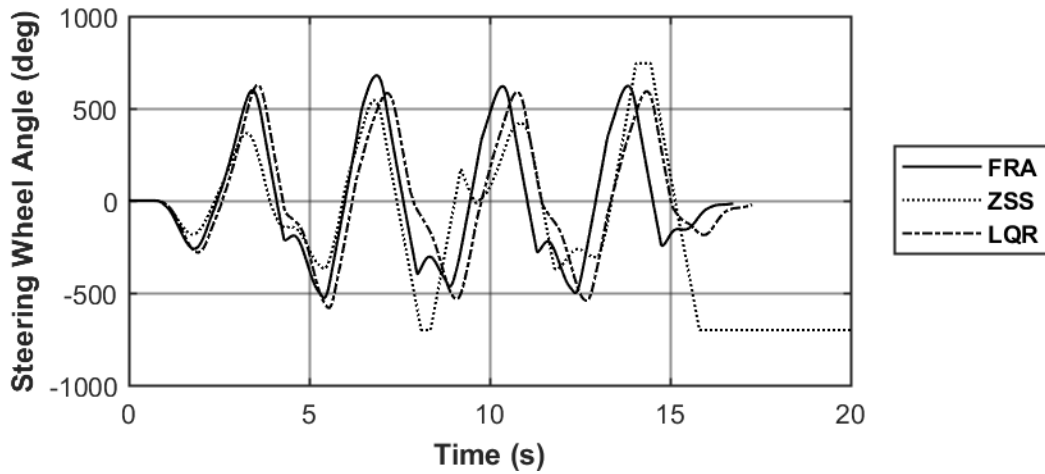**Figure 5-12 Vehicle Speed: 15m slalom at max speed over μ=0.85**

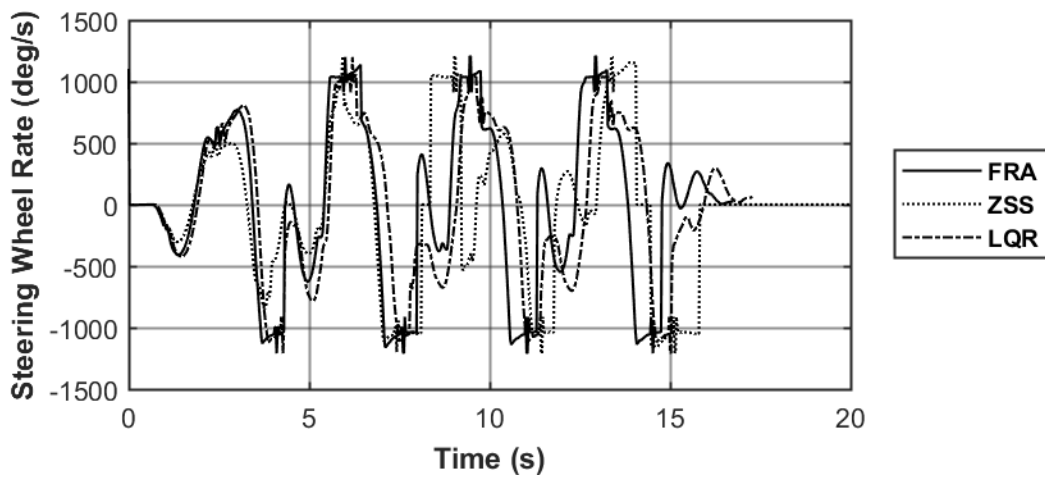**Figure 5-13 Steering Wheel Angle: 15m slalom at max speed over μ=0.85**

Figure 5-14 Steering Wheel Rate: 15m slalom at max speed over μ=0.85

The required steering inputs for all of these vehicles are extremely high, but reasonable. The ZSS requires the full range of the steering wheel in order to correct the oversteer produced by the ZSS controller (Figure 5-13). Peak steering wheel rates are all similar over the whole maneuver (Figure 5-14) with a peak of around 1200 deg/s. In a 2005 study by the NHTSA, Forkenbrock et al. [77] indicate the maximum steering rate achievable by humans is 1819 deg/s over a maximum one second duration. This test was also performed using an SUV, which theoretically does not require as much steering torque as a combat vehicle with the two front axles steered. If following the conclusions from [77], the steering requirements during this test are acceptable. However, through professional advice, which cannot be properly cited, the maximum steering wheel rate for heavy trucks is 540 deg/s, which is much lower than all vehicles during this test maneuver. This suggests the maximum attainable speeds for these vehicles would be much lower in order to have significant steering input.
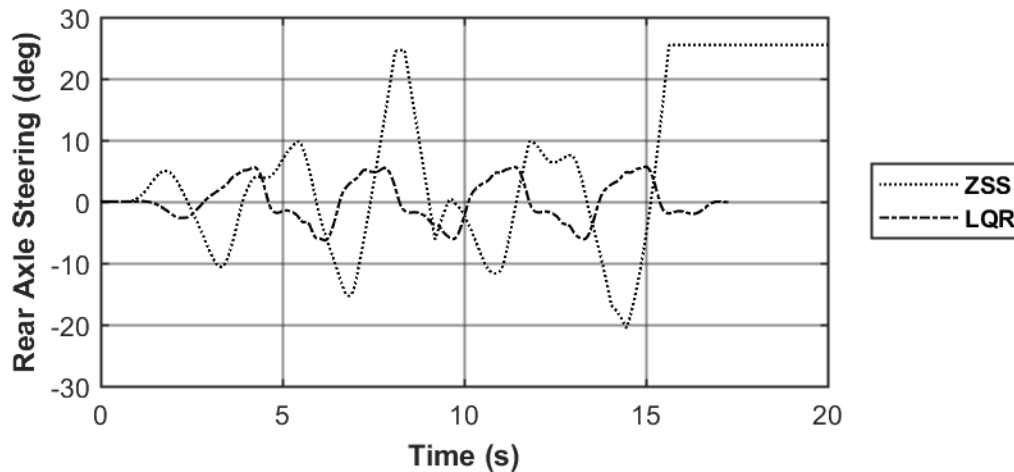

Figure 5-15 Rear Axle Steering Angle: 15m slalom at max speed over μ=0.85

The rear axle of the ZSS vehicle reaches saturation several times during the maneuver as seen in Figure 5-15. The LQR rear axle, for the majority of the maneuver, steers in the same direction of the front axles, which is opposite of the ZSS rear axle. This oversteering of the ZSS vehicle as shown in Figure 5-16 is a result of the responsiveness of the controller. Since the rear axle is directly related to the steering of the front axle, oversteering becomes a significant problem with repetitive full side to side steering input.
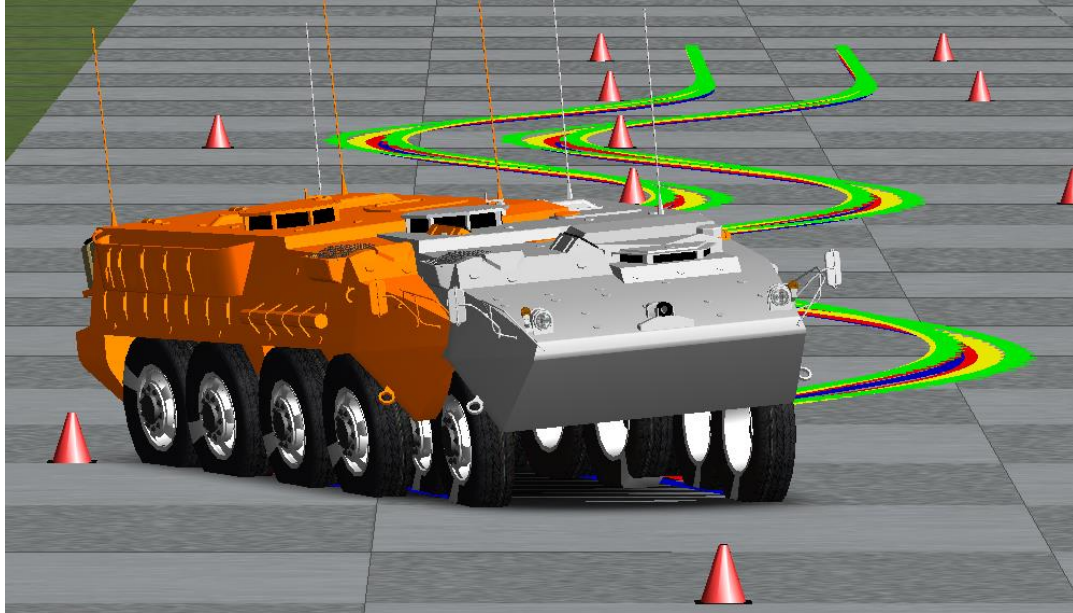
61

Figure 5-16 Result of oversteering for ZSS vehicle (orange) compared to LQR (grey) understeering behaviour
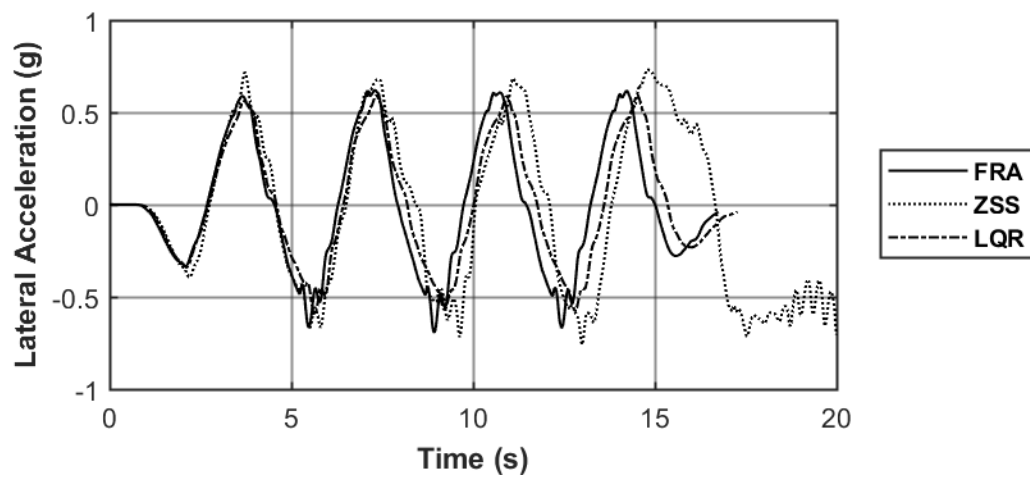

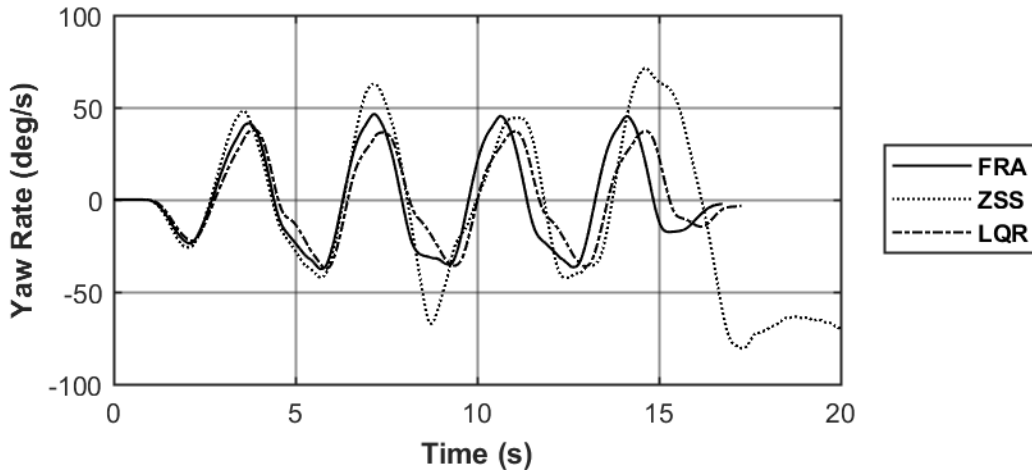**Figure 5-17 Lateral Acceleration: 15m slalom at max speed over μ=0.85**

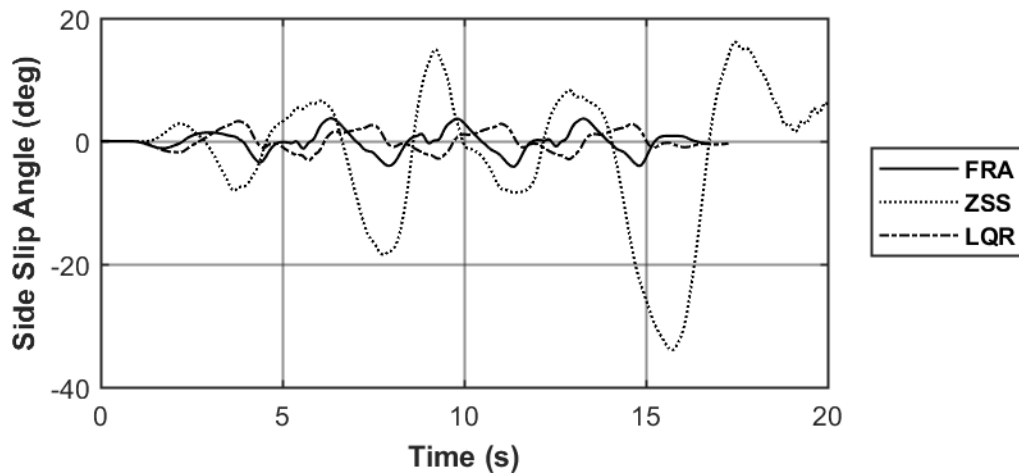**Figure 5-18 Yaw Rate: 15m slalom at max speed over µ=0.85**

Figure 5-19 Side Slip Angle: 15m slalom at max speed over µ=0.85

The performance of the conventional FRA vehicle is most desirable at this speed over high surface friction based on the speed, lateral acceleration, yaw rate, and sideslip measures. The peak lateral accelerations of the ZSS vehicle are the highest at around 0.7 g's (Figure 5-17). The yaw rate (Figure 5-18) and sideslip angle (Figure 5-19) of the ZSS vehicle represent a vehicle that is losing control with a sequential tight turning demand. The LQR vehicle results in a lower yaw rate than both the ZSS and conventional vehicle. This is provided by the steering of the rear axle. At a speed of 32 km/h the ZSS steering input provides extra yaw rate required for increased maneuverability, but the repeated demand results in an oversteering condition after the saturation of the steering system.
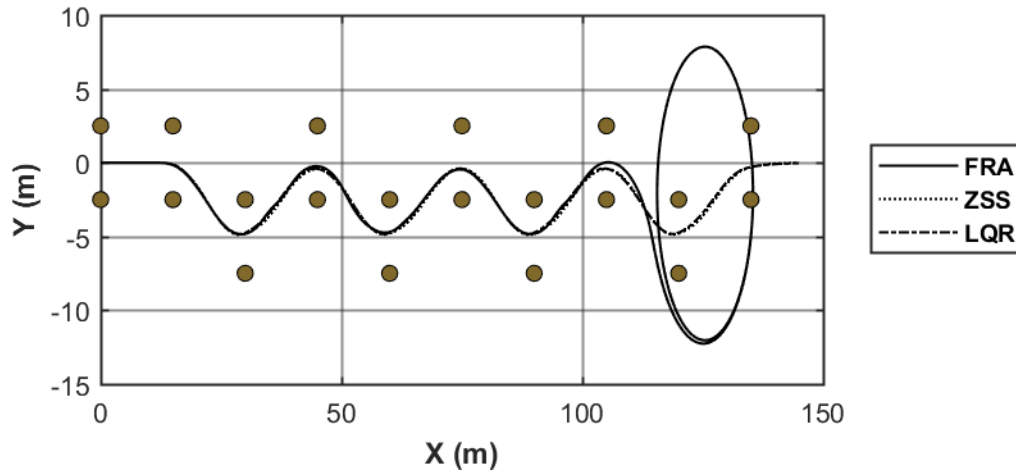
5.2.1.3 Maximum speed – µ=0.35

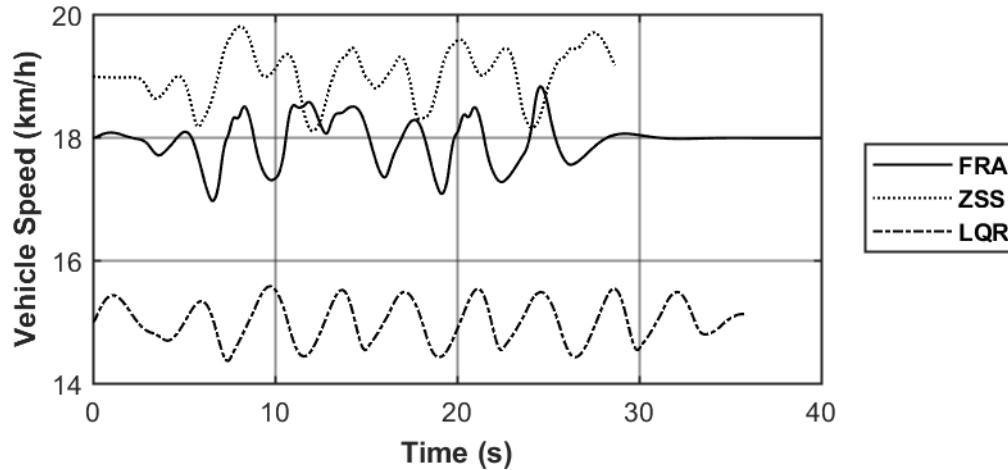**Figure 5-20 Vehicle Trajectory: 15m slalom at max speed over µ=0.35**

Figure 5-21 Maximum Vehicle Speed: 15m slalom at max speed over µ=0.35

In order for the vehicles to complete the 15-meter slalom maneuver over a surface friction of 0.35, the speed was decreased from 20 km/h until each vehicle completed the maneuver. The FRA vehicle completed the majority of the maneuver at 18 km/h as seen in Figure 5-20, until the amplification of the lateral acceleration catches up and causes the vehicle to lose control. The steering wheel input of the FRA vehicle (Figure 5-24) also reached the peak steering input through this maneuver, which caused a delay in the change of trajectory. The vehicle that completed the maneuver with the highest speed is the ZSS vehicle at the targeted 19 km/h, as seen in Figure 5-21. The LQR controlled vehicle required the lowest speed of 15 km/h to complete the maneuver, which further demonstrates how the LQR controller is not appropriate for low speed maneuvers, even over low friction surfaces.

64

The increased performance of the ZSS can be attributed to the rear axle steering increasing the maneuverability. The rear axle steering allows the vehicle to enter the set of cones with a better heading, as seen in Figure 5-22, by promoting the rear of the vehicle to follow the same path as the front of the vehicle. Over low friction surface, however, the rear axle takes a wider path than the front of the vehicle which could lead to oversteering if the speed increased as 19 km/h is the fastest the ZSS vehicle could complete this maneuver.
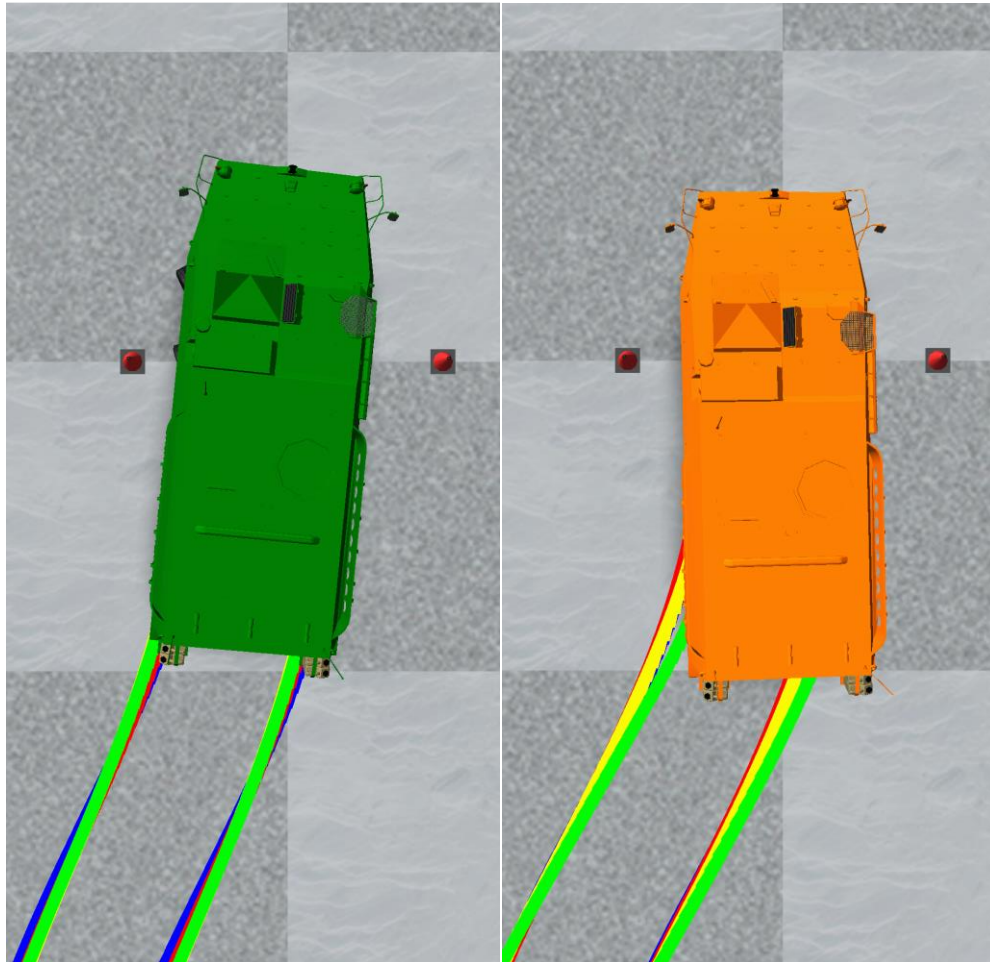
Figure 5-22 Vehicle Approach: 15m slalom at max speed over μ=0.35, FRA (green), ZSS (orange)

Both the LQR and ZSS steering wheel inputs have been decreased compared to the conventional FRA vehicle which reached the peak steering input. The steering wheel rate (Figure 5-23) of the FRA vehicle reaches over 1000 deg/s for a significant amount of times further showcasing how over low friction surface, the performance of this vehicle in tight areas is not ideal.
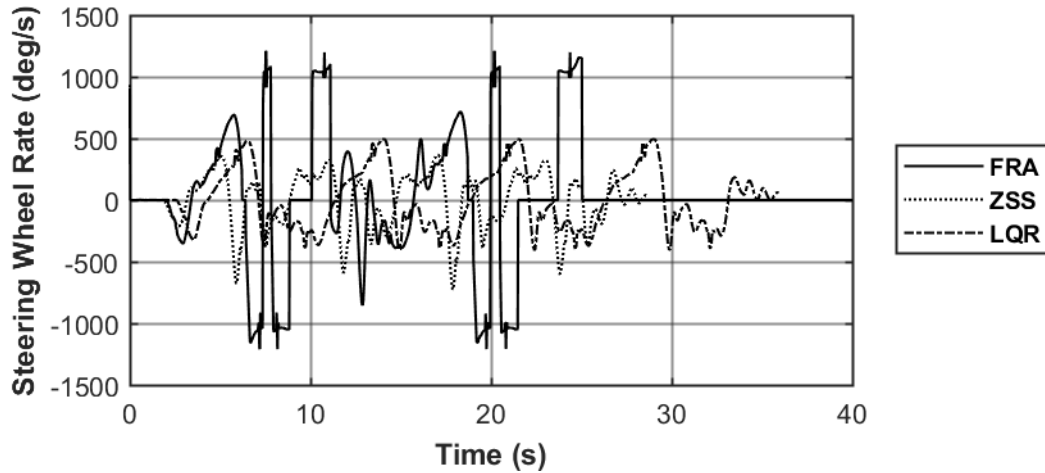
Figure 5-23 Steering Wheel Rate: 15m slalom at max speed over μ=0.35
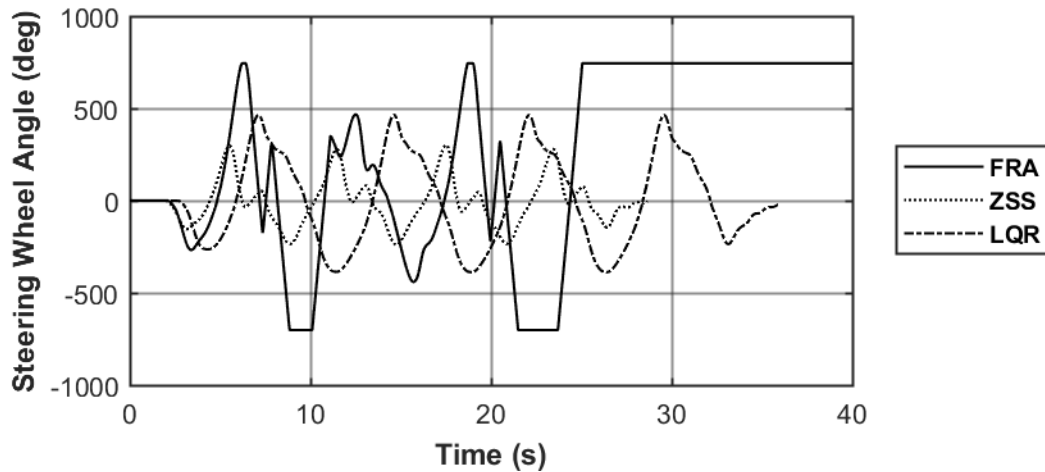
Figure 5-24 Rear Axle Steering Angle: 15m slalom at max speed over μ=0.35

The vehicle with the highest steering angle on the rear axle, ZSS, is the best performing vehicle for this 15-meter slalom maneuver. The ZSS vehicle is the feed-forward-controlled vehicle, which increases the responsiveness of the controller, resulting in better control over the low friction surface. At this speed it also helps that the ZSS steers the rear axle opposite to the front axle, increasing the maneuverability even over low friction surface.

Figure 5-25 Vehicle Sideslip Angle: 15m slalom at max speed over μ=0.35

Figure 5-26 Lateral Acceleration: 15m slalom at max speed over μ=0.35

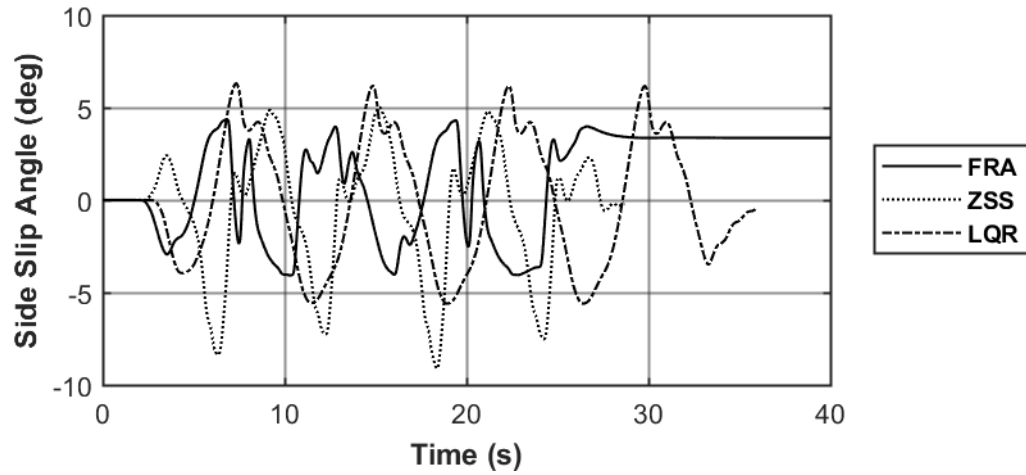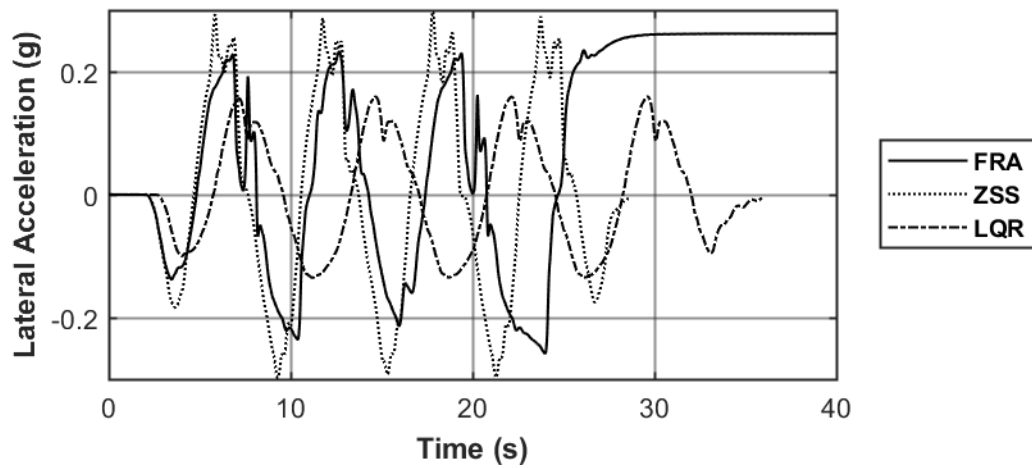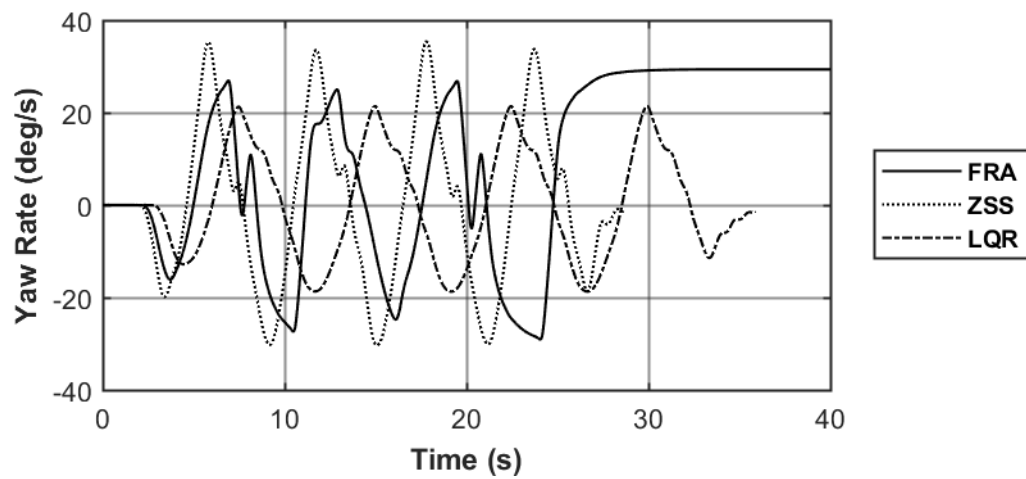**Figure 5-27 Yaw Rate: 15m slalom at max speed over μ=0.35**

The vehicle with the highest speed during this maneuver, ZSS, has the highest lateral acceleration and yaw rate (Figure 5-26 and Figure 5-27 respectively). This vehicle also has the highest sideslip angle, Figure 5-25, however it is opposite in amplitude compared to the FRA and LQR vehicles, meaning the vehicle is oversteering as a result of the rear axles steering opposite to the front axle. For low speeds this is desired, as well as higher yaw rates, indicating better maneuverability. This desired value is also dependant on the experience of the driver, as high yaw rates can sometimes be hard to get used to.

The conventional vehicle loses control resulting in constant high sideslip angle, lateral acceleration, and yaw rate during the oversteering event occurring at the end of the simulation (17-25 seconds).

5.3 LOW-MEDIUM SPEED TRANSITION

The low-medium speed transition maneuvers will help develop conclusions supporting suggestions for the activation speeds for each controller as the FRA, ZSS and LQR vehicles all have optimal performance at different speeds.

5.3.1 Modified J-turn maneuver – 40 km/h

The modified J-turn maneuver uses a steering input which was determined from a reference combat vehicle performing a 75 ft. (22 meter) J-turn maneuver at 40 km/h. This test will serve as an evaluation tool for the vehicles maneuverability and stability at this speed. Since the performance is evaluated at a fixed steering input, this simulation will compare the vehicle's ability to resist rollover as well as turning radius performance. The steering input seen in Figure 5-28 is comprised of an increasing steering wheel angle to a peak of 376.2 degrees followed by a return to center and a correction to straighten the vehicle. The speed of 40 km is chosen as it is in the range where the vehicle is transitioning from low speed operation to high speed operation. The three vehicle configurations are compared over high friction (μ=0.85) and low friction (μ=0.35) surfaces.
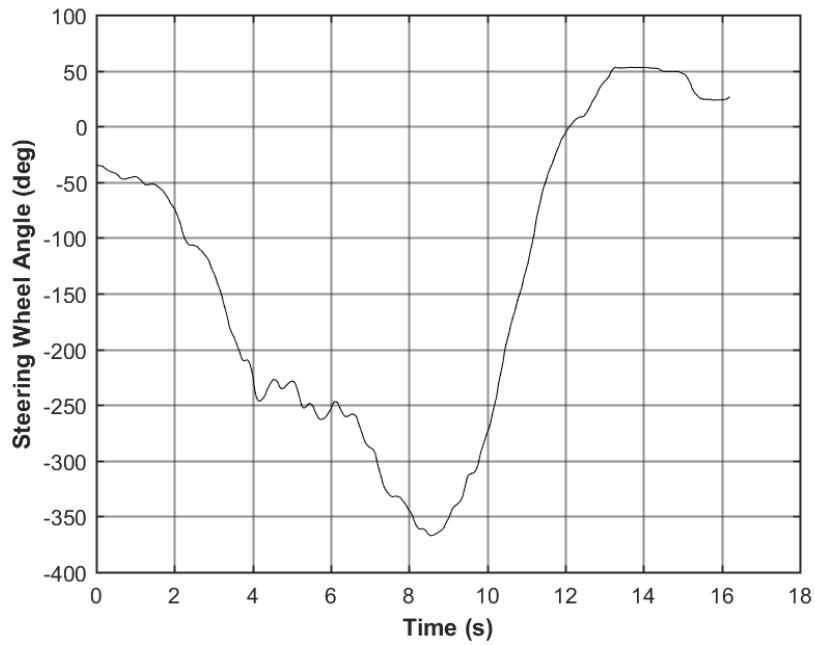
Figure 5-28 Modified J-Turn Steering wheel input

5.3.1.1 High friction – μ =0.85
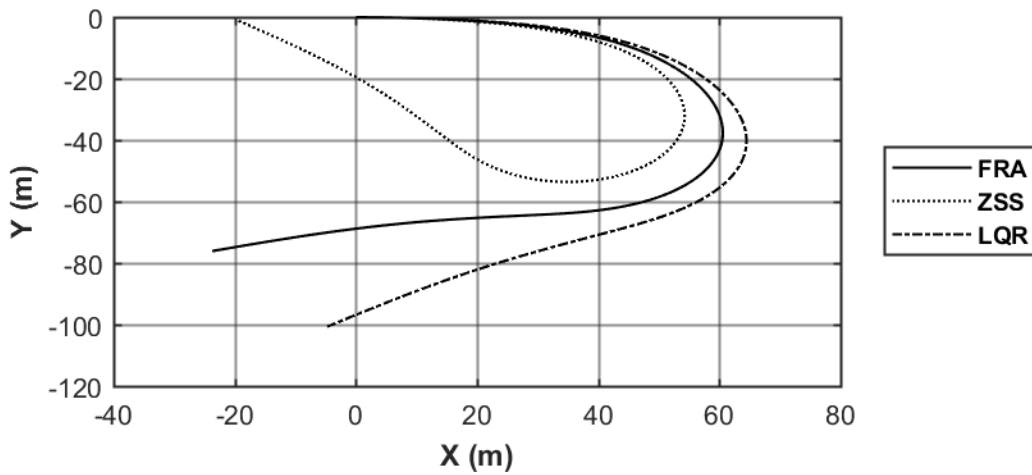
Figure 5-29 Vehicle Trajectory: Modified J-turn over μ=0.85

The turning radius of the ZSS controlled vehicle is a lot tighter than the FRA vehicle due to the feed-forward nature of the controller and the contra-steer that is used at speeds below 49.5 km/hr (Figure 2-5). The LQR controlled vehicle operates with a larger turning radius in an effort to reduce the yaw rate and sideslip angle and satisfy the control parameters.
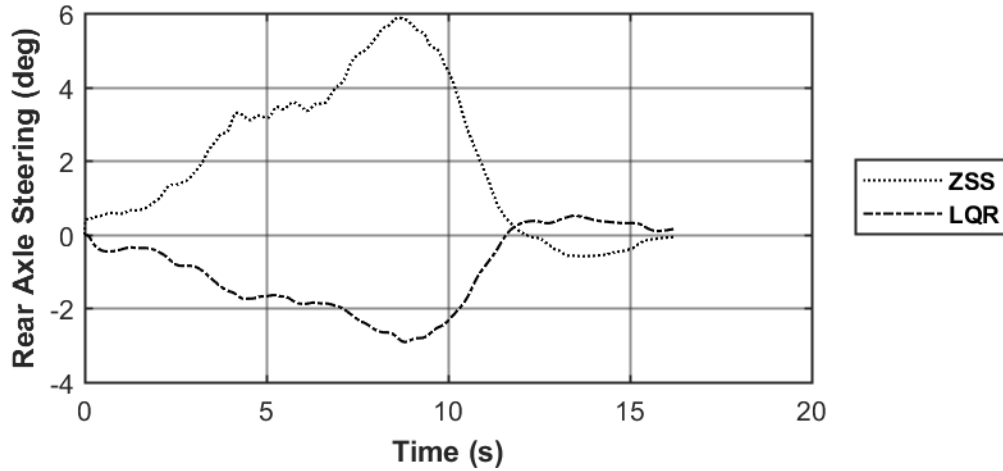
Figure 5-30 Rear Axle Steering Angle: Modified J-turn over µ=0.85

At the speed of 40 km/h, the ZSS vehicle will steer the rear axle opposite of the front axle, reducing the turning radius with the same steering input compared to the conventional vehicle. The LQR controller steers the rear axle in the same direction as the front axle, which explains why the trajectory is a wider turn as seen in Figure 5-29. The LQR rear axle is steered a maximum of three degrees, which will not provide as significant of a change in dynamic performance as the six degrees of contra-steer seen with the ZSS controller.

Figure 5-31 Lateral Acceleration: Modified J-turn over µ=0.85
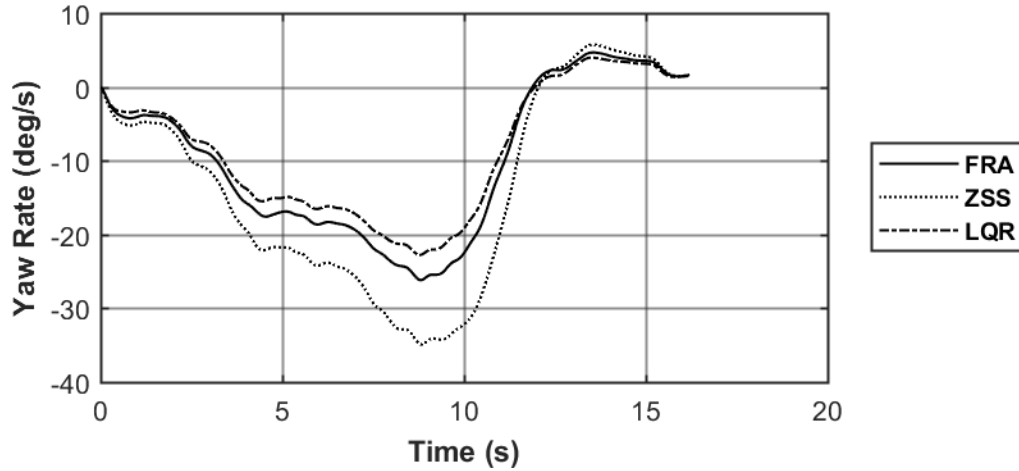
Figure 5-32 Yaw Rate: Modified J-turn over µ=0.85
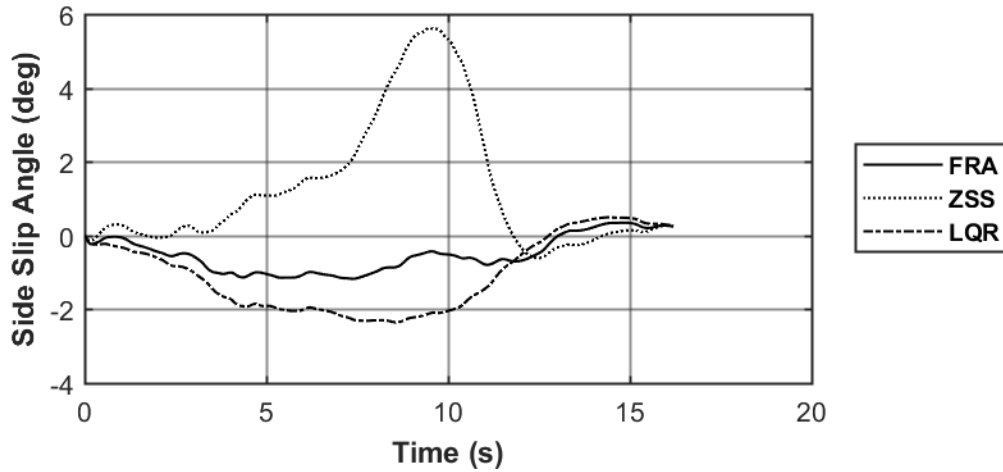
Figure 5-33 Side Slip Angle: Modified J-turn over µ=0.85

The lateral acceleration performance (Figure 5-31) indicates the contra-steer induced by the ZSS controller increases the lateral acceleration. The lateral acceleration is not increased significantly, and rollover is not a concern. Since the LQR controller is using the conventional vehicle as a reference model, the vehicle behaviour is not dramatically different from the conventional vehicle. The LQR reduces the yaw rate (Figure 5-32) and increases the sideslip angle (Figure 5-33) of the vehicle compared to the conventional vehicle. This can be explained by the reference model being calculated at steady state, so in this case, the steady state of the vehicle includes a slight sideslip angle and a decreased yaw rate from the dynamic results of the conventional vehicle.

During this maneuver the ZSS vehicle induces a contra-steer, which as a result decreases the turning radius of the vehicle, but also introduces a sideslip angle opposite of the conventional vehicle. At lower speeds, such as 40km/h, the added maneuverability is useful. The ZSS steering output to the rear axle is calculated based on vehicle dynamic calculations and should provide a reliable steering output over high friction surfaces that increases maneuverability and remains stable.

5.3.1.2 Low friction – μ =0.35
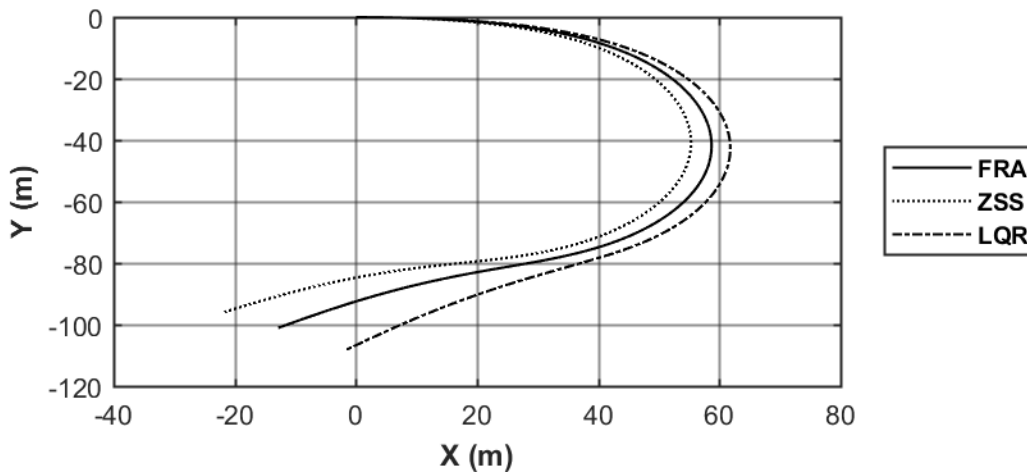
Figure 5-34 Vehicle Trajectory: Modified J-turn over µ=0.35

Over a low friction surface, the difference in performance with the controllers is not as exaggerated as over ideal surface. Regardless the trajectory of the ZSS vehicle is still tighter, and the LQR radius is larger. This pattern is due to the similar rear axle steering angles presented in Figure 5-30.
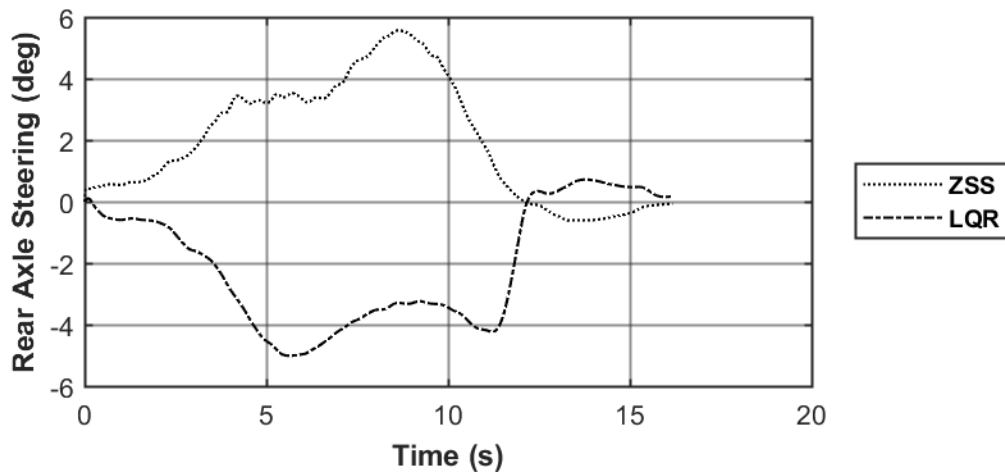
Figure 5-35 Rear Axle Steering Angle: Modified J-turn over μ=0.35
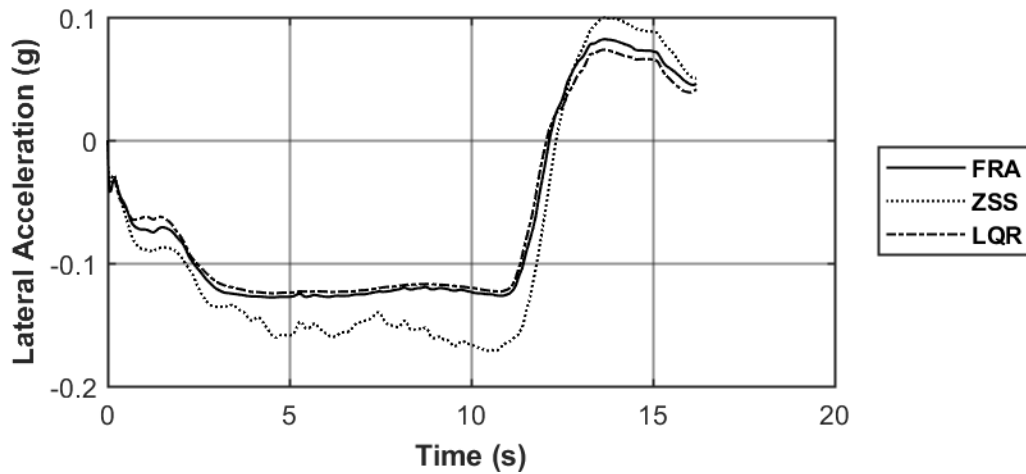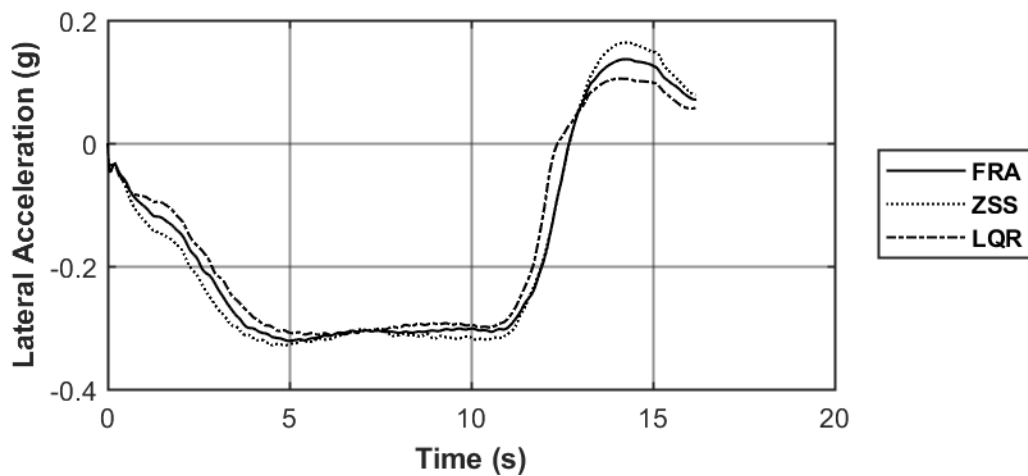

Figure 5-36 Lateral Acceleration: Modified J-turn over μ=0.35
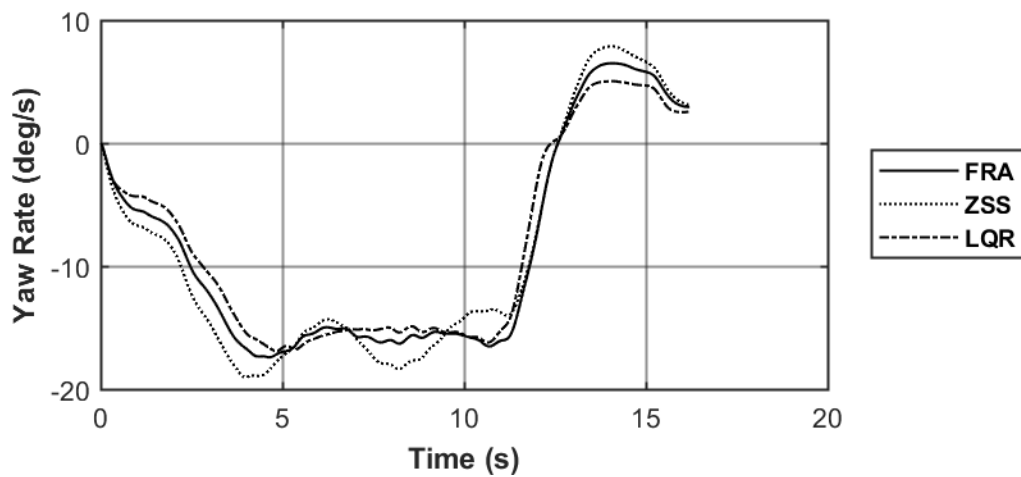
Figure 5-37 Yaw Rate: Modified J-turn over μ=0.35
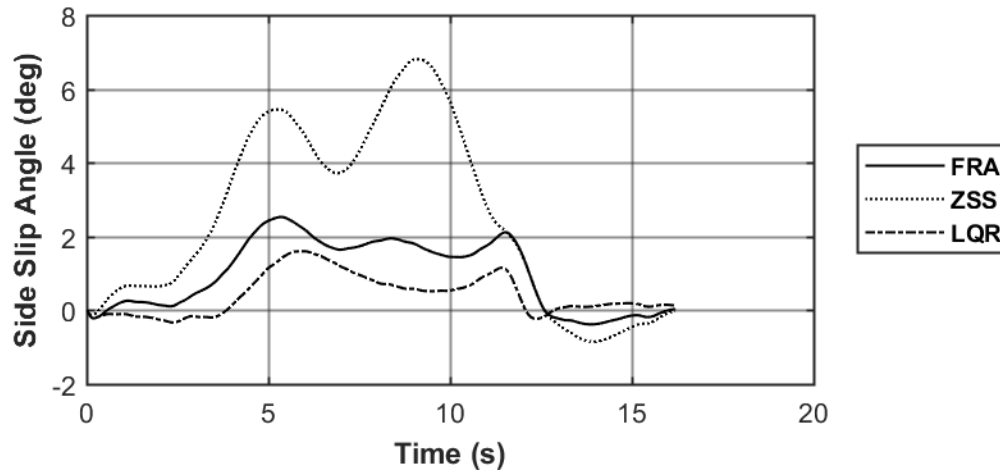
Figure 5-38 Side Slip Angle: Modified J-turn over μ=0.35

The performance of the vehicles over low friction surface does not differ too much. The peak lateral accelerations (Figure 5-31) and yaw rates (Figure 5-32) of the ZSS vehicle have a slightly higher amplitude, however do not indicate major performance improvements. The LQR controller reduces the sideslip angle seen in Figure 5-33, which shows the most significant performance improvement from this set of results. A reduced sideslip angle describes a vehicle that is pointing more in the direction of travel, rather then slipping sideways. This is desired over low friction surface as spin out is more likely with increasing sideslip angle and lack of recoverability of low friction surface.

5.3.2   Low-Medium Speed Transition – 100-ft Skid Pad Constant Acceleration

The 100ft diameter circle constant acceleration is a good simulation to analyze the steering input required for each controlled vehicle. The addition of a rear steering angle should decrease the steering input at lower speeds and increase the required steering inputs at higher speeds.
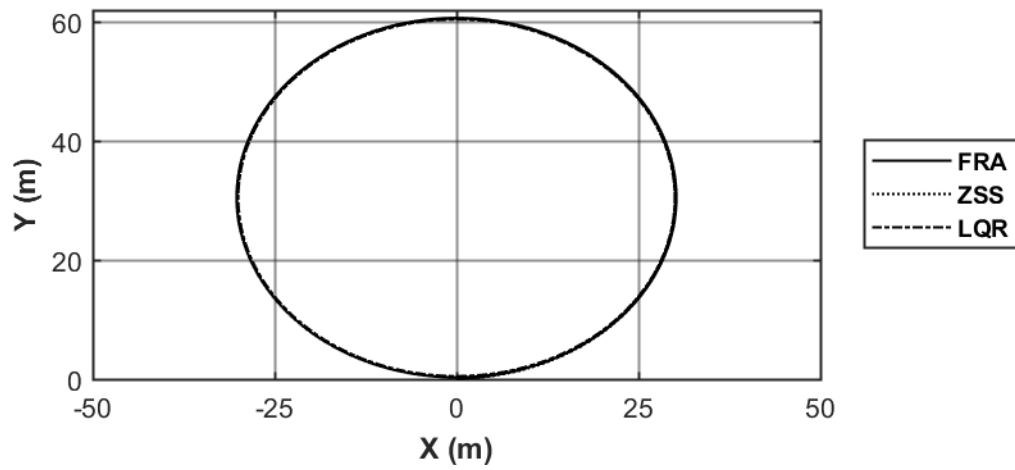
Figure 5-39 Vehicle Trajectory:100-ft skid pad over μ=0.85
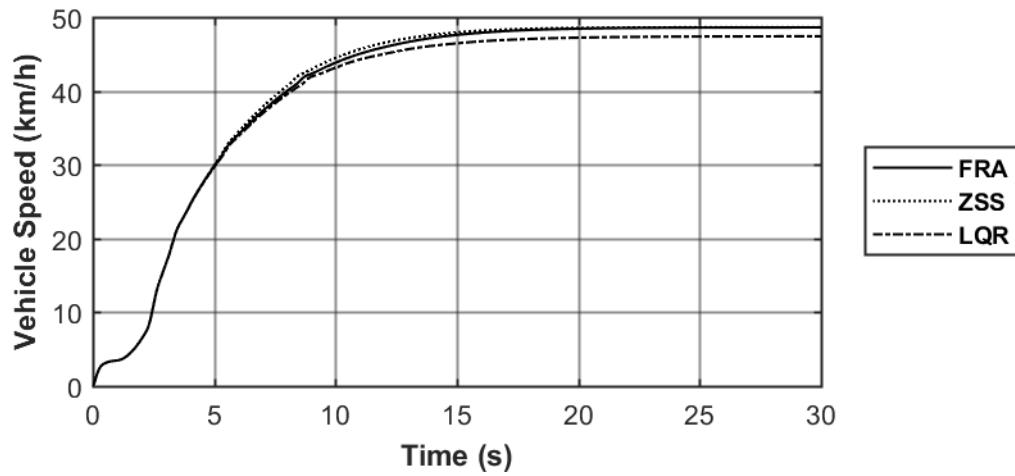
Figure 5-40 Vehicle Speed: 100-ft skid pad over μ=0.85
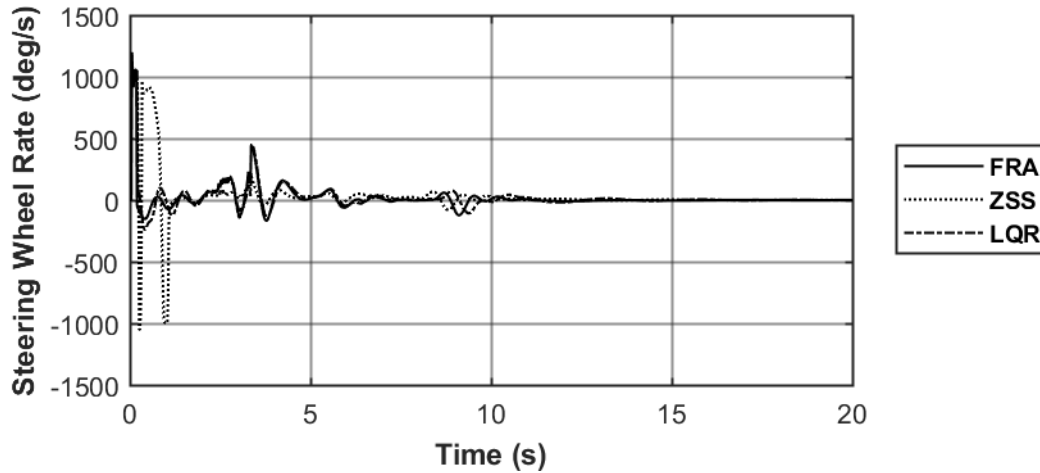
Figure 5-41 Steering Wheel Rate: 100-ft skid pad over μ=0.85

The 100-ft circle skid pad maneuver offers analysis on steering behaviour for the different control methods. All four vehicle controllers offer similar performance when analyzing the trajectory (Figure 5-39). The speed performance of the vehicles (Figure 5-40) indicate the LQR controller has the lowest peak speed under steady state steering, however this minor speed deficiency is not a very big concern as it steers more neutrally with minor decrease in yaw rate and lateral acceleration. The steering wheel rate (Figure 5-41) is also very similar with every vehicle after the initialization of the test. Other vehicle dynamic parameters will offer more insight into the effectiveness of the controllers.
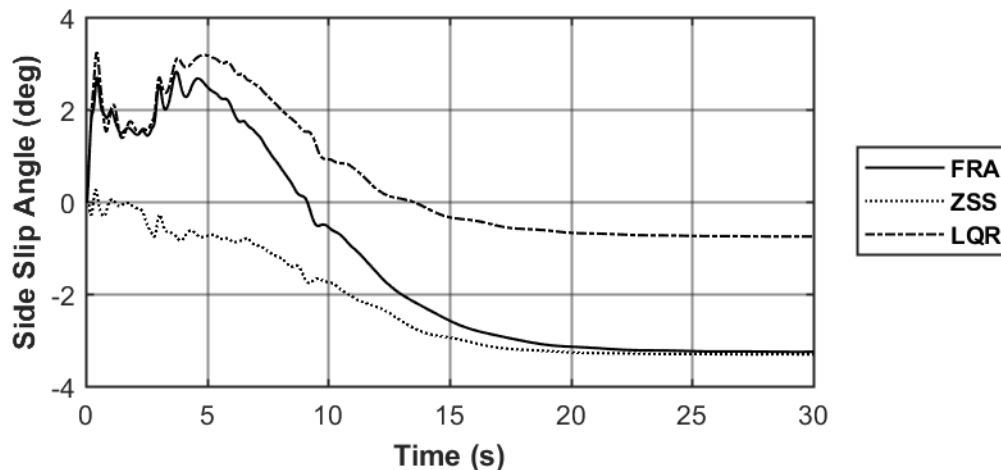
Figure 5-42 Side Slip Angle: 100-ft skid pad over μ=0.85
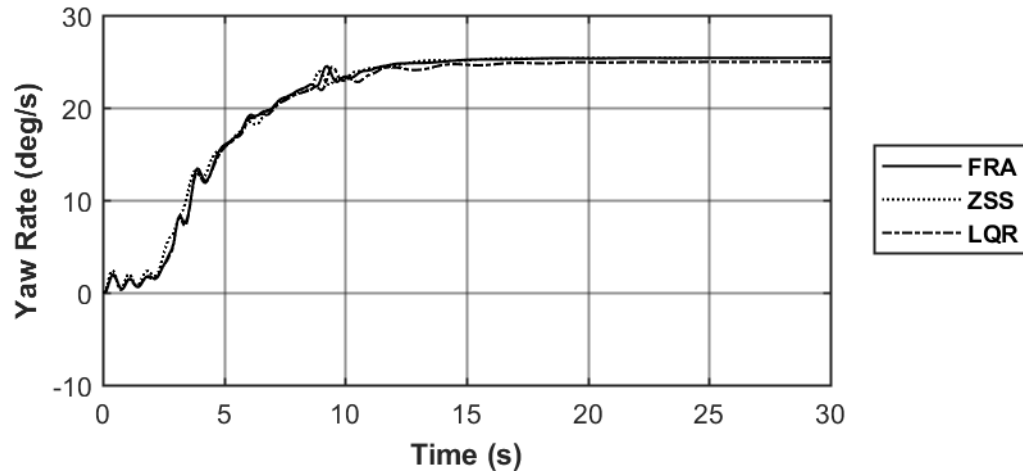
Figure 5-43 Yaw Rate: 100-ft skid pad over μ=0.85
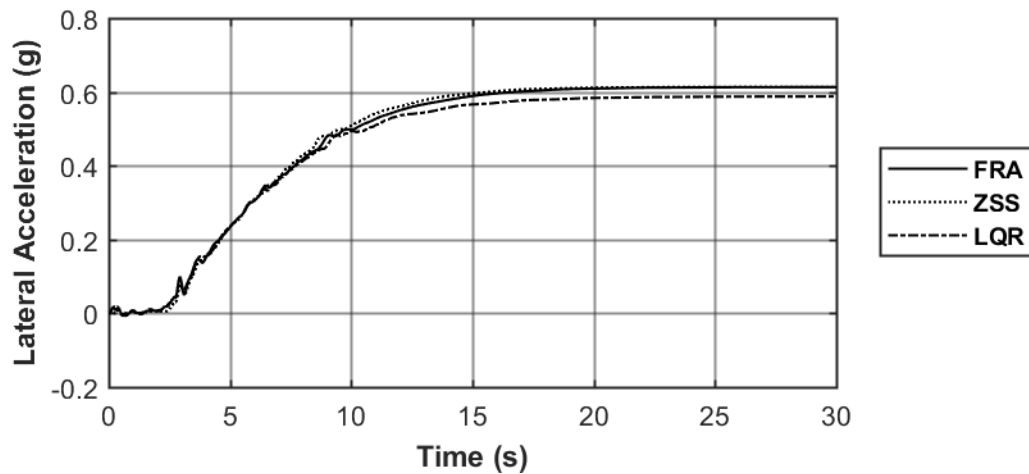
Figure 5-44 Lateral Acceleration: 100-ft skid pad over μ=0.85

The 100 ft skid pad simulation demonstrates that every configuration tested does not have the power in order to lose control during a steady state maneuver. The included simulated mechanical differentials do a very good job at distributing the torque in order to remain under control and following the projected path. This simulation most likely would have different results with locked differential configurations including increased speeds and further off-tracking from target path.

The most notable difference performance measure is the sideslip angle (Figure 5-42). The LQR controller does a decent job at maintaining a smaller sideslip angle than the ZSS controller or FRA vehicle. The lower sideslip angle represents a more neutral steering vehicle which is desirable as the vehicle is pointing in the direction of travel resulting in

less tire wear and makes the vehicle more predictable. The sideslip angle of the ZSS controlled vehicle is closer to zero at low speeds, which is due to the ZSS controller solving the rear axle steering angle for a sideslip angle of zero at steady state. However, as the speed increases, the ZSS has no reference to the steady state causing the performance measures to stray away from the desired steady state motion. The LQR references the desired steady state performance of the conventional FRA vehicle (yaw rate and side slip angle), which explains why at low speeds the performance is similar, and at higher speeds the LQR reduces the performance measures to satisfy the desired vehicle performance at steady state.

The yaw rate and lateral acceleration (Figure 5-43 Figure 5-44) of the ZSS controlled vehicle is very similar to the conventional vehicle, as the rear axle steering angle approaches zero (Figure 5-45) when the maximum speed is reached and steady state steering is achieved. Since every vehicle is staying to a similar turning radius, the lateral acceleration and yaw rate are directly affected by the forward speed of the vehicle. The LQR controlled vehicle results show lower yaw rate and lower lateral accelerations during the steady state steering and speed portion of the maneuver which is partially due to the reduced speed resulting from the rear axle steering input. The LQR vehicle performs the best at steady state steering input by decreasing the sideslip angle the most and achieving the most neutral steering results.

The minor differences in the vehicle performances are a direct result of the method of the controlled rear axle. LQR controller requires the largest steering input for this maneuver (Figure 5-46) and is also the only controller that induces a rear steer angle in the same direction as the front axle. The maximum speed reached for the ZSS vehicle is just less than the threshold speed (49.5 km/h) for the controller which determines the rear axle remains counter-steered during the entirety of the maneuver.

During this maneuver all vehicles approach a lateral acceleration of 0.6 g's (Figure 5-44) relatively high for a large vehicle. The LQR controller minimizes this slightly, but as a

result forward speed is lost (Figure 5-40). This is an example of how performance may need to be slightly compromised as a method of increasing stability.
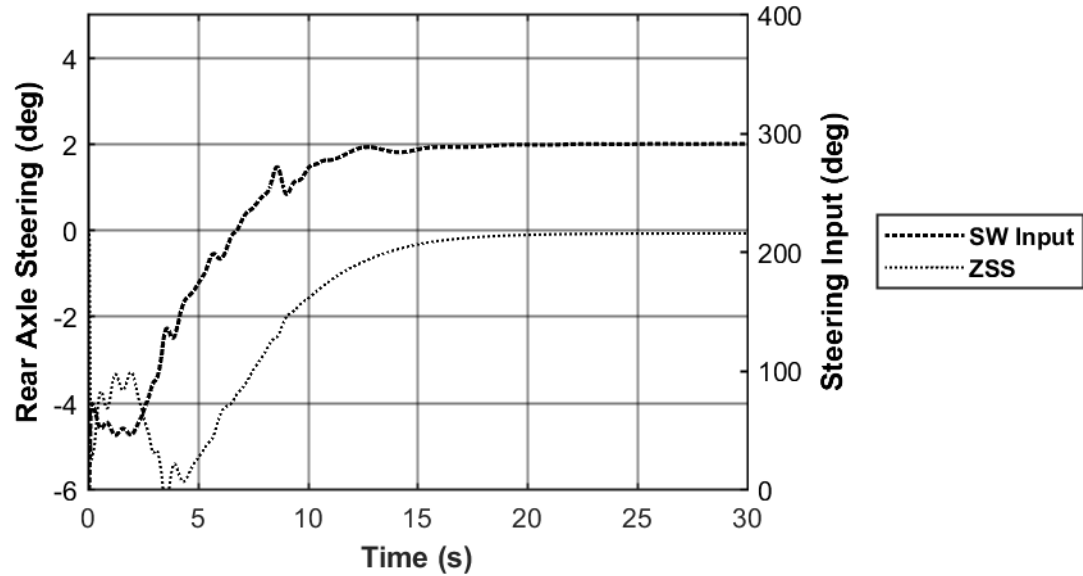
Figure 5-45 Zero-Sideslip Rear Axle Steering:100-ft skid pad over μ=0.85
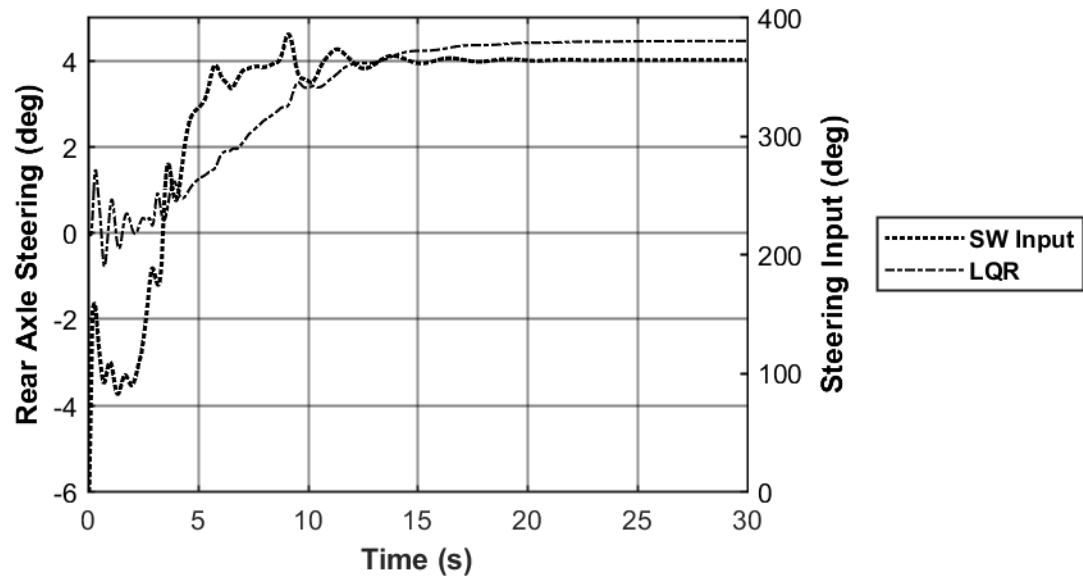
Figure 5-46 LQR Rear Axle Steering:100-ft skid pad over μ=0.85a

5.4 HIGH SPEED STABILITY TESTING

5.4.1 FMVSS 126 ESC

FMVSS 126 ESC is designed by the Federal Motor Vehicle Safety Standard (FMVSS) [78] as a method to evaluate the Electronic Stability Control (ESC) in production vehicles. This test includes a steering wheel input rather than a path to follow. The steering wheel input consists of a sine wave path with a 0.7 Hz Frequency with a 400-millisecond delay in the second half of the wave and an amplitude of 234 degrees. Generally, the amplitude is determined using a ramp steer maneuver with a "slowly increasing steering angle" until the vehicle lateral acceleration reaches 0.3 g at a speed of 80 km/h. In order produce comparable results, the same steering wheel input will be used on each vehicle based off of the requirements for the conventional vehicle. The steering input is represented in Figure 5-47.
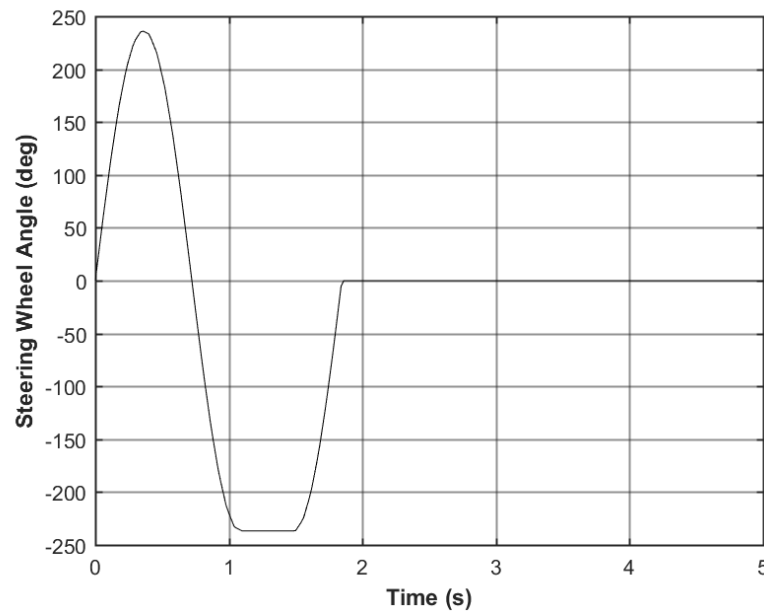
Figure 5-47: FMVSS 126 ESC steering wheel input
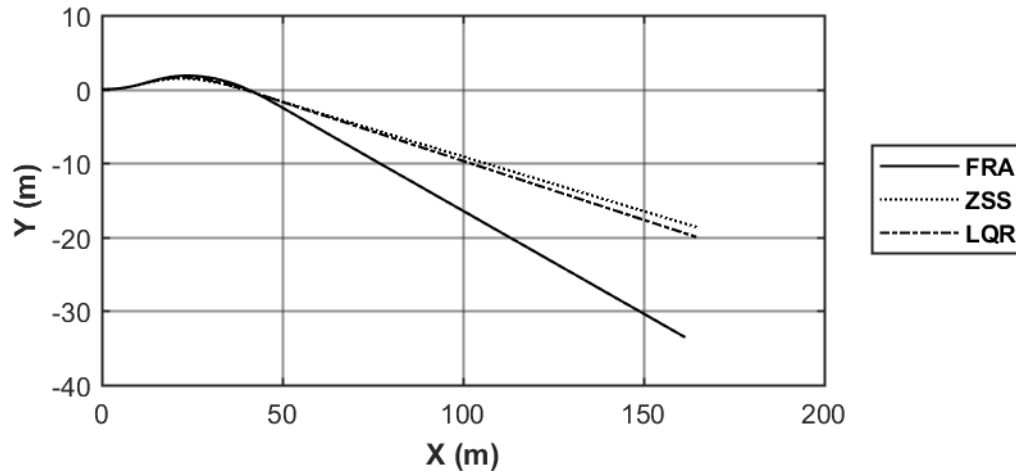
Figure 5-48 Vehicle Trajectory: FMVSS 126 ESC at 60 km/h over μ=0.85: Vehicle Trajectory

The overall trajectory of the vehicle indicates that the conventional (FRA) vehicle has the most change in path. The ZSS and LQR controlled vehicles have less change in trajectory because of the rear axle steering which is steered in the same direction as the front wheels (Figure 5-50) which dampens the yaw rate. Upon close inspection of the lateral displacement (Figure 5-49), the FRA vehicle has the most lateral displacement, which is desirable for this maneuver as peak lateral displacement is one of the measures for this maneuver [79].
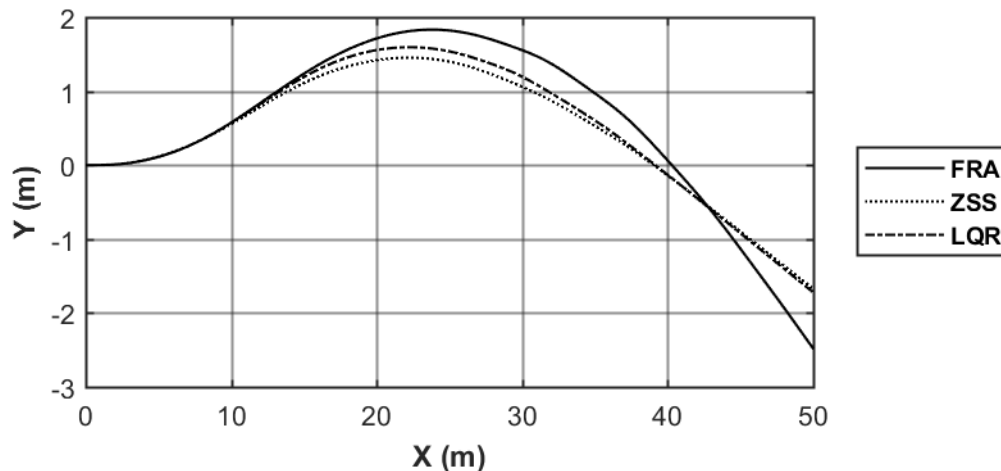
Figure 5-49 Vehicle Lateral Displacement: FMVSS 126 ESC at 60 km/h over μ=0.85

Figure 5-50 Rear Axle Steering Angle: FMVSS 126 ESC at 60 km/h over μ=0.85
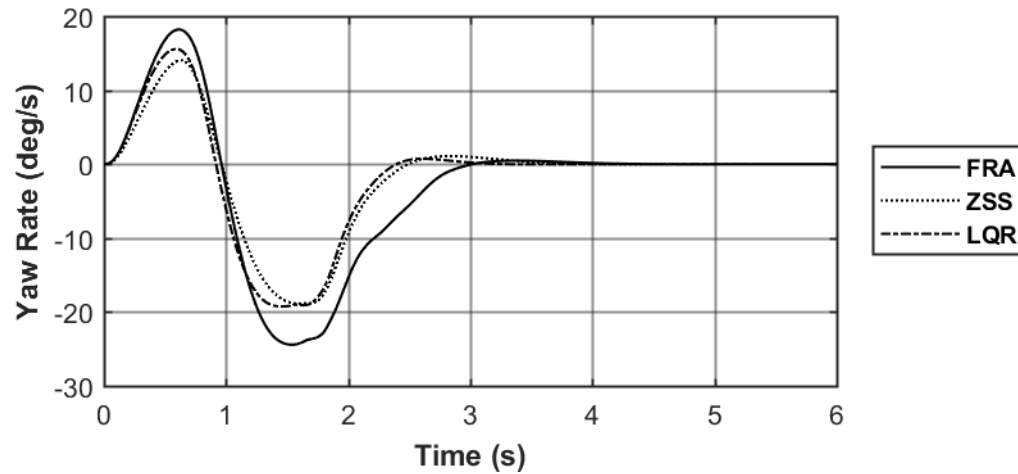
Figure 5-51 Yaw Rate: FMVSS 126 ESC at 60 km/h over μ=0.85

During the FMVSS 125 ESC maneuver at 60 km/h both the LQR and ZSS controllers are able to dampen the yaw rate (Figure 5-51) and decrease the severity and duration of the vehicle sideslip (Figure 5-52). The duration of high lateral acceleration seen in the FRA vehicle is decreased in the LQR and ZSS vehicles as well (Figure 5-53). The lateral acceleration of the ZSS vehicle has been damped due to the responsiveness of the feed-forward controller. The rear axle steering signal (Figure 5-50) of the ZSS controller is directly related to the steering input seen in Figure 5-47 while the LQR controlled rear axle is not directly related. This is due to the imposed 0.3 second time delay in the controller and the feed-back nature of the controller.

Figure 5-52 Side Slip Angle: FMVSS 126 ESC at 60 km/h over μ=0.85
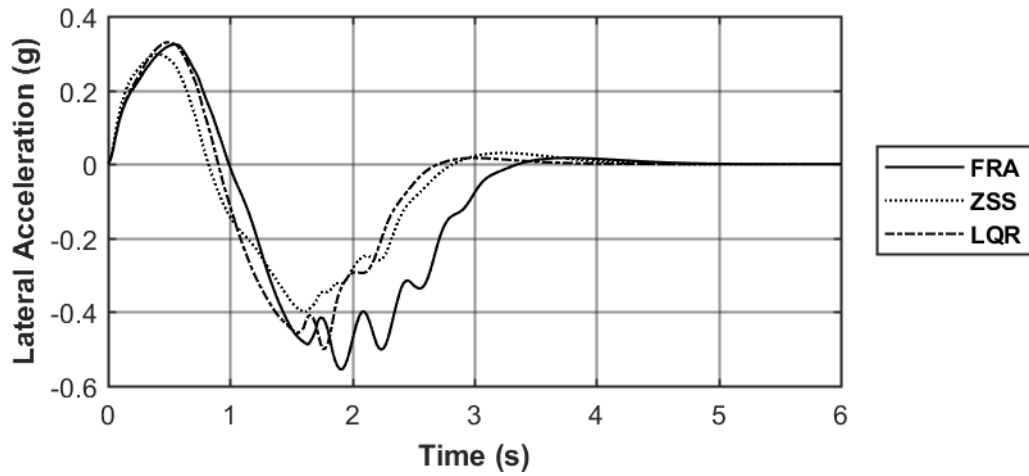
Figure 5-53 Lateral Acceleration: FMVSS 126 ESC at 60 km/h over μ=0.85

The lateral accelerations as shown in in Figure 5-53 demonstrate the FRA vehicle is skidding due to the high sideslip angle. By decreasing the sideslip angle, the vehicle skids less which indicates the tires are still in their controllable range.

Figure 5-54 Vehicle Trajectory: FMVSS 126 ESC at 80 km/h over μ=0.85: Vehicle Trajectory
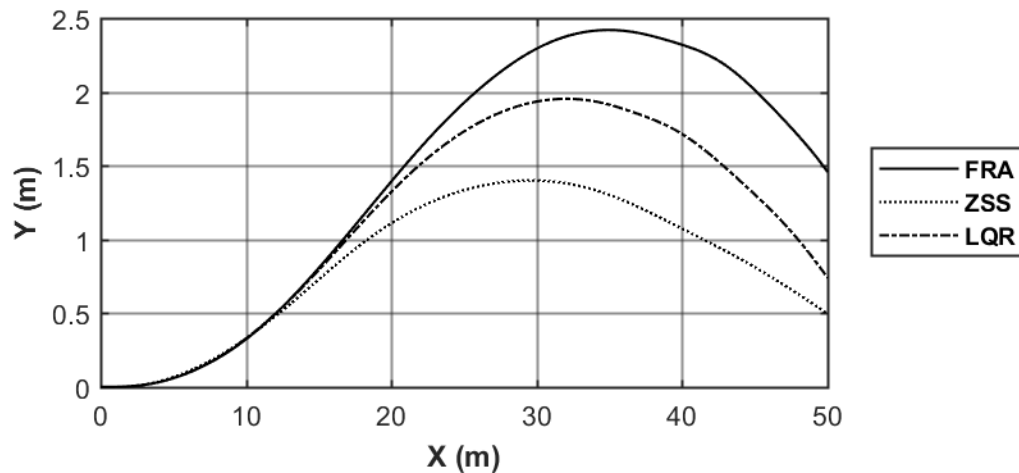
Figure 5-55 Vehicle Lateral Displacement: FMVSS 126 ESC at 80 km/h over μ=0.85

At a speed of 80 km/h over a high friction surface, the lateral displacement of the controlled vehicles is comparatively less than the conventional vehicle (Figure 5-55). At higher speeds the steering input to the rear axle is in the same direction as the front axles which results in less lateral displacement than the fixed rear axle vehicle with identical steering inputs. By referring to the ZSS steering output, the higher the speed, the more the rear axle is to steer in the same direction which decreases the lateral displacement. The LQR vehicle has a higher lateral displacement than the ZSS vehicle which is more desirable in an emergency situation.

Figure 5-56 Rear Axle Steering Angle: FMVSS 126 ESC at 80 km/h over μ=0.85
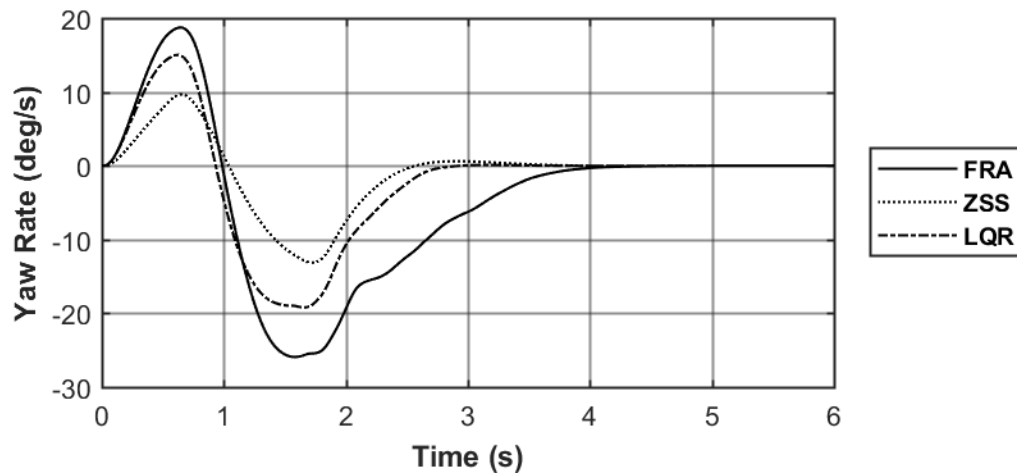
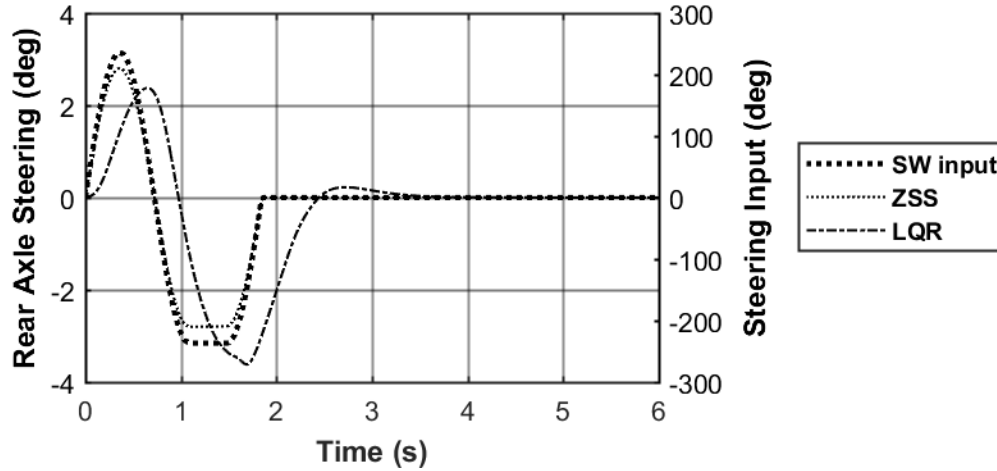**Figure 5-57 Yaw Rate: FMVSS 126 ESC at 80 km/h over μ=0.85**

Figure 5-58 Side Slip Angle: FMVSS 126 ESC at 80 km/h over μ=0.85

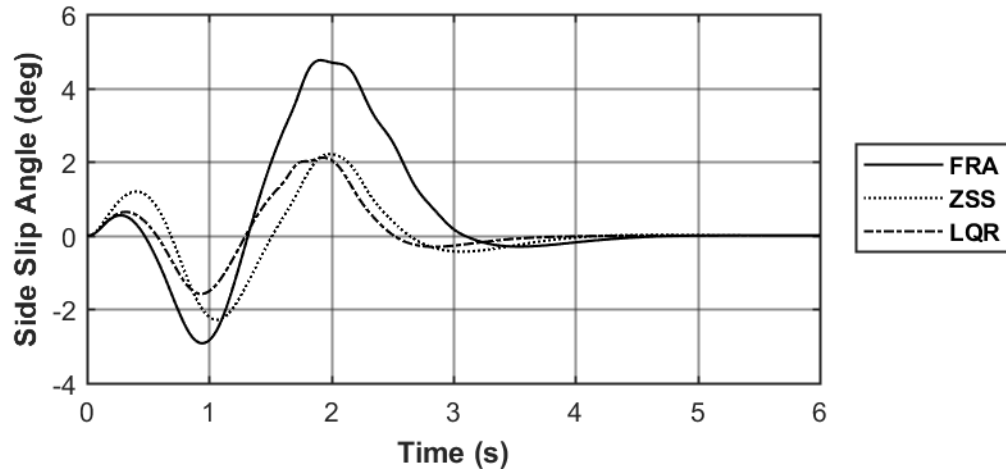**Figure 5-59 Lateral Acceleration: FMVSS 126 ESC at 80 km/h over μ=0.85**

The FMVSS 126 maneuver over high friction surface provides an interesting lateral acceleration behaviour for the LQR and FRA vehicles. The lateral acceleration from 1.5 seconds to when the vehicle is settled in Figure 5-53 has an oscillation indicating the rapid increase and decrease of the lateral acceleration rather than a smooth transition. This is likely due to skidding of the tires during drift. The LQR and FRA vehicles have higher sideslip angles than the ZSS vehicle during this maneuver (Figure 5-58) which is a result of the responsiveness of the feed-forward controller that is designed to reduce the sideslip angle.

Much like the FMVSS 126 over high friction surface at 60 km/h, the yaw rate, lateral acceleration, and sideslip angle of the controlled vehicles are reduced (Figure 5-57, Figure 5-59, Figure 5-58). These results also settle to zero quicker than the conventional vehicle. The yaw, lateral acceleration, and sideslip behaviour of the LQR controlled vehicle is similar to the conventional vehicle as the reference yaw rate and sideslip angle is determined based on the reference model that is the conventional vehicle. The ZSS rear axle steers without delay to the front axle which causes a peak in the lateral acceleration when the steering returns to zero just before two seconds. However, this would likely not be an issue with proper damping in the system which is typically seen on physical models.
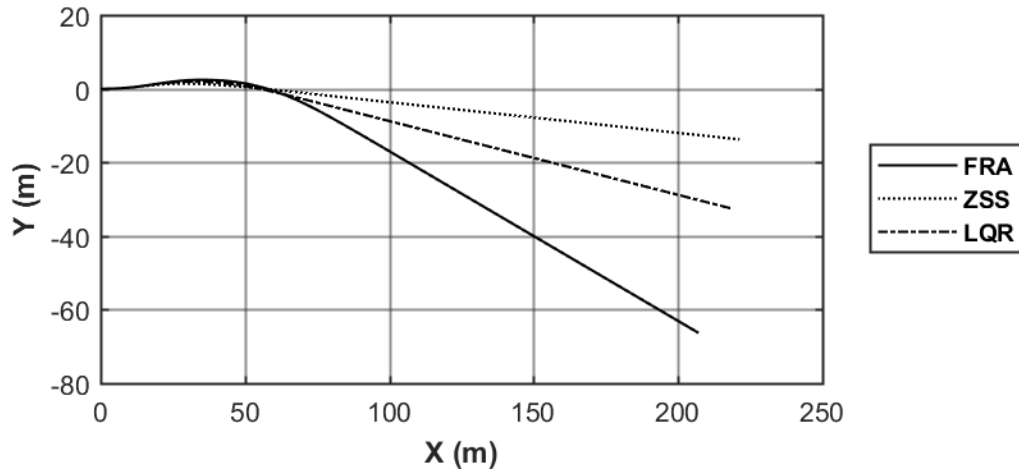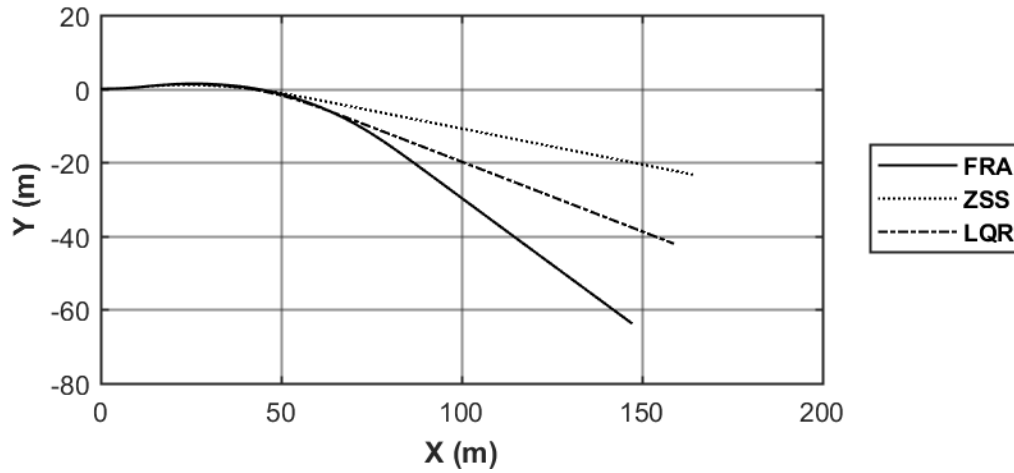
Figure 5-60 Vehicle Trajectory: FMVSS 126 ESC at 60 km/h over μ=0.35
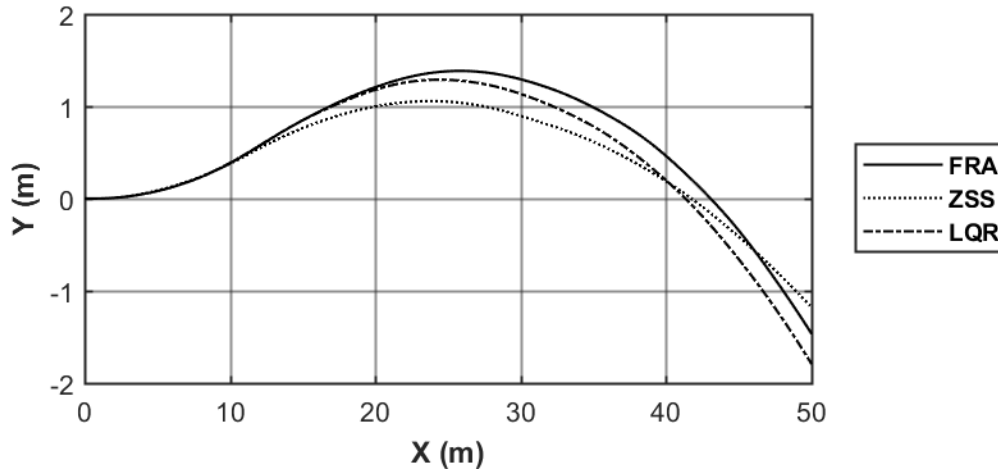
Figure 5-61 Vehicle Lateral Displacement: FMVSS 126 ESC at 60 km/h over μ=0.35

The trajectory performance of the three configurations is very similar over low friction surface (Figure 5-60) when compared to high friction surface (Figure 5-48). The lateral displacement is in a similar range, however the direction the vehicles are travelling after settling back to steady state is different due to the sideslip performance.

The rear axle of the ZSS controlled vehicle is directly related to the steering input while the LQR rear axle steering is steered for a longer duration to dampen the yaw rate and sideslip angle (Figure 5-62).
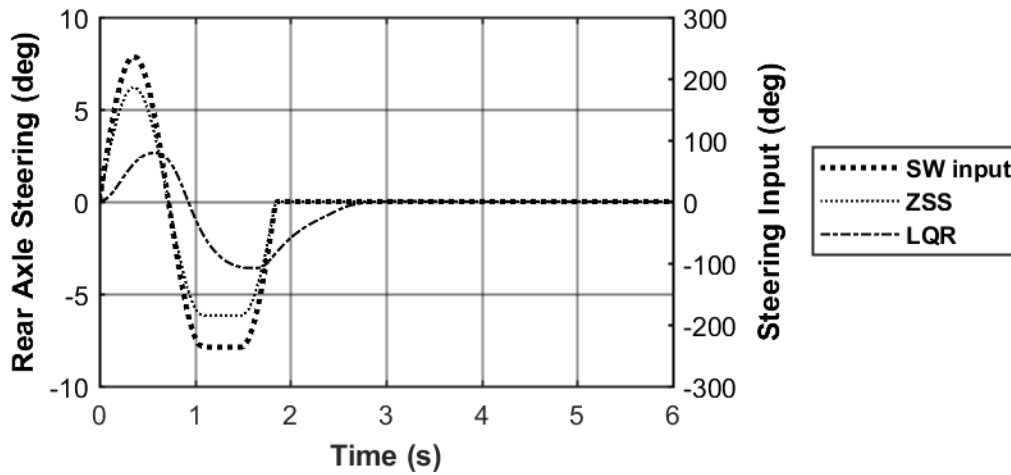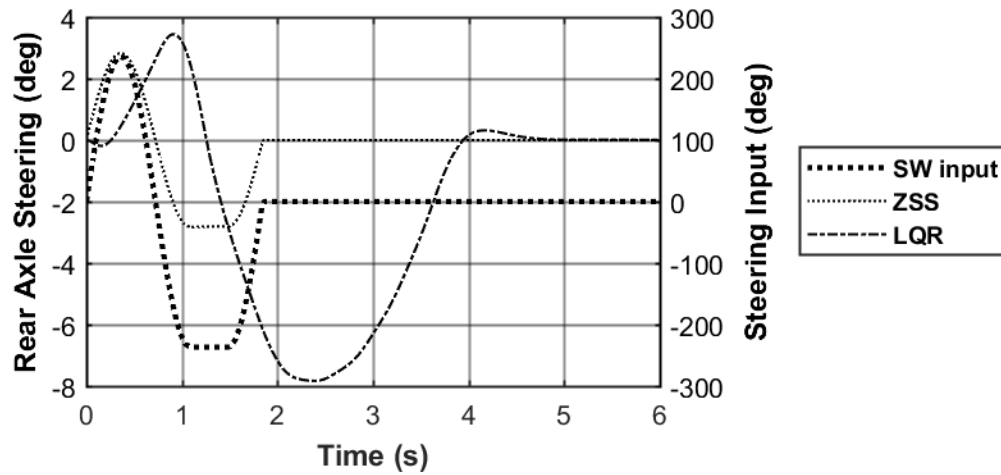
**Figure 5-62 Rear Axle Steering Angle: FMVSS 126 ESC at 60 km/h over μ=0.35**
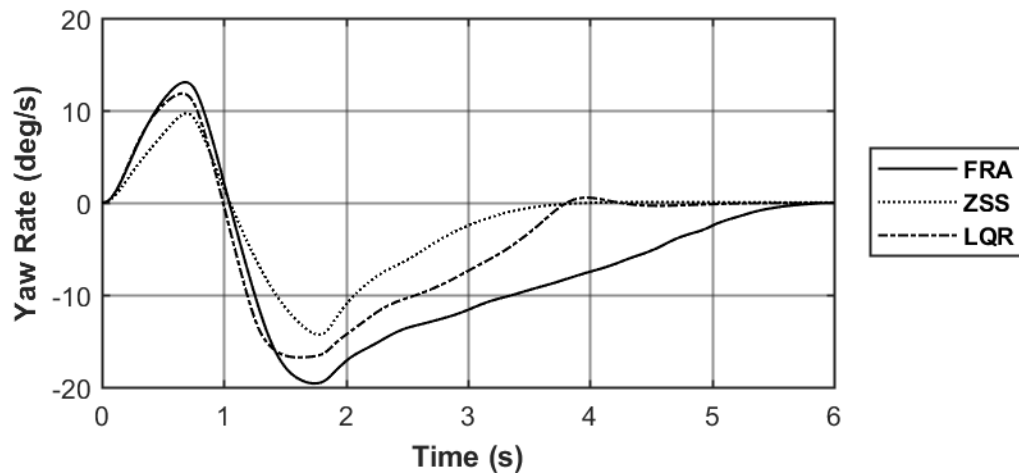
Figure 5-63 Yaw Rate: FMVSS 126 ESC at 60 km/h over μ=0.35
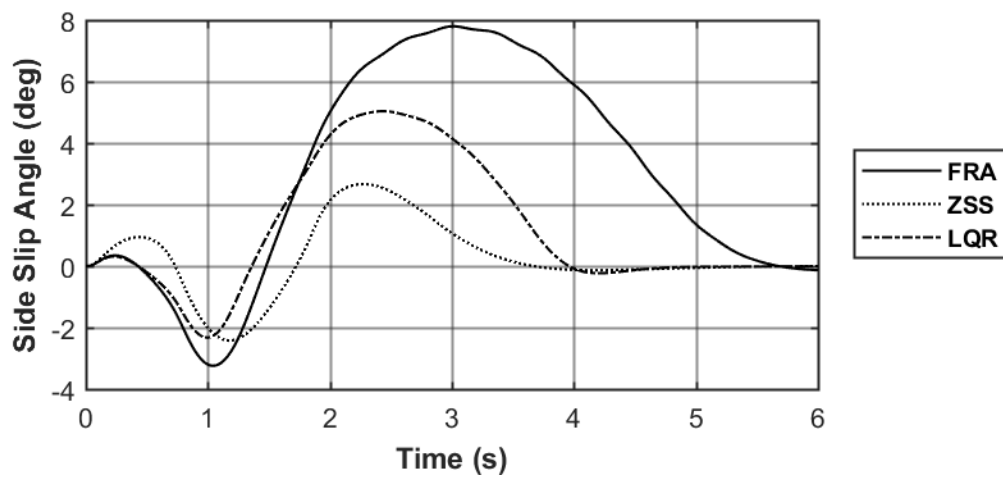
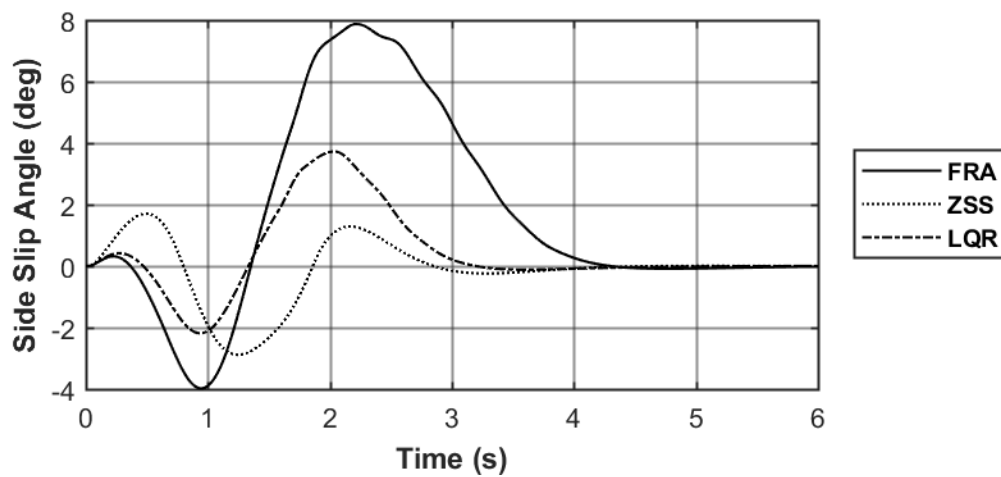**Figure 5-64 Side Slip Angle: FMVSS 126 ESC at 60 km/h over μ=0.35**
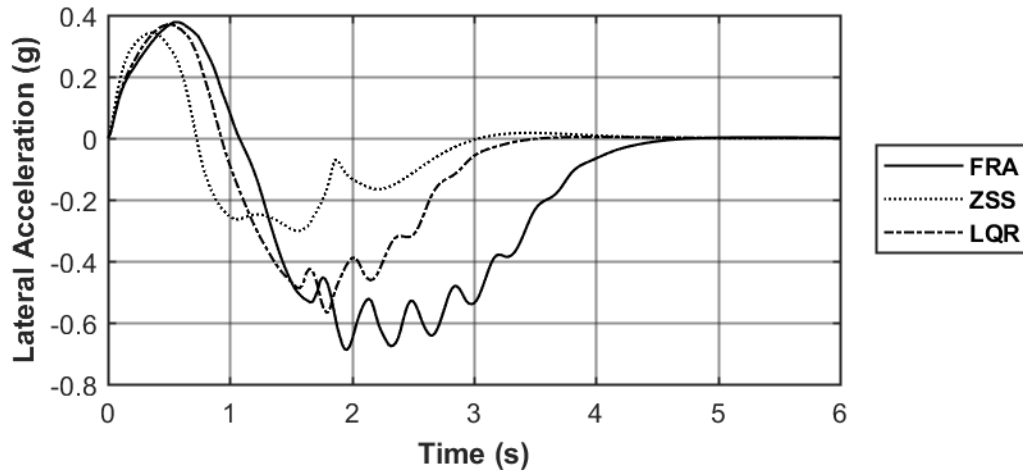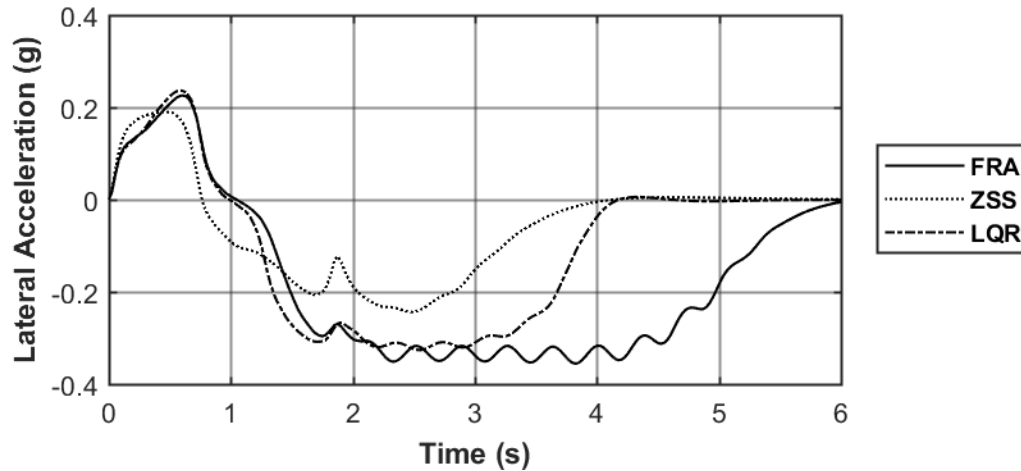
Figure 5-65 Lateral Acceleration: FMVSS 126 ESC at 60 km/h over μ=0.35

When comparing the yaw rates of the different controller configurations in Figure 5-63 the LQR controller dampens the yaw rate better than the conventional vehicle. This allows the LQR vehicle to gain directional stability quicker. The ZSS vehicle has a better response, returning to steady state sooner than the conventional and LQR vehicles. The ZSS controller reduces the sideslip angle (Figure 5-64) as it is designed to, but results in a lower yaw rate and lateral displacement. The LQR and conventional vehicles both have large sideslip angles, around five and eight degrees respectfully, which is not ideal as it is generally more difficult to regain directional stability over a low friction surface.

5.4.1.4   80 km/h – μ=0.35
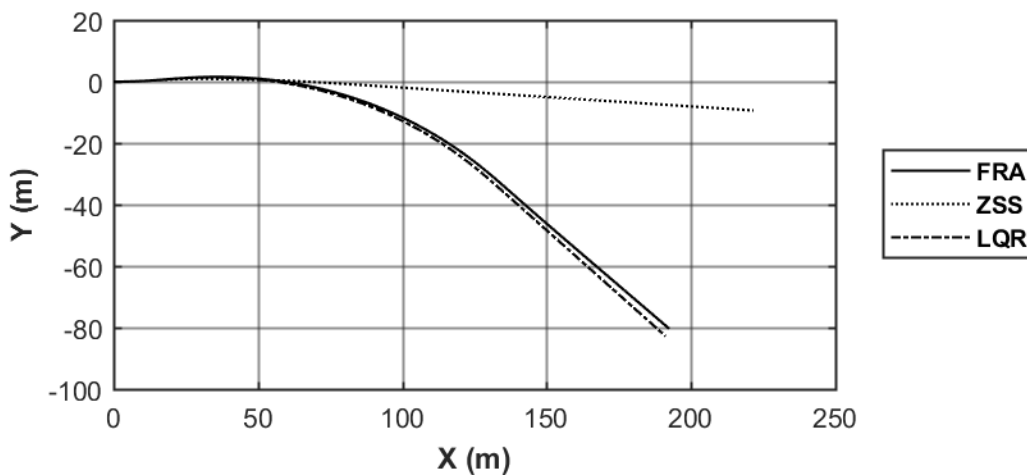
Figure 5-66 Vehicle Trajectory: FMVSS 126 ESC at 80 km/h over μ=0.35
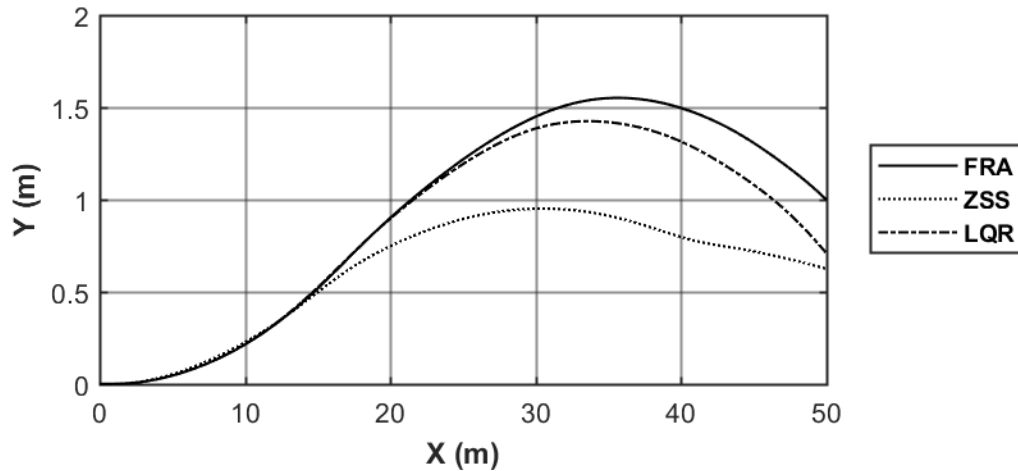
Figure 5-67 Vehicle Lateral Displacement: FMVSS 126 ESC at 80 km/h over μ=0.35
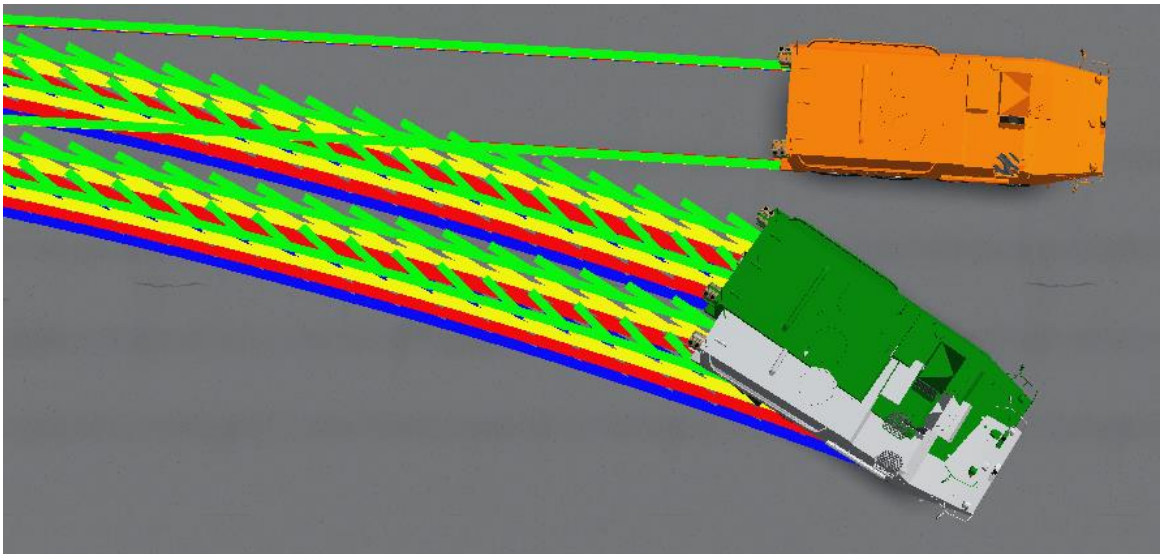
Figure 5-68 Simulation Results: FMVSS 126 ESC at 80 km/h over μ=0.35

Figure 5-68 shows the LQR (grey) and FRA (green) vehicles drifting while the ZSS vehicle (orange) is able to maintain stability over low friction surface at high speeds.

At 80 km/h over a low friction surface, the trajectories of the LQR and FRA vehicles (Figure 5-66) are very similar, despite the extended rear axle steering output seen in Figure 5-69. The direct relationship for the ZSS rear axle steering to the steering input results in better response even at high speeds, which reduces the lateral displacement due to the reduction of vehicle performance measures below.
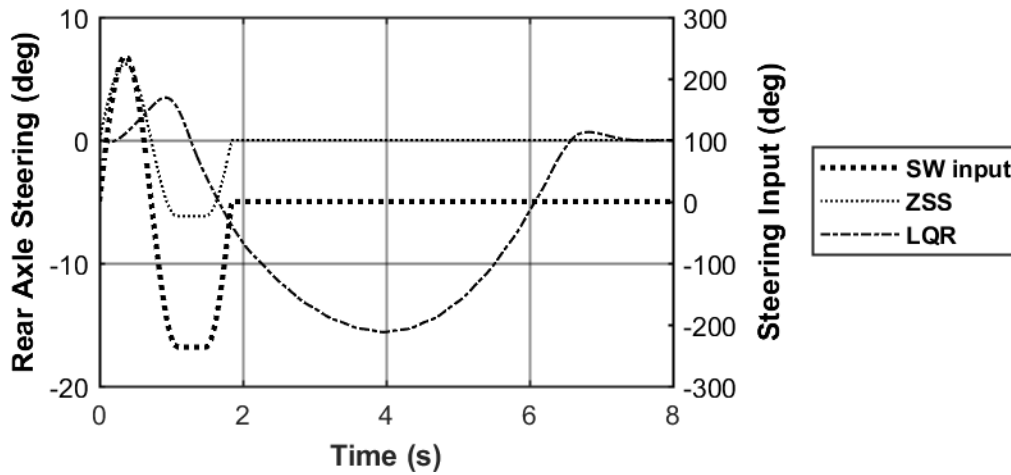
Figure 5-69 Rear Axle Steering Angle: FMVSS 126 ESC at 80 km/h over μ=0.35
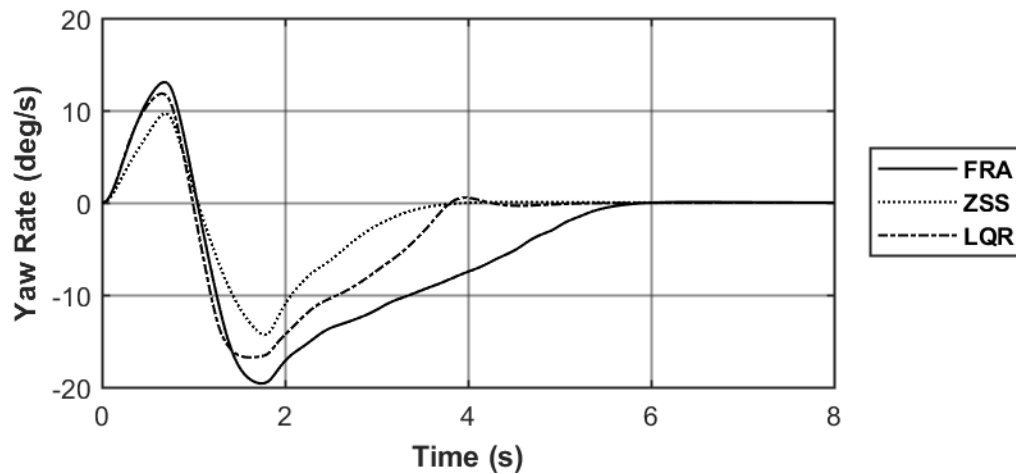
Figure 5-70 Yaw Rate: FMVSS 126 ESC at 80 km/h over μ=0.35
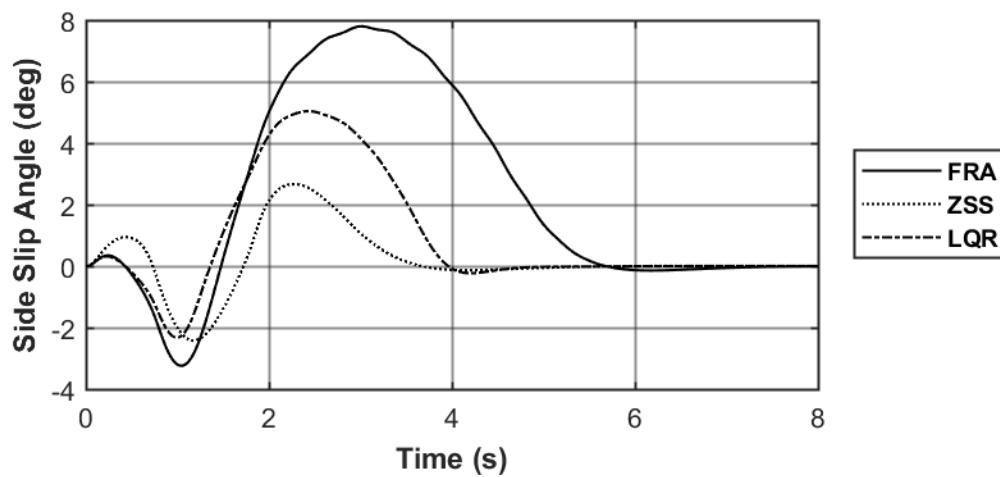
Figure 5-71 Side Slip Angle: FMVSS 126 ESC at 80 km/h over μ=0.35
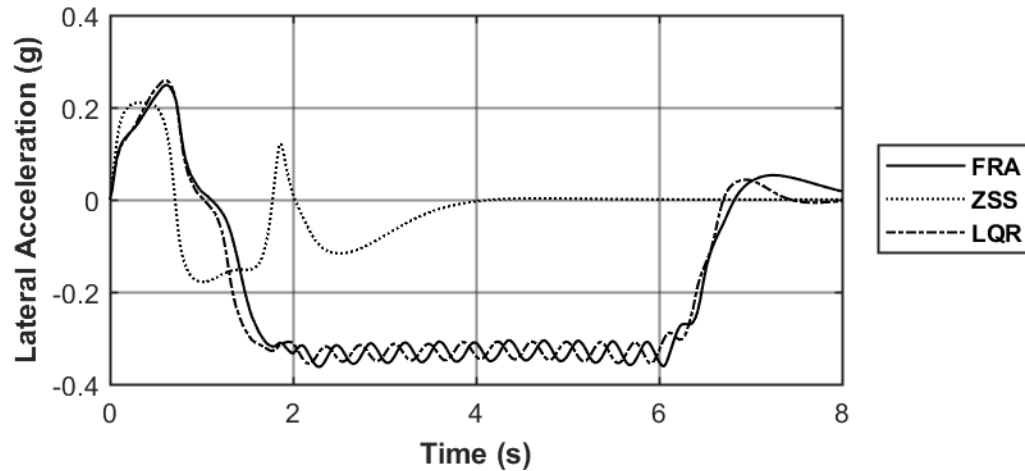
Figure 5-72 Lateral Acceleration: FMVSS 126 ESC at 80 km/h over μ=0.35

Despite the decrease in amplitude of the ZSS vehicle performance measures, the behaviour of the vehicle is not ideal in an emergency maneuver. The LQR controller manages to decrease the settling time of the yaw rate (Figure 5-70), side slip angle (Figure 5-71), and the lateral acceleration (Figure 5-72). The similar lateral displacement seen between the LQR and the conventional vehicle and the decreased settling time by the LQR vehicle suggest the LQR controller performs ideally over low friction surface at high speeds.

5.4.1.5   FMVSS 126 ESC lateral displacement summary

Table 5-3 FMVSS 126 Maximum Lateral Displacement

	High Friction Surface 80 km/h	Low Friction Surface 80 km/h	High Friction Surface 60 km/h	Low Friction Surface 60 km/h
FRA	2.420m	0.797m	1.833m	0.722m
ZSS	1.400m	0.575m	1.454m	0.577m
LQR	1.954m	0.748m	1.595m	0.688m

The overall maximum lateral displacement has an expected trend with proper assumptions of rear axle behaviour for the controlled vehicles. At both 80 and 60 km/h it is expected the rear axle will steer in the same direction as the front axle, therefore the lateral displacement is expected to be less than the conventional vehicle with the same steering input. The rear axle steered vehicles require more steering input to achieve the same lateral displacement as the FRA vehicle

The conventional vehicle has the highest lateral displacement for all scenarios and ZSS has the least lateral displacement for all scenarios. At lower speeds the ZSS controller actually increases its lateral displacement, while the FRA and LQR vehicles decrease the lateral displacement. This is due to the rear steering angle of the ZSS vehicle decreasing as speed decreases.

The FMVSS 126 criterion requires an ESC equipped vehicle to have a lateral displacement of at least 1.22 meters when operating at 80.5 km/h for a vehicle with a GVWR of greater than 3500 kg at 1.07 seconds after the initiation of the steering input [79]. This time is chosen as it is the start of the dwell and is generally easy to identify in field testing. The following table will provide the lateral displacement at 1.07 seconds.

Table 5-4 FMVSS 126 Lateral Displacement at 1.07 seconds

	High Friction Surface 80 km/h	Low Friction Surface 80 km/h	High Friction Surface 60 km/h	Low Friction Surface 60 km/h
FRA	1.792	0.642	1.533	0.605
ZSS	1.291	0.527	1.319	0.5263
LQR	1.648	0.527	1.437	0.596

Over the high surface at 80 km/h, all vehicles pass the FMVSS criteria with a lateral displacement of greater than 1.22 meters.

The LQR controller performs ideally in this situation by passing the lateral displacement measures and returning the vehicle to steady state quicker than the conventional vehicle. This is important in high speed situations when lesser amounts of time can result in the difference between a safe maneuver and an accident. The ZSS controller provides the least lateral displacement but, in every scenario, decreases the magnitudes of the yaw rate, sideslip angle and lateral acceleration which could be interpreted as beneficial.

5.4.2 Double Lane Change (DLC)

The NATO AVTP 03-160 W lane change test consists of a lane change with a quick return to original lane. The results from this maneuver are used to analyze the transient lateral dynamics of a vehicle. The maneuver will be completed at the speeds of 60 km/h and 80 km/h to assess the stability of the vehicle as well as the ability to complete the maneuver without hitting the cones. This maneuver will only be performed over high friction surface (μ=0.85) as it is unlikely to see this type of maneuver over low friction surfaces.
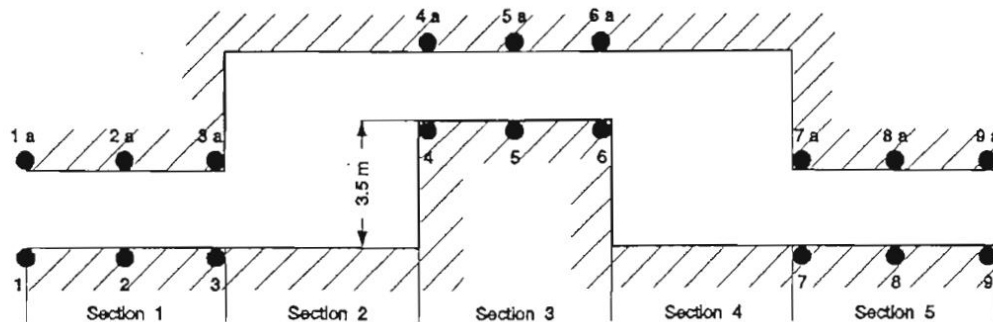
Figure 5-73: NATO AVTP 03-160 W lane change course [76]

> Section 1: Length = 15 m (49.2 ft)
>   Width = 1.1 * vehicle width + 0.25 m (0.82 ft)
> Section 2: Length = vehicle length + 24 m (78.72 ft)
>   Width = 3.5 m (11.48 ft) + Section 3 width
> Section 3: Length = 25 m (82 ft)
>   Width = 1.2 * vehicle width + 0.25m (0.82 ft)
> Section 4: Length = vehicle length + 24 m (78.72 ft)
>   Width = 3.5 m (11.48 ft) + Section 3 width
> Section 5: Length = 15 m (49.2 ft)
>   Width = 1.1 * vehicle width + 0.25 m (0.82 ft)

The lane change course as seen in Figure 5-73 includes three sections for the vehicle to pass through. The lane change width is 3.5 meters and the distance between the cones is determined by the effective length of the vehicle plus 24 meters. This course has been adapted into a path following maneuver in TruckSim© as seen in Figure 5-74. This path uses a sine curve to meet the centerline of the cones.
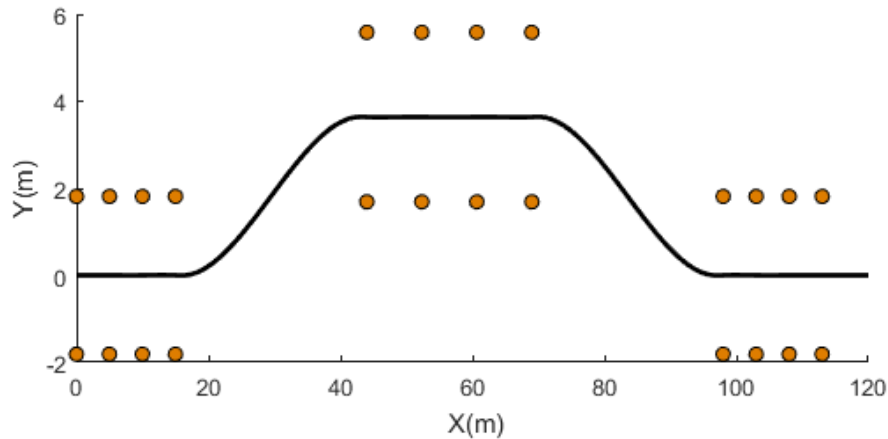
Figure 5-74: NATO AVTP 03-160 W lane change course (Path in TruckSim©)

The NATO double lane change is used to analyze the transient performance of the vehicle as well as performance based on completeness while avoiding the cone layout.

NOTE: The maneuver within TruckSim© is a path following maneuver where the path is the center of the cones with a ½ sine curve connecting the paths in between the lane changes. Even if the maneuver is a failure due to interaction with the cones, the relevant data can still be compared against one another. The driver model for all of these simulations is identical, meaning the preview time and decision algorithm are the same for each vehicle. Identical paths will be used rather than altering the path to follow for each independent vehicle and will represent a driver that is familiar with the conventional vehicle .
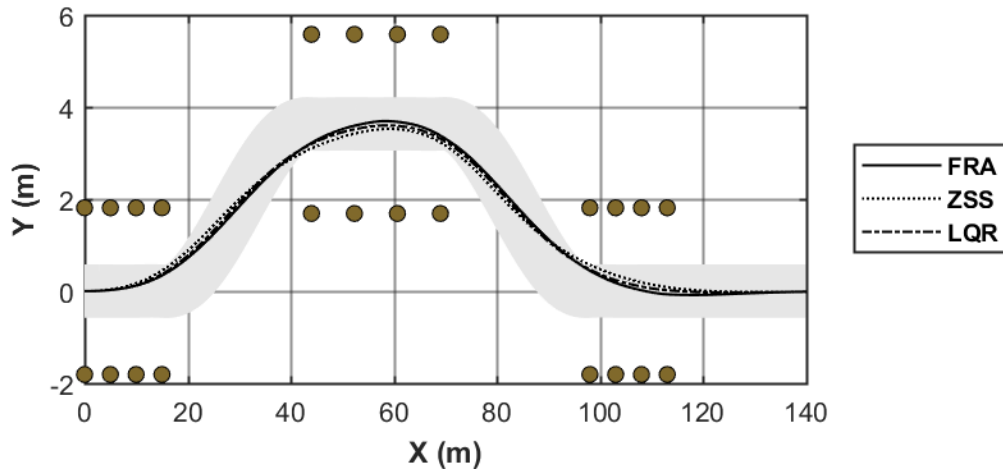
Figure 5-75 Vehicle Trajectory: NATO double lane change 80km/h over μ=0.85

| (a) | (b) | (c) |
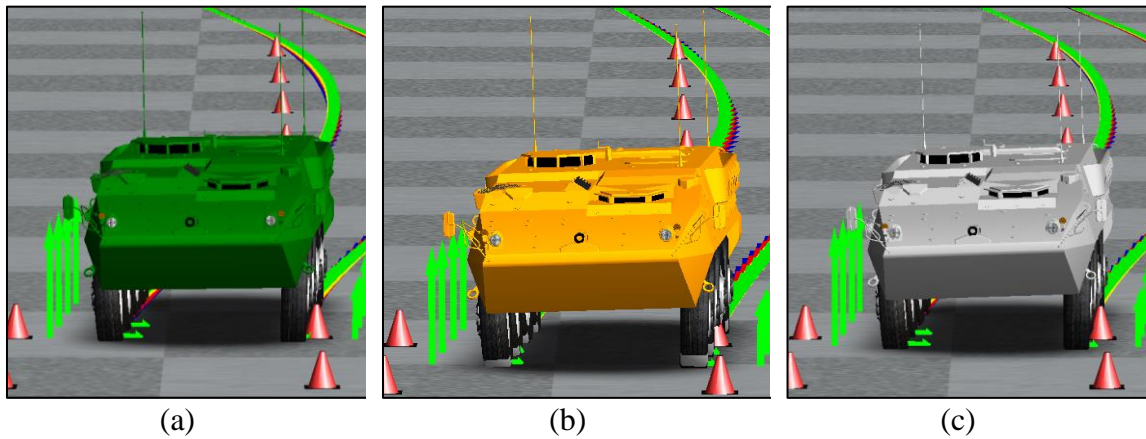
Figure 5-76 Failure point for NATO DLC on conventional vehicle (a), ZSS vehicle (b), LQR vehicle (c)

The results show that all vehicles fail the NATO double lane change at 80 km/hr over high friction surface (Figure 5-76). There is not a major deviation from the course, however upon close inspection it can be seen that the ZSS vehicle fails the maneuver with the most interference with the cones (Figure 5-76(b)). All vehicle configurations managed to stay in a reasonable speed range (Figure 5-78), decreasing only 0.7 km/h. Since this maneuver is based on a path following maneuver in TruckSim©, Figure 5-74, and a simple driver model, the interaction with the cones should not be interpreted as a complete fail.
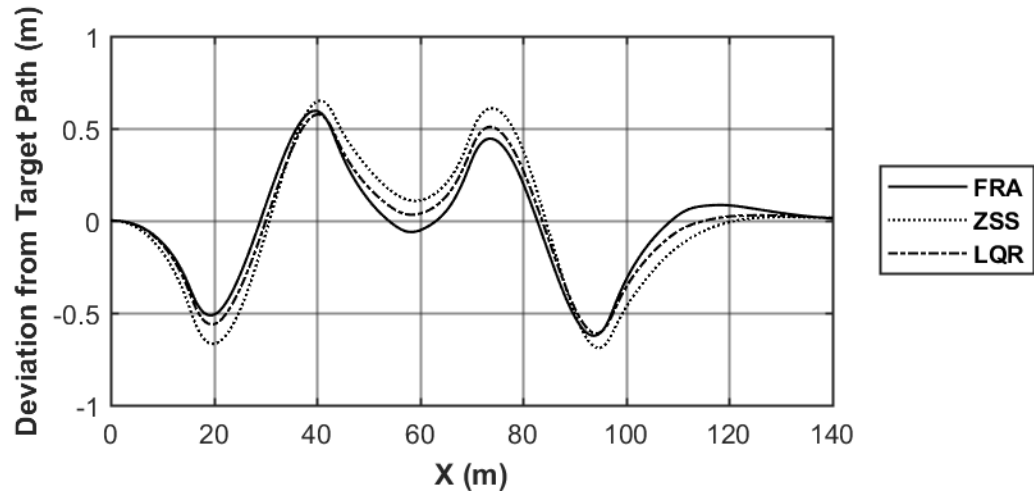
Figure 5-77 Lateral Deviation from Target Path: NATO double lane change 80km/h over μ=0.85
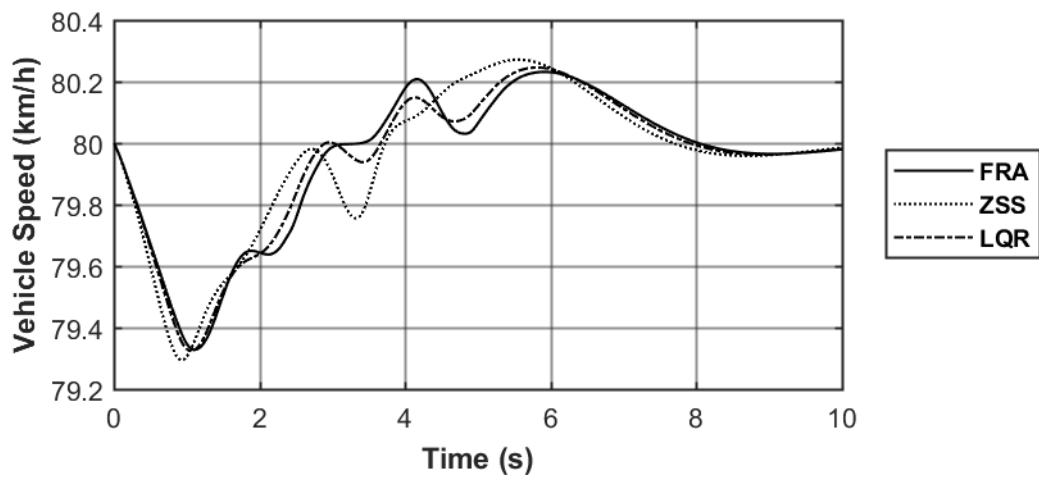
Figure 5-78 Vehicle Speed: NATO double lane change 80km/h over μ=0.85
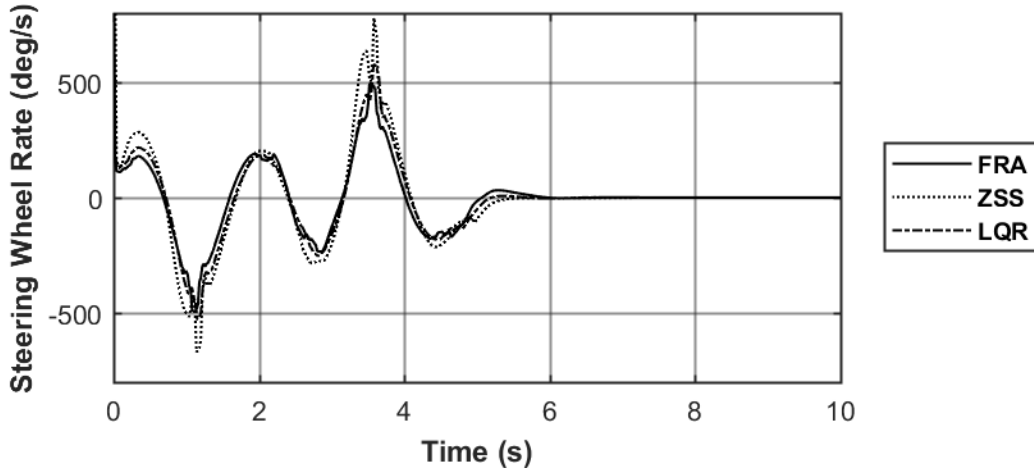
Figure 5-79 Steering Wheel Rate: NATO double lane change 80km/h over μ=0.85
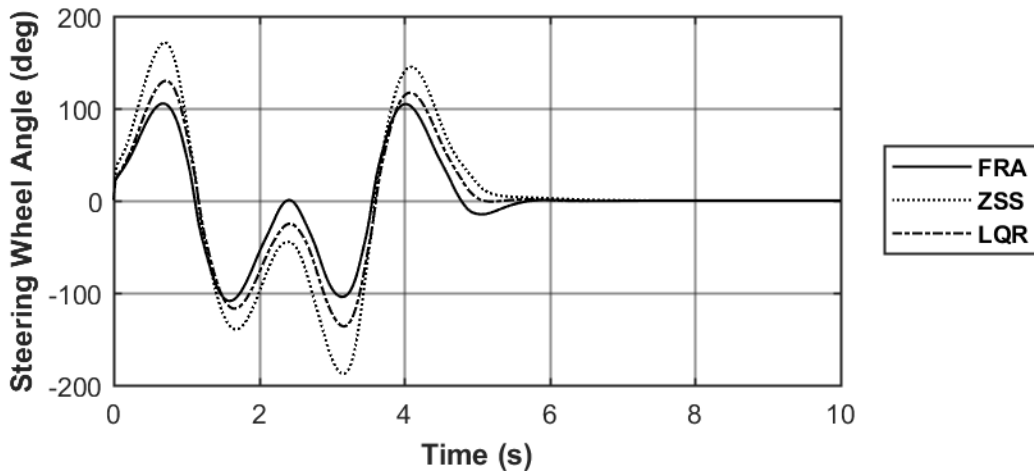
Figure 5-80 Steering Wheel Input: NATO double lane change 80km/h μ=0.85

The steering wheel rates (Figure 5-79) for all of the controller configurations are similar. The ZSS controller requires the largest steering wheel rate of around 778 deg/s, which is also a result of a required increase in steering wheel input for ZSS seen in Figure 5-80. This is a much higher steering wheel rate than the conventional vehicle which has a maximum steering wheel rate of just below 500 deg/s. The LQR controlled vehicle reaches a peak of approximately 576 deg/s. This is much lower than the maximum steering wheel rate of 1819 deg/s over a maximum one second duration discussed in [77]. Large steering wheel rates demand a lot from a driver, especially with larger vehicles which require heavier steering input. Smaller steering wheel rates will be less fatiguing for the driver which makes the ZSS controller not desirable at higher speeds.
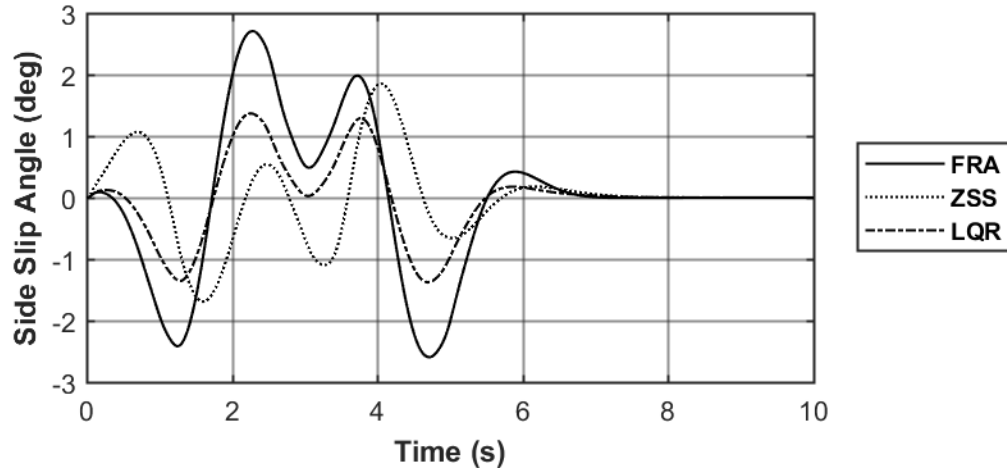
Figure 5-81 Side Slip Angle: NATO double lane change 80km/h over μ=0.85
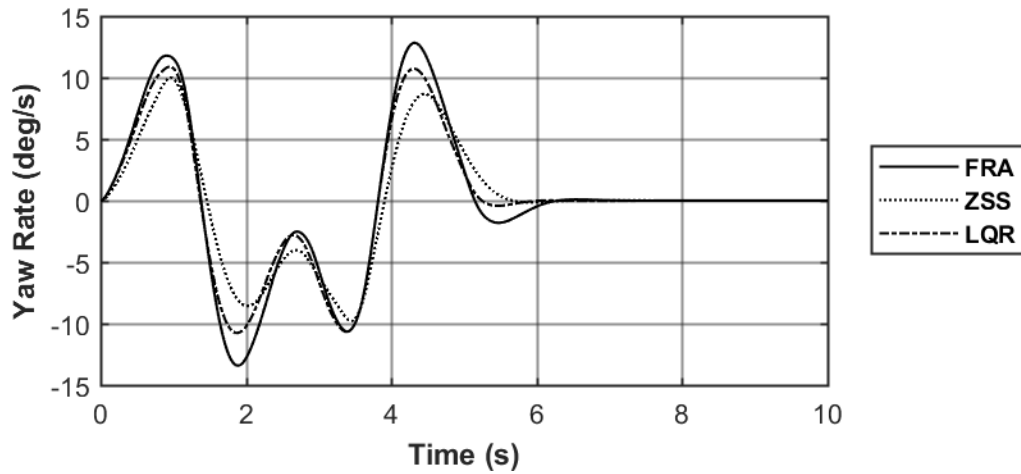
Figure 5-82 Yaw Rate: NATO double lane change 80km/h over μ=0.85

The sideslip angles and the yaw rates of the vehicles are as expected. The conventional vehicle sees the highest sideslip angle (Figure 5-81) as well as the highest yaw rate (Figure 5-82). The maximum sideslip angle is below three degrees for all vehicles which is within an acceptable performance range. The sideslip angle of the LQR vehicle is minimized the most which promotes better performance. The lateral accelerations of all vehicles are all within range which does not promote rollover (Figure 5-83).
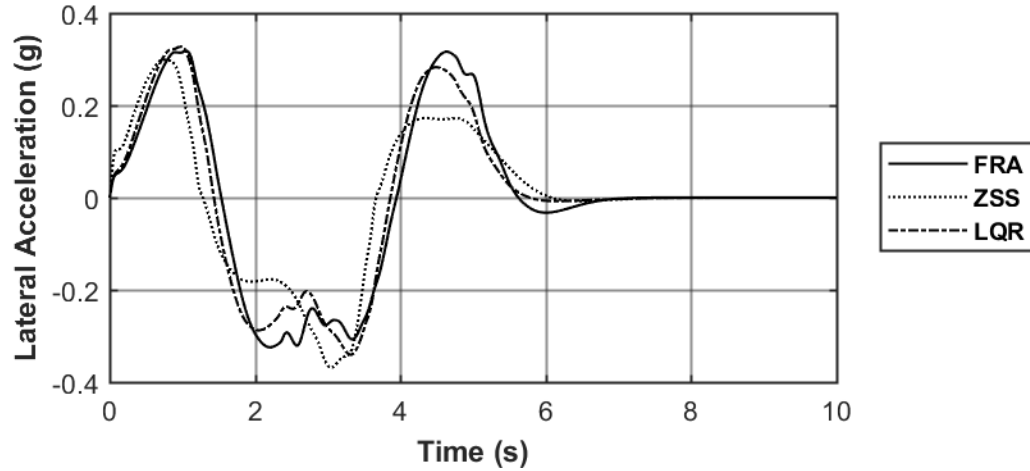
Figure 5-83 Lateral Acceleration: NATO double lane change 80km/h over μ=0.85
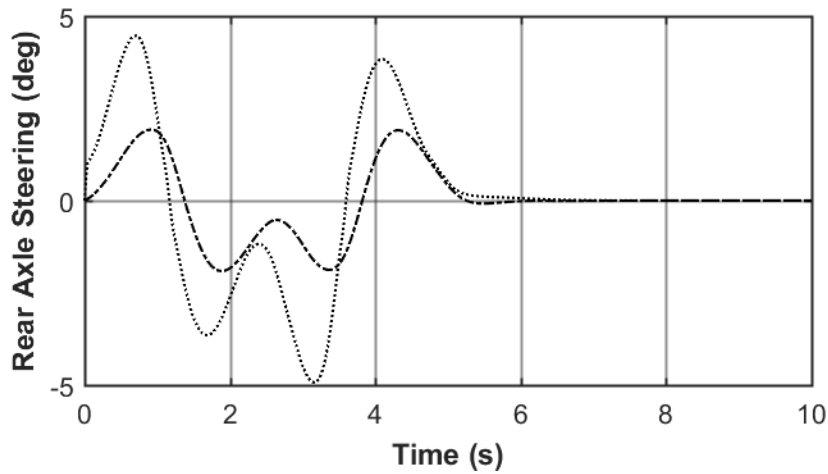
Figure 5-84 Rear Axle Steering: NATO double lane change 80km/h μ=0.85

The rear axle steering output from the ZSS controller is directly related to the speed and steering wheel angle. At a relatively constant speed, the ZSS steering output is directly proportional to the steering wheel angle. The LQR controller includes a time delay which offsets the physical steering of the rear axle (Figure 5-84). The LQR controller outputs a much smaller rear steering angle of just below two degrees than the five degrees the ZSS controller outputs. This extra steering of the rear axle in the direction of the front axle results in higher steering input required for the ZSS vehicle. This directly results in the higher steering wheel rate discussed earlier in this section.
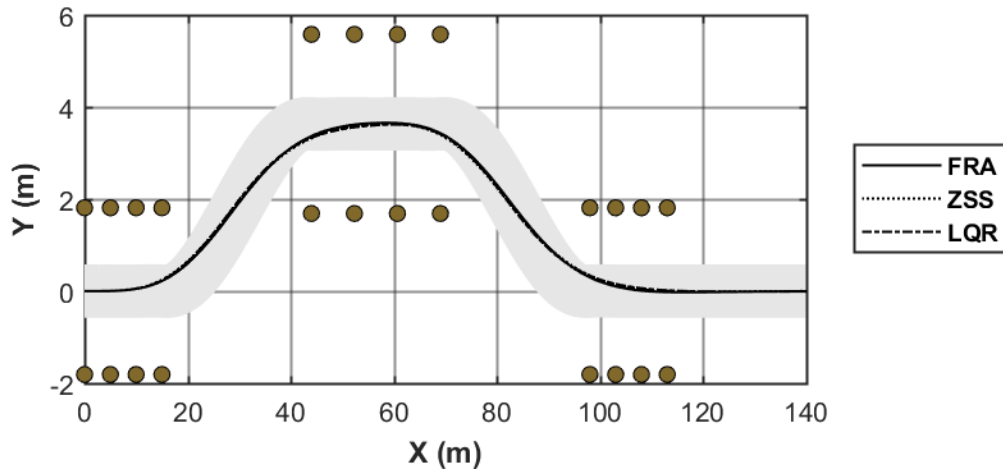
Figure 5-85 Vehicle Trajectory: NATO double lane change 60km/h µ=0.85
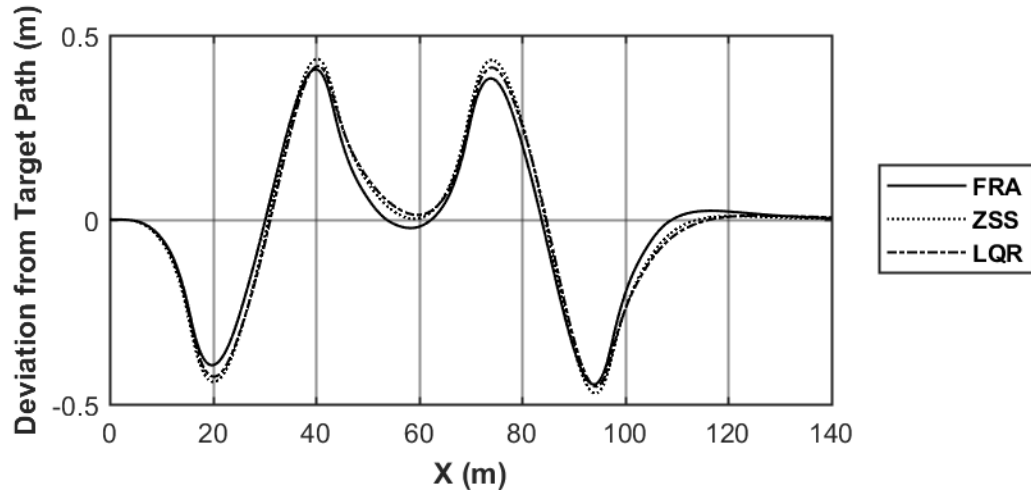
Figure 5-86 Lateral Deviation from Target Path: NATO double lane change 60km/h over µ=0.85

When reviewing the simulation, all vehicles passed the NATO DLC at 60 km/h by not interfering with the cones. The paths of the vehicles are very similar (Figure 5-85) and all stayed within an acceptable range of speed (Figure 5-87).
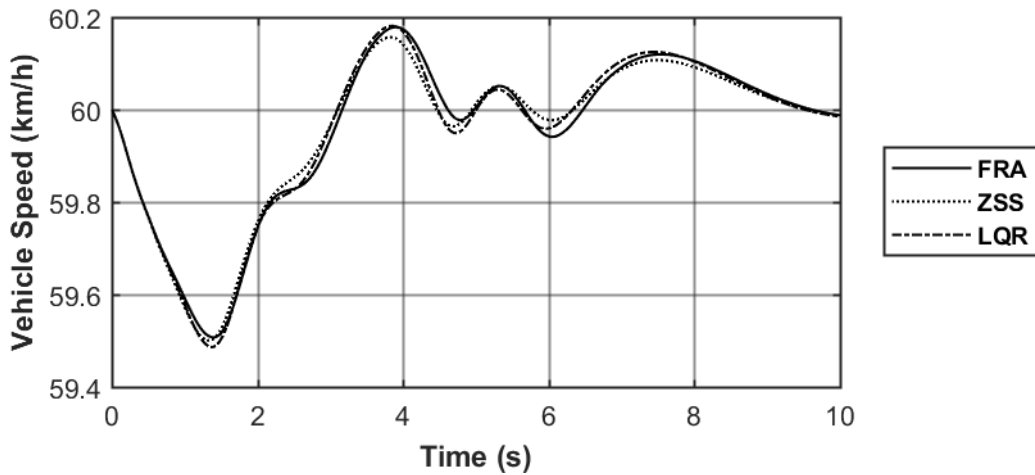
Figure 5-87 Vehicle Speed: NATO double lane change 60km/h μ=0.85
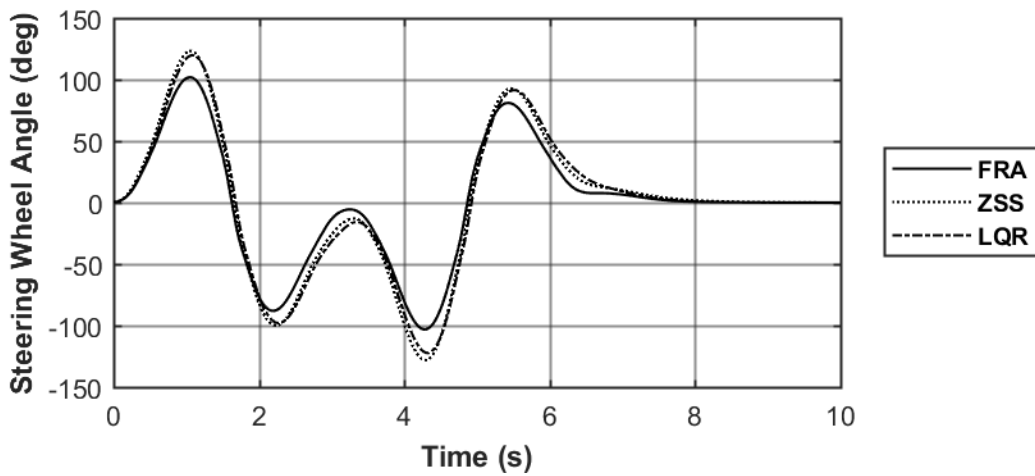
Figure 5-88 Steering Wheel Input: NATO double lane change 60km/h over μ=0.85
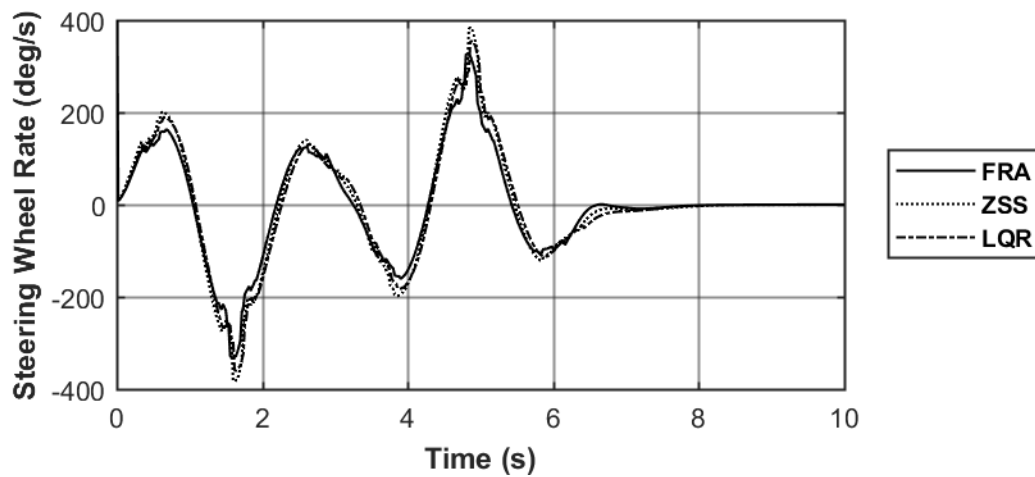
Figure 5-89 Steering Wheel Rate: NATO double lane change 60km/h over μ=0.85

The steering wheel rates for all vehicles are within acceptable range (Figure 5-89) with ZSS seeing the highest rate, same as during the 80 km/ hr simulation. This is due to higher steering input required (Figure 5-88) because of higher rear axle steering angle output from the ZSS controller in the same direction as the front wheels (Figure 5-93)
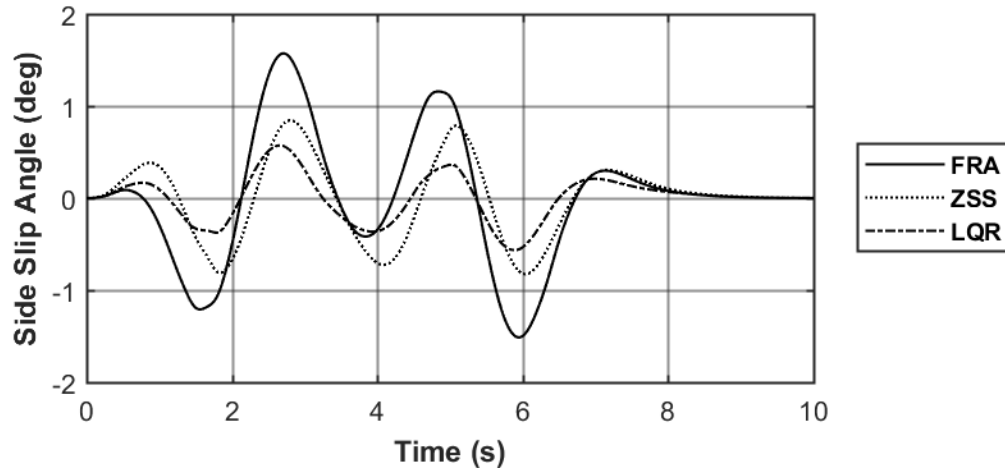
Figure 5-90 Side Slip Angle: NATO double lane change 60km/h over μ=0.85
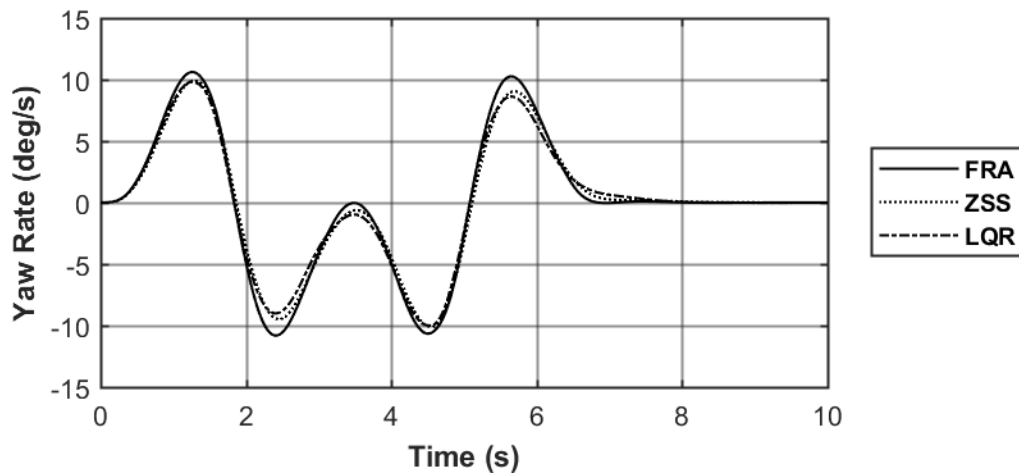
Figure 5-91 Yaw Rate: NATO double lane change 60km/h over μ=0.85
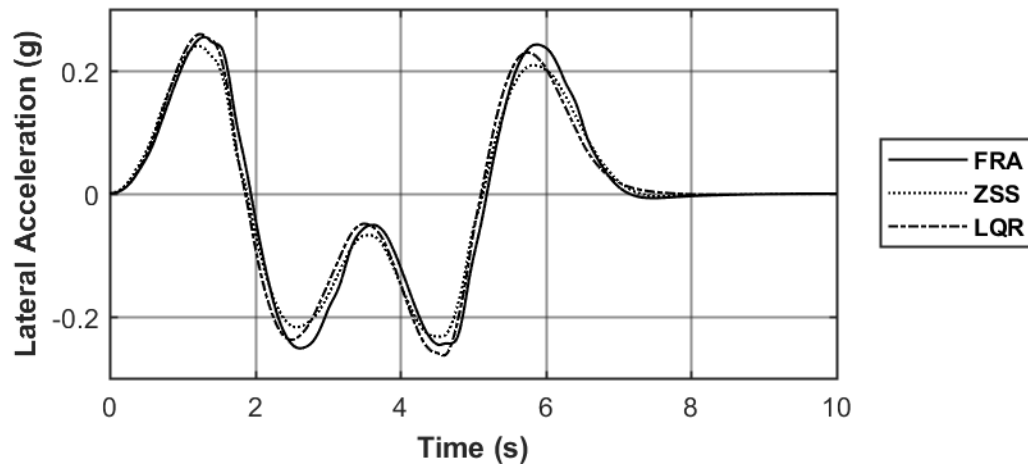
Figure 5-92 Lateral Acceleration: NATO double lane change 60km/h over μ=0.85

The LQR and ZSS controlled vehicles show handling improvements with resulting lower sideslip angles than the conventional vehicle (Figure 5-90) as well as slightly lower yaw rate and lateral acceleration peak values (Figure 5-91, Figure 5-92). The LQR controller was able to minimize the sideslip angle to a peak amplitude of 0.55 degrees and slightly reduce the yaw rate compared to the ZSS controller. This is completed with slight increased RAS output on the first, second and fourth peaks by the LQR controller compared to the ZSS controller (Figure 5-93).
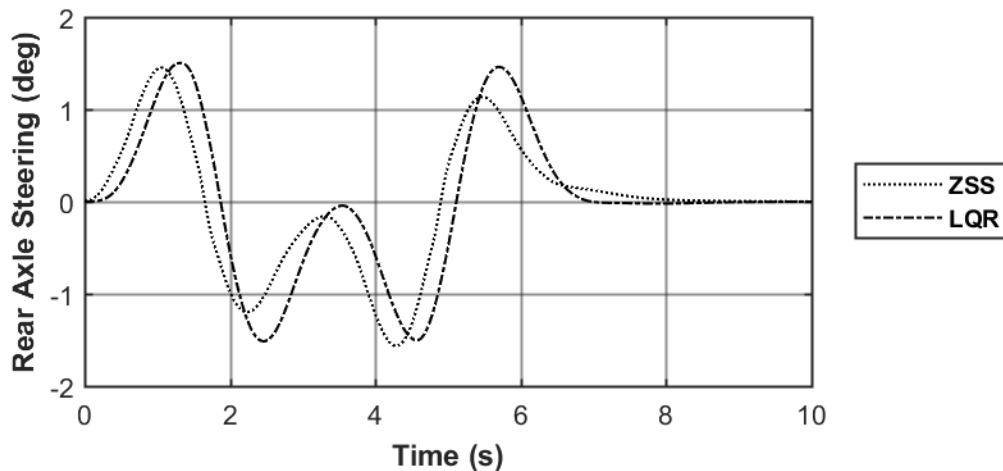
Figure 5-93 Rear Axle Steering: NATO double lane change 60km/h over μ=0.85

5.5   SUMMARY OF CHAPTER

The overall performance of the controllers defines the best performing control setup for low, high and the transition speed. For low speed turning maneuvers, it is ideal to have high maneuverability which results from a high yaw rate and high rate of yaw rate generation. This was achieved best by the ZSS controller. The objective controlling the vehicle at a high speed is to increase the stability. This is achieved by steering the rear axle in the same direction as the front axles. Both the ZSS and the LQR controllers use this method when steering at higher speeds. The ZSS controller is much more responsive as it is a direct relationship between the steering of the front axle and the rear axle. The LQR controller calculates the necessary steering angle for the rear axle in addition to including a time delay. This allows for the rear axle steering angle to respond to the current vehicle state rather than input the steering angle without any vehicle performance input.

5.5.1   Low Speed Simulation Conclusions

The maneuver completed for the low speed simulation was the constant step slalom with 15-meter cone spacing over high friction surface. Performance at 20 km/h and the maximum achievable speed was analyzed. It was determined that the LQR controller was not practical for increasing the maneuverability at low speeds. The ZSS controller implemented the rear axle steering to successfully increase the maneuverability of the vehicle by steering the rear axle strategically in the opposite direction of the front axle. The ZSS controller did not perform well for the tight maneuver at 32 km/h, resulting in oversteer and over correcting by the driver model which caused saturation of the steering input.

- LQR controller is not ideal for increasing the maneuverability of the vehicle at low speeds.
- ZSS controller using direct feed-forward steering input to rear axle steering angle results in increased maneuverability for the speed of 20 km/h. The feed-forward controller however did not perform well as the speed was increased over 30 km/h.
- The ZSS vehicle performed the best over low friction surface, achieving the highest speed without losing control.

- The conventional (FRA) vehicle and the LQR vehicle performed similarly with the FRA vehicle completing the course at a maximum 32 km/h and the LQR vehicle completing the course at 31 km/h. The decrease in lateral acceleration, yaw rate, and sideslip angle are either not noticeable, or negligible. This suggests that around the speed of 30 km/h the conventional vehicle has the most desirable behaviour by maintaining stability while having comparable performance measures to the controlled vehicles.

5.5.2 Low-Medium Speed Transition Conclusions

To analyze the vehicle response during the speed transition, a modified J-turn maneuver was used. This was a steering input based on the steering measurement of the physical vehicle completing a 75-foot (22 meter) J-turn at 40 km/h. The 100 ft radius constant acceleration test is used to assist in defining the speed transition behaviour. By analyzing the lateral accelerations and the path tracked by the different vehicle configurations, conclusions can be made for the performance at mid-range speeds.

- Over high friction surface, the ZSS controller has the tightest turning radius with the same steering input. This is a result of the contra-steer that ZSS controller induces at 40 km/h. This also results in the ZSS controlled vehicle to experience oversteer rather than the understeer experienced by the conventional and LQR vehicles. The LQR controller increases the radius by steering the rear axle in the same direction as the front axle.
- The LQR reduces the lateral acceleration and yaw rate slightly over the conventional vehicle as a result of the increase turning radius. The sideslip angle is also reduced, inducing more understeer than the conventional vehicle is already experiencing.
- Over the low friction surface all vehicles are experiencing oversteer, with the ZSS experiencing up to seven degrees of sideslip angle. The LQR controller is effective at reducing the sideslip behaviour over low friction surface with a peak sideslip angle of just less than two degrees.

- The yaw lateral acceleration and yaw rates of the different vehicles over low friction surface all behave as expected when analyzing the trajectories. The ZSS vehicle has a slightly tighter turning radius resulting in a higher yaw rate and lateral acceleration. The LQR has the larges turning radius and results in the lowest lateral accelerations and yaw rates.

- The LQR controller provides a low side slip angle when the steering is at steady state during the 100-ft constant radius acceleration simulation which occurs close to 50 km/h. This suggest the LQR controller is more appropriate when the speed increases.

- The ZSS vehicle provides the lowest sideslip angle at lower speeds and as the speed increases during the 100-ft radius constant acceleration maneuver, the rear axle steering input reduces until the performance is similar to the conventional vehicle due to low rear axle steering angle.

5.5.3 High Speed Testing Results

Two simulations were used to test the vehicle controller configuration performance at higher speeds of 60 km/h and 80 km/h. The FMVSS 126 ESC maneuver is an emergency steering input which simulates a driver avoiding an obstacle as speed. The best results for this maneuver is high lateral displacement while still remaining in control. The second maneuver is a path following double lane change maneuver that is good for analyzing the transient response of the vehicle to a typical maneuver.

- At the speeds selected for this simulation (60 km/h and 80 km/h) both the ZSS and LQR controlled vehicles steer the rear axle in the same direction as the front axle typically reducing the lateral acceleration, yaw rate and sideslip angle compared to the conventional fixed rear axle vehicle.

- The conventional vehicle as the baseline vehicle performed as a production vehicle should. The lateral displacement is reasonable (higher than requirements for FMVSS 126 ESC standards [79]), and the vehicle remains stable. The conventional vehicle tends to take longer than the other controllers to reach steady state after the steering returns to zero.

107

- The rear axle steering of the ZSS vehicle is directly related to the steering wheel input. This leads to a more responsive steering of the rear axle compared to the LQR controller. When the steering input returns to zero, so does the rear axle steering, which results in a local peak of the lateral acceleration even over low friction surfaces. The responsiveness for the feed-forward controller leads to the smallest sideslip angles as well as the lowest yaw rates and lateral accelerations.

- The DLC simulation shows the conventional FRA vehicle requires the least steering input out of the vehicles and has the least deviation from the target path. This could be due to the driver model being tuned for the conventional vehicle.

- The LQR controlled vehicle has the most reduced sideslip angle for both the 80 km/h and 60 km/h DLC maneuver. The steering input is increased slightly from the ZSS vehicle.

- The ZSS controller shows the lowest lateral acceleration magnitude for both speeds in the DLC maneuver. This is likely due to the responsiveness of the controller.

- Despite the FRA vehicle having the best performance measures in terms of steering input and deviation from the target path, there has to be some consideration for the gains in stability from these controllers at high speed.

5.5.4 Overall Conclusions

Overall the ZSS controller is suitable for increasing the maneuverability of the 8x8 combat vehicle at low speeds. The ZSS controller requires less steering input than the FRA and LQR vehicles which makes the vehicle more maneuverable by increasing the yaw acceleration with less input from the driver. Neither the LQR or ZSS prove any benefit over the conventional vehicle during mid-range speed maneuvers (30-40 km/h). The LQR controller performs the best at higher speeds by having a good compromise for the lateral displacement achieved with the FRA vehicle and the stability resulting from the ZSS controller during the FMVSS 126 ESC steering wheel input maneuver. The LQR controller also assists in the vehicle handling more neutral than either oversteer or understeer during the steady state portion of the 100-ft radius constant acceleration and the higher speed DLC

maneuvers. At higher speeds a lower yaw rate is also seen which is desired for drivers in training.

From these results it is suggested the ZSS controller be adopted for lower speeds from 0-30 km/h to increase the maneuverability at lower speeds when the likely hood of low radius turns is higher and losing control is less likely. The conventional vehicle performs well between 30-45 km/h and should be adopted for these speeds. The LQR reduces the yaw rate and lateral accelerations at higher speeds and should be included in the final design of the controller for speeds above 45 km/h.

CHAPTER 6

ROLLOVER PREVENTION AND EXTERNAL DISTURBANCE MANAGEMENT

Rollover of a vehicle is highly dependent on the lateral acceleration of the vehicle. The results from the simulations in Chapter 5 determine that lateral accelerations are reduced by the control of the rear axles steering at higher speeds. Since the previous section did not cause rollover, this chapter will present a severe steering input that causes rollover for the conventional vehicle. In the literature review it was discussed that active steering can assist in dampening the effects of external resistance. The external resistance will be provided by a crosswind as this is one of the issues that effects vehicles that have a high center of gravity and a large side profile.

6.1 ROLLOVER AVOIDANCE – FISHHOOK MANEUVER

To appropriately demonstrate the effectiveness of the rear axle steering ROM system, conditions need to be set that cause rollover on the conventional vehicle. The maneuver used is a fishhook steering input, seen in Figure 6-1, and similar to the FMVSS 126 ESC except with steep steer input to 294 degrees rather than a sinusoidal steering input.
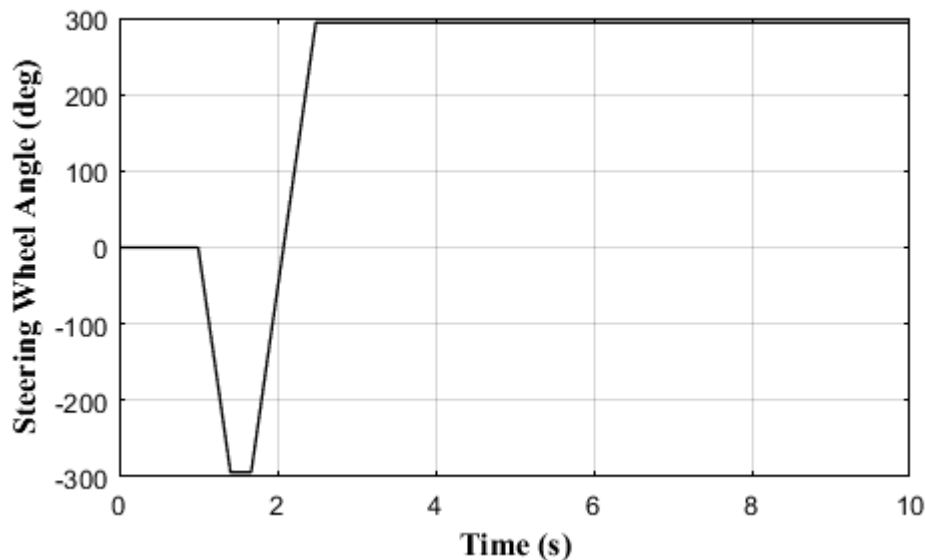
Figure 6-1 Fishhook steering wheel input

The surface friction for this simulation is 0.95 to represent a high friction surface such as concrete. Rollover is more likely over a high friction surface. This test will be performed at 60 km/h, until one second into the simulation (when the steering input is initiated), when the throttle will be released, and the vehicle will be placed in neutral.

The term introduced in this section is the Load Transfer Ratio (LTR), which was briefly discussed in the literature review. This term describes the ratio of the load on each side of the vehicle. An LTR with a magnitude of one describes a vehicle that has all of its load on one side, otherwise known as rollover.

6.1.1   Fishhook Results – 60 km/h, μ=0.95
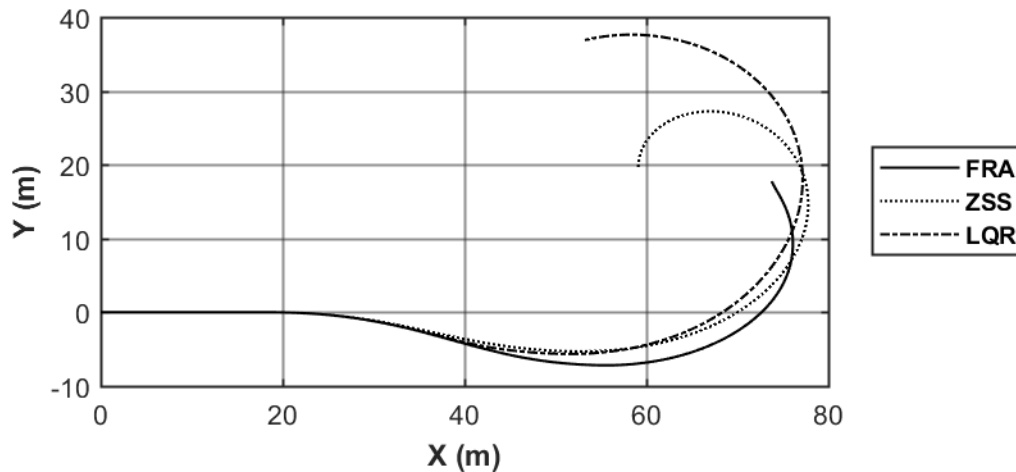
Figure 6-2 Vehicle Trajectory: Fishhook at 60 km/h over μ=0.95

In this fishhook maneuver at 60 km/h over a high friction surface, the conventional vehicle reaches a rollover condition as seen by the FRA vehicle rolling in Figure 6-3 (green). All of the vehicle speeds decrease during this maneuver as the throttle is released at one second (Figure 6-4).
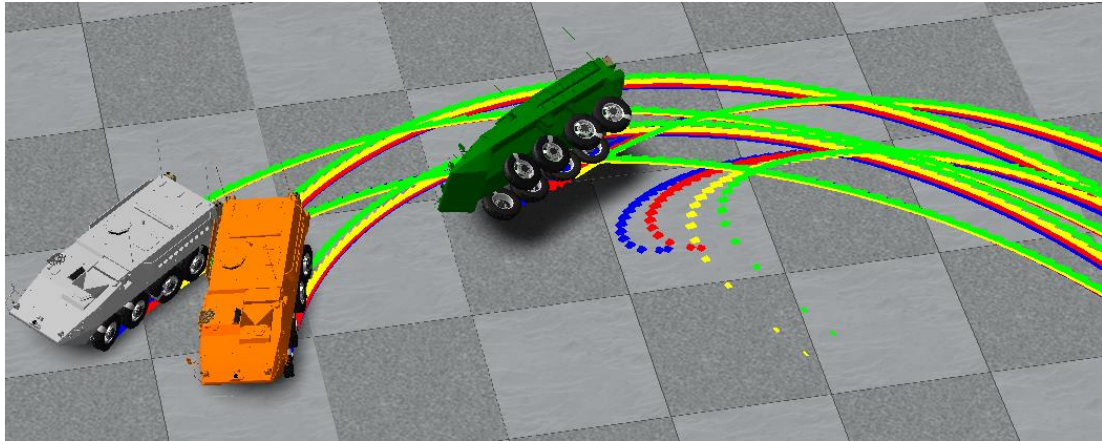
Figure 6-3 Fishhook maneuver trajectory; FRA (green), ZSS (orange), LQR (grey)
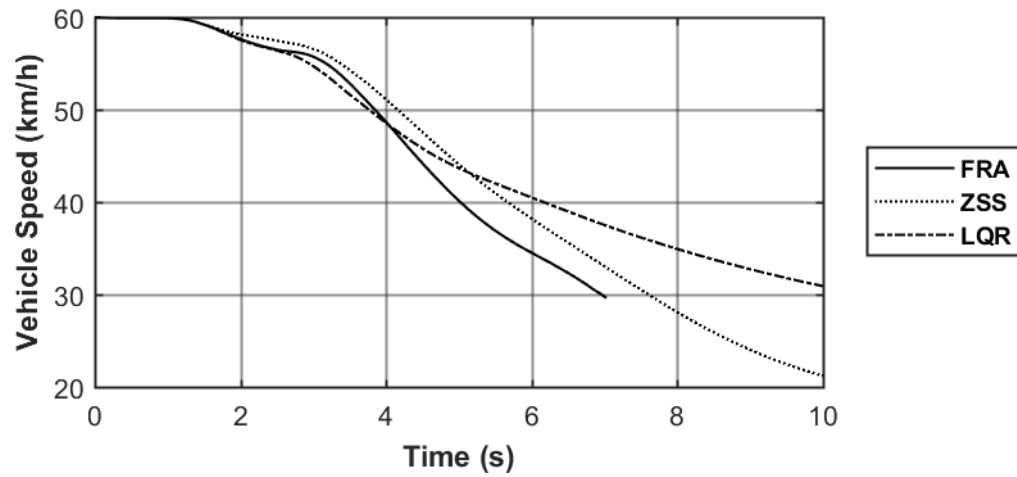
Figure 6-4 Vehicle Speed: Fishhook at 60 km/h over μ=0.95
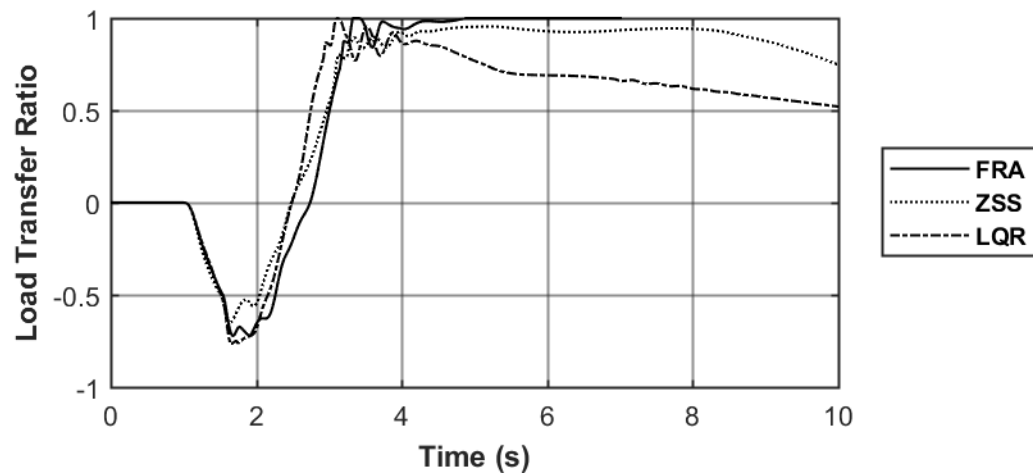
Figure 6-5 Load Transfer Ratio: Fishhook at 60 km/h over μ=0.95

By analyzing Figure 6-5, it can be determined that every vehicle reaches close to rollover condition. The LQR controlled vehicle reaches rollover condition (LTR=1) but reduces the transfer before the physical rollover occurs. The ZSS controlled vehicle never reaches rollover, most likely due to the responsiveness of the feed-forward controller, however as the speed decreases below 49.5 km/h, just after 4 seconds into the maneuver (Figure 6-4), the LTR remains high and the vehicle would be more susceptible to a tripped rollover. This is caused by the induced contra-steering at lower speeds. The LQR controller reduces the LTR despite the decreasing speeds with the rear axle remaining steered in the same direction as the front axle for the duration of the maneuver (Figure 6-6).
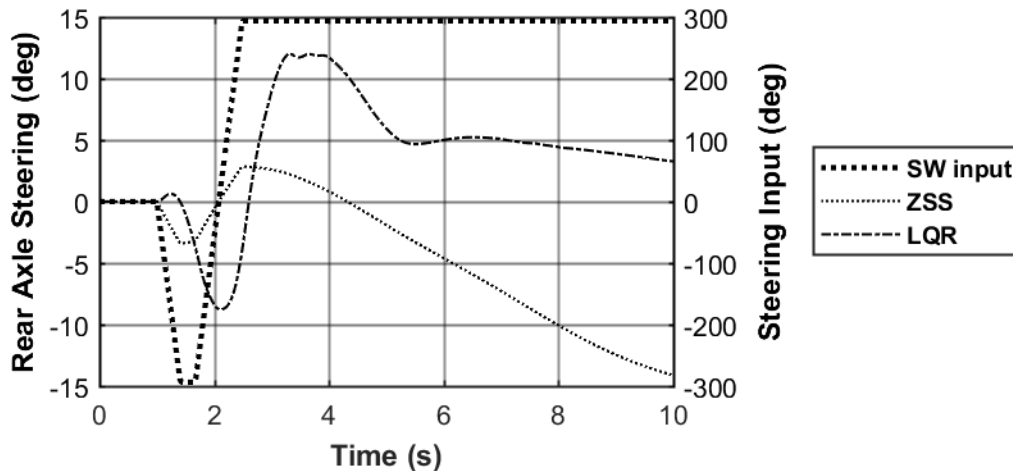
Figure 6-6 Rear Axle Steering Angle: Fishhook at 60 km/h over μ=0.95

The active steering of the LQR and ZSS controllers intuitively decrease the LTR without monitoring the LTR directly. As discussed previously, the responsiveness of the ZSS controller reduces the risk of rollover. The LQR controller monitors the yaw rate and sideslip angle and the rear axle steering angle is calculated to minimize these performance measures to the steady state calculation.
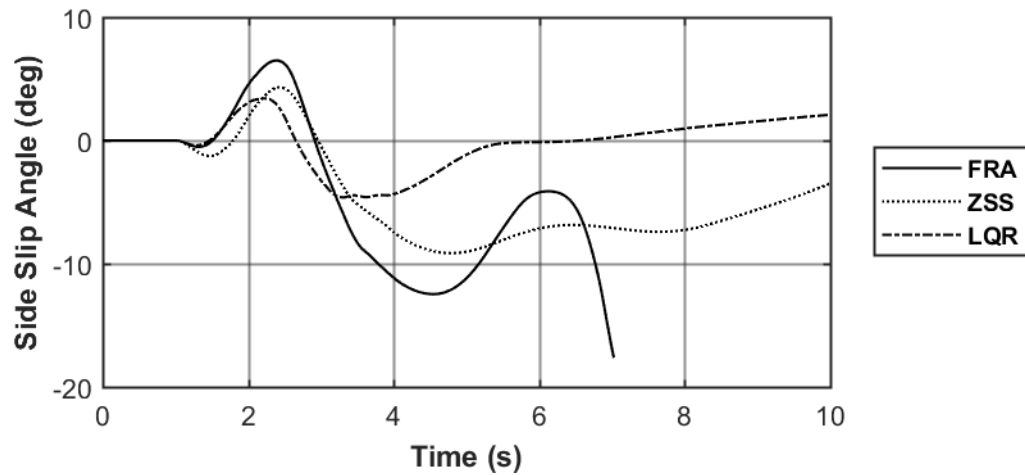
Figure 6-7 Vehicle Side Slip Angle: Fishhook at 60 km/h over μ=0.95
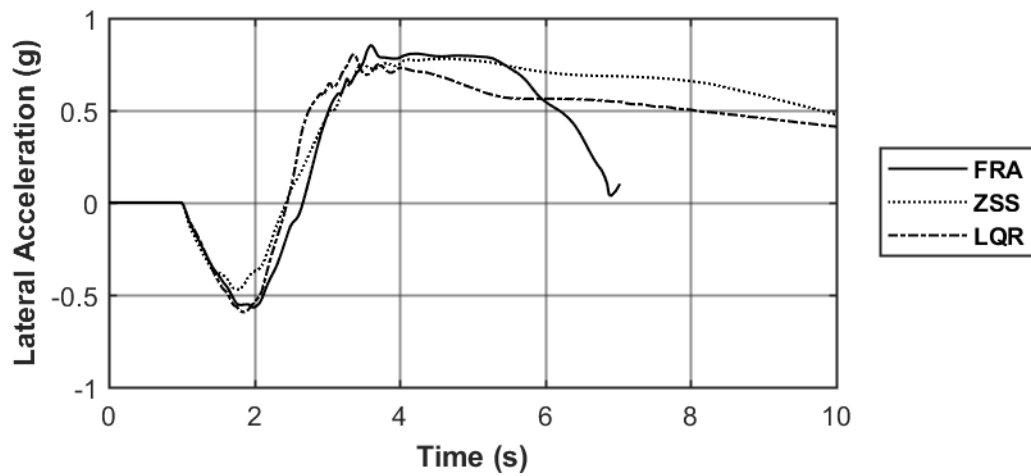
Figure 6-8 Vehicle Lateral Acceleration: Fishhook at 60 km/h over μ=0.95
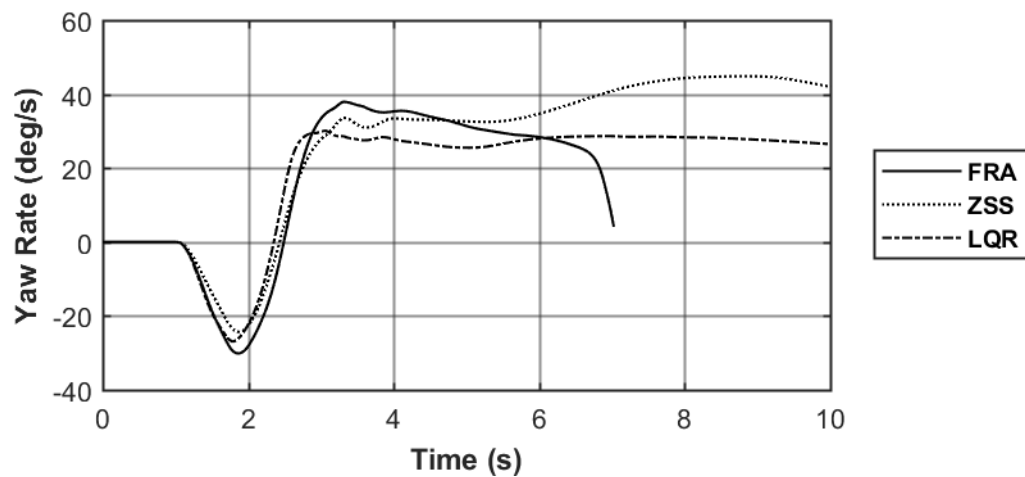
Figure 6-9 Vehicle Yaw Rate: Fishhook at 60 km/h over μ=0.95

The LQR controller is the most effective at decreasing the sideslip angle at 60 km/h (Figure 6-7). The ROM controller allows for the vehicle to behave as the conventional FRA vehicle was designed until near rollover is detected. The ZSS controlled vehicle allows the vehicle to continue to oversteer with an increased lateral acceleration and increased yaw rate when the other controlled vehicles reach steady state.

This maneuver was performed at the limits of the FRA vehicle to show the effectiveness of the RAS controllers. This maneuver was also tested at 80 km/h over the high friction surface where all of the vehicles failed. In this case it would be necessary to include a secondary ESC system using braking or some method of differential torque application as the lateral tire limits of the tires were reached. This was not tested in this work as it was out of the scope of this thesis.

6.2 EXTERNAL DISTURBANCE

External disturbances can have a significant impact on the behaviour of a vehicle. Larger vehicles such as tractor trailers and even the combat vehicles are affected by a crosswind due to the large surface area of the side of the vehicle. Braking over split-μ surfaces can cause an unwanted torque to the vehicle due to the low traction on one side of the vehicle.

6.2.1 Crosswind Simulation

The crosswind simulation is used to predict vehicle behaviour during a severe crosswind. This test is performed over a straight path with a surface friction of μ=0.85. The crosswind is 100km/h perpendicular to the vehicle direction, from the right side for a portion and from the left side for the next portion (Figure 6-11, Figure 6-10). The vehicle will be driving with a target speed of 80 km/h through these crosswinds.
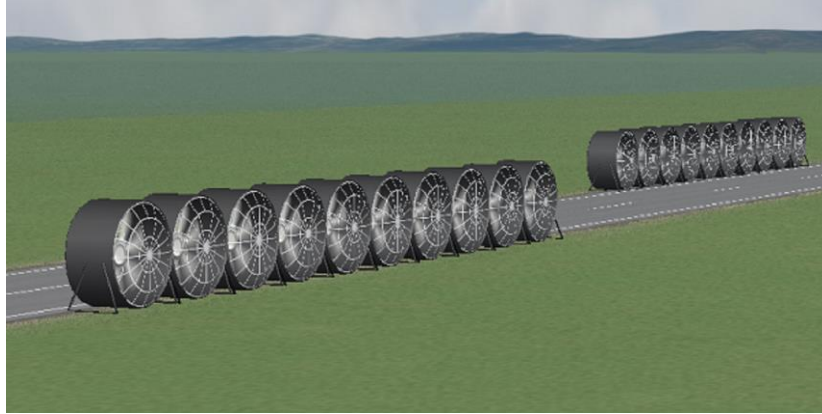
Figure 6-10 Crosswind facility physical representation
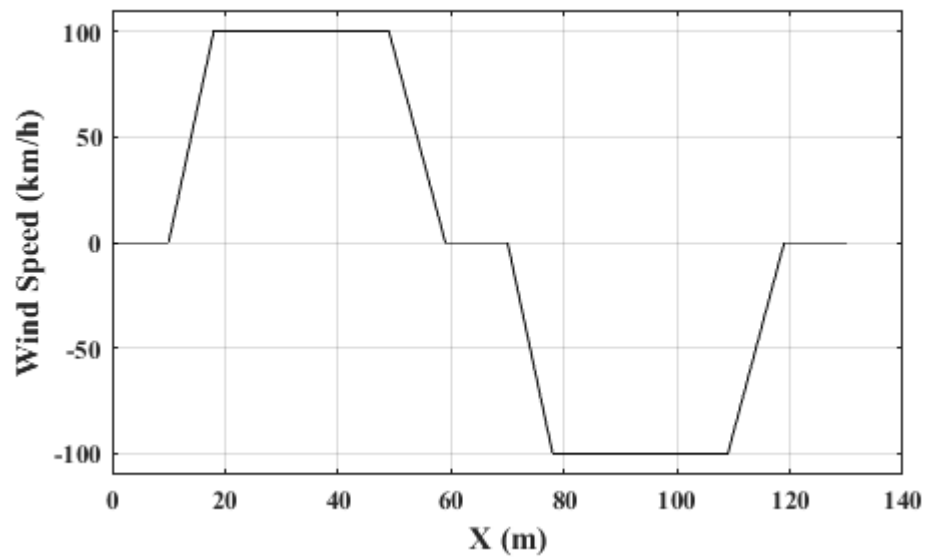
Figure 6-11 Crosswind speed and direction
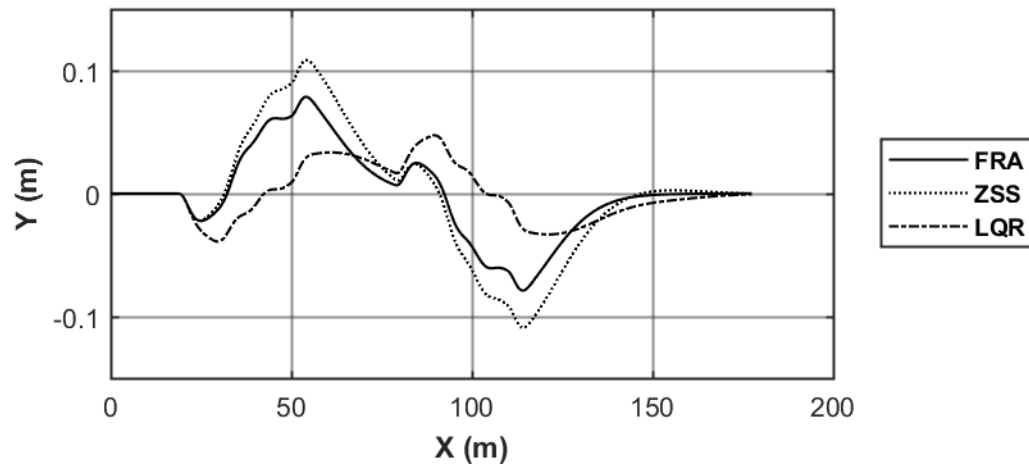
Figure 6-12 Vehicle Trajectory: Crosswind test at 80 km/h over μ=0.85

During the crosswind test the ZSS vehicle has the largest displacement from the intended path and the LQR controlled vehicle has the lowest displacement (Figure 6-12). It is interesting to note the corrective steering input for the LQR vehicle is for the most part opposite of the ZSS and FRA vehicles (Figure 6-13).

The crosswind applies a moment about the center of gravity of the vehicle, which rotates the vehicle with the rear away from the wind source as seen in Figure 6-14. On the FRA and ZSS vehicles, the driver is required to steer away from the wind source in order to correct the applied moment from the wind and continue straight. This results in the RAS of the ZSS vehicle to be steered away from the wind source, damping the moment applied by the wind source but causing the vehicle to drift more in a "crabbing" fashion. This leads the vehicles to stray from the center of the path more than the LQR vehicle. The LQR controller corrects the external moment with the rear axle steering and the driver can continue to correct the path with the front steering resulting in less deviation from the center of the path. This also allows the LQR vehicle to have less of a heading angle change (Figure 6-15) and little crabbing behaviour.
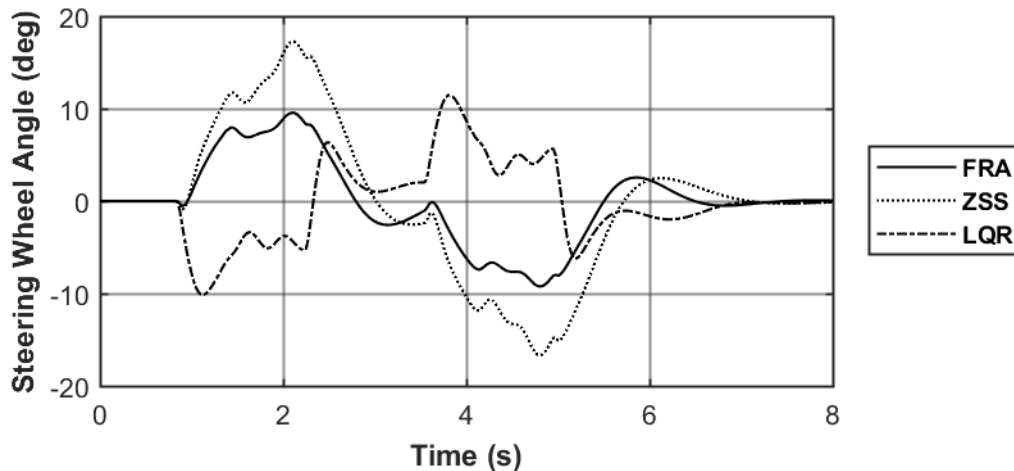
Figure 6-13 Steering Wheel Angle: Crosswind test at 80 km/h over μ=0.85
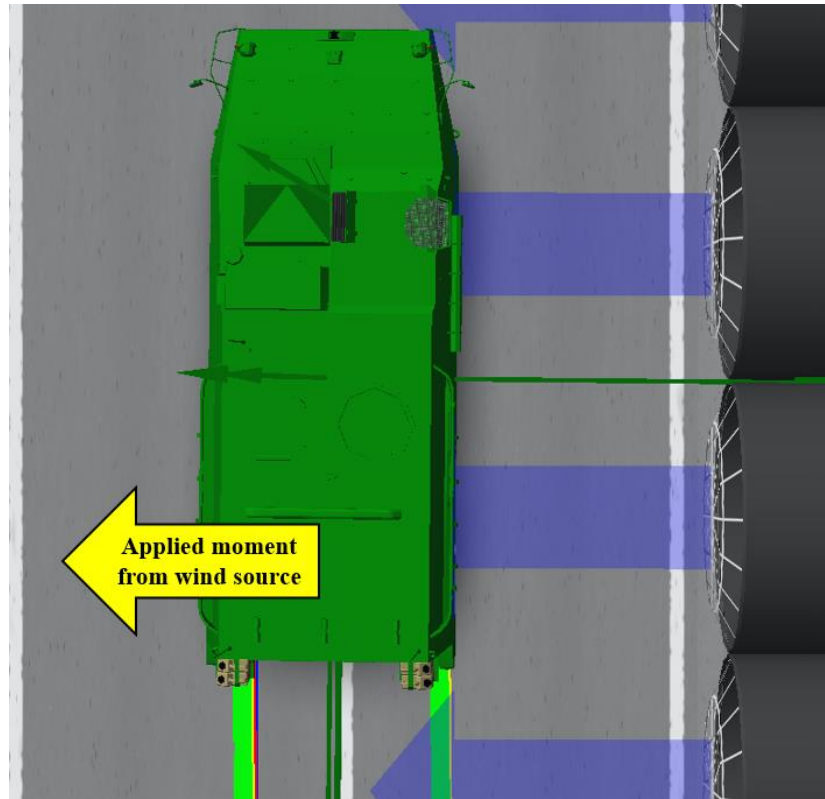
Figure 6-14 Applied moment from wind source (assumed due to decreased surface area on front of vehicle.)
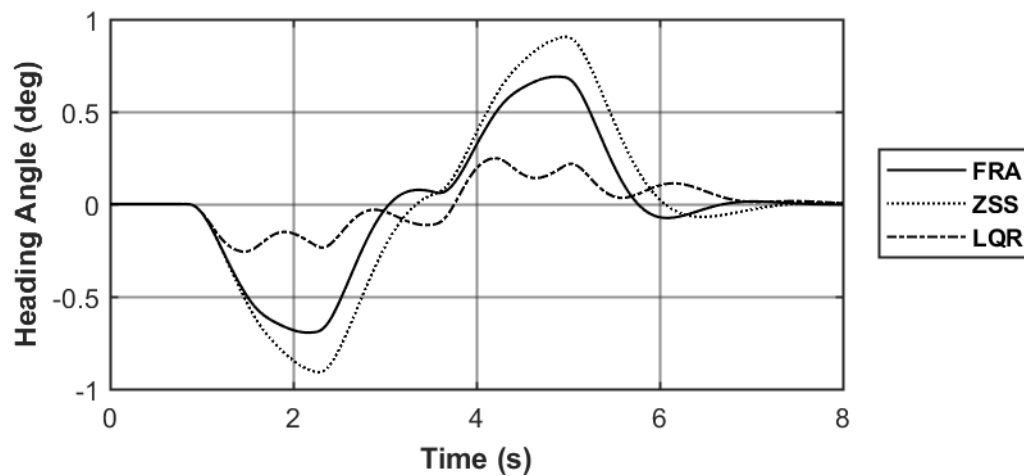
Figure 6-15 Heading Angle: Crosswind test at 80 km/h over μ=0.85
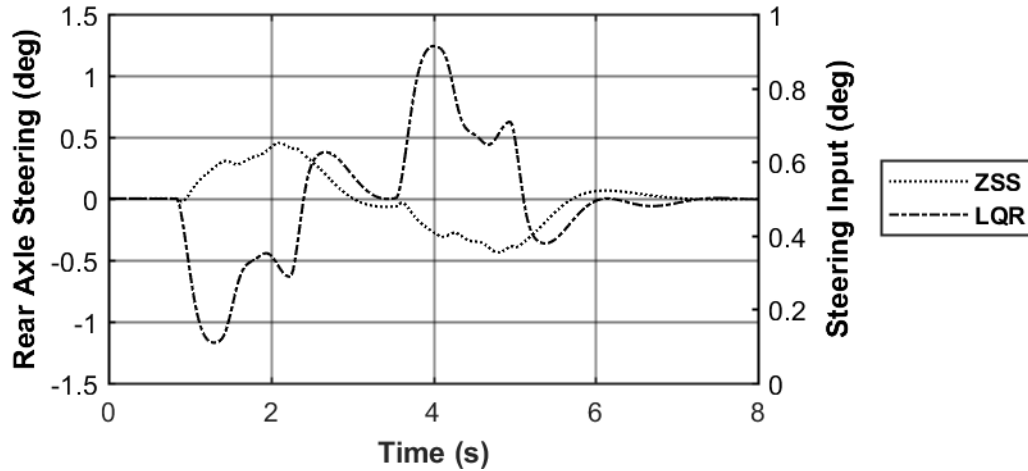
Figure 6-16 Rear Axle Steering: Crosswind test at 80 km/h over μ=0.85

Since the LQR controller calculates the required rear axle steering angle depending on the requirements to reach steady state, it makes the controller more useful for non-transient maneuvers. In Chapter 5 it was determined that at higher speeds both the LQR and ZSS controllers would steer in the same direction as the front axle at higher speeds. The steering input is low, which results in the reference yaw rate to be low, therefore, the outcome of the calculated rear steering angle to correct the external yaw moment is in the direction of the wind source. The driver is forced to steer into the wind source to remain straight.
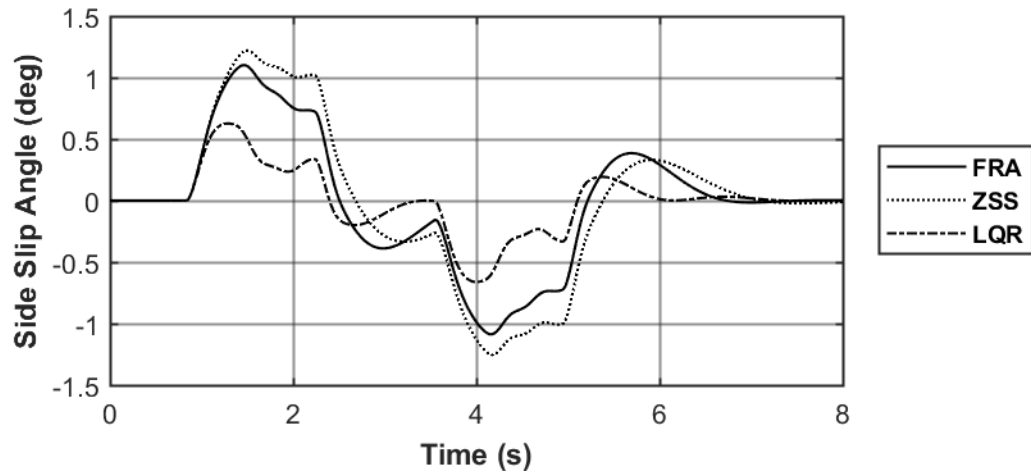
Figure 6-17 Vehicle Side Slip Angle: Crosswind test at 80 km/h over μ=0.85
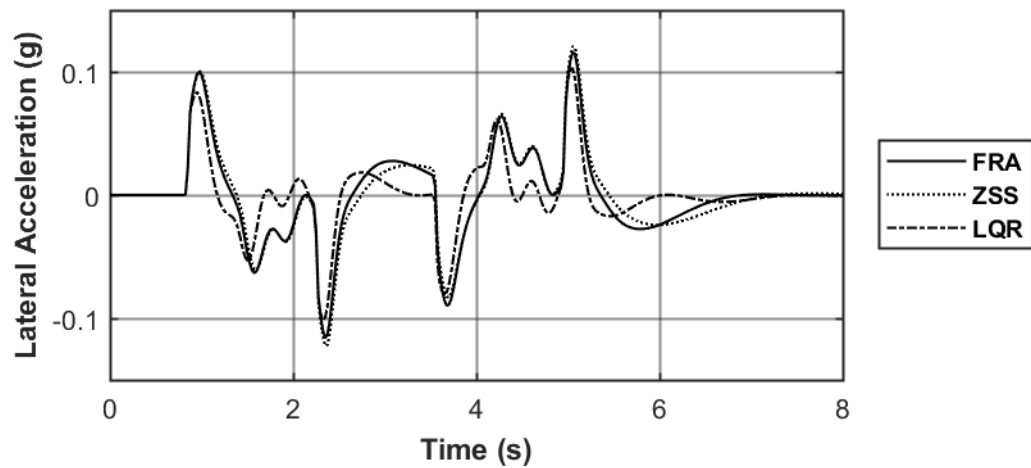
Figure 6-18 Lateral Acceleration: Crosswind test at 80 km/h over μ=0.85
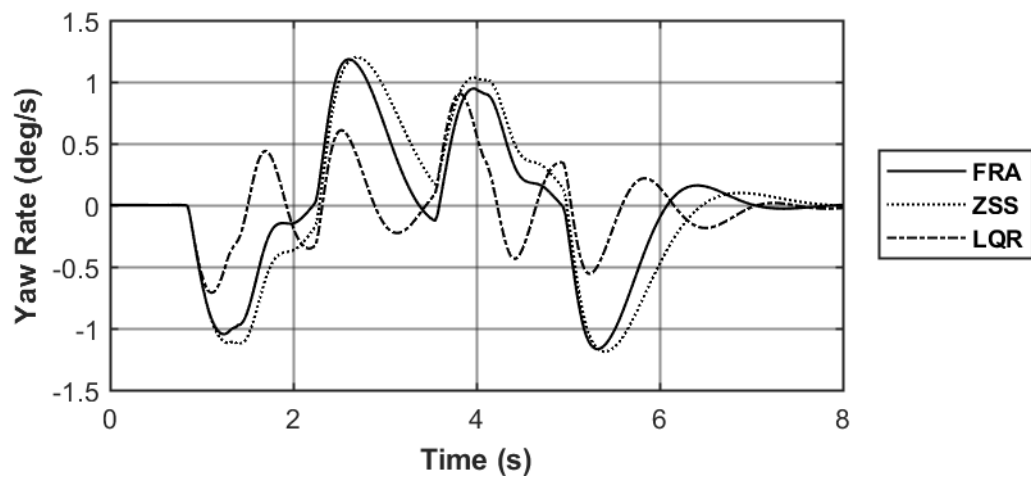
Figure 6-19 Yaw Rate: Crosswind test at 80 km/h over μ=0.85

The lateral accelerations (Figure 6-18) of the vehicles are all similar as this is an in-line maneuver. The behaviour of the rear axle steering of the LQR vehicle results in the lowest side slip angle (Figure 6-17) as well as yaw rate (Figure 6-19). Despite the differences being minimal, the LQR controller dampens the yaw rate and side slip angle as designed.

6.3   SUMMARY OF CHAPTER

This chapter presented results from two simulations to test the versatility of rear axle steering on an 8x8 combat vehicle. Other than added stability the proper control of rear axle steering can prevent rollover when the conventional vehicle reaches rollover in the same maneuver and reduce the effects of external yaw on the vehicle.

6.3.1   Conclusions – Rollover Avoidance

Rollover avoidance evaluation was conducted at a single speed of 60 km/h. The maneuver included a fishhook steering input over high friction surface (μ=0.95) which resulted in the conventional vehicle to rollover. All three presented controllers were able to prevent the rollover from occurring, each with advantages from different perspectives. This simulation demonstrates the potential of using these control systems to prevent rollover under these conditions.

- The ZSS vehicle was the only vehicle to not reach full rollover condition (LTR=1), meaning one side did not lift off. This is due to the responsiveness of the controller, and as the vehicle is travelling at higher speeds the rear axle steers in the same direction of the front axle. This results in the rate of lateral acceleration generation to decrease and the vehicle to stay in contact with the ground.
- The LQR vehicle reaches rollover condition (LTR=1) however is able to recover. The LQR controller has the most reduced yaw rate and sideslip angles, suggesting the controller operates as designed. The feed-back control of the RAS returns the vehicle to steady state when the steering is constant towards the end of the simulation.

6.3.2 Conclusions – External Disturbance

The external disturbance was simulated using the crosswind facility test. A direct crosswind of 100 km/h was simulated on both the left and right sides of the vehicle which was travelling at 80 km/h over high friction surface. The crosswind applied a force on the whole side of the vehicle resulting in a moment with the majority of the force on the rear of the vehicle.

- The conventional vehicle requires the driver to steer away from the wind source, causing the vehicle to be travelling slightly sideways, meaning the heading of the vehicle is towards the wind source rather than straight ahead.

- The ZSS vehicle also requires the driver to steer away from the wind source, but with more steering input than the conventional vehicle. The rear axle is steering in the same direction as the front axle, which results in the vehicle to be travelling slightly more sideways than the conventional vehicle.

- The LQR vehicle operates completely different in this simulation. The LQR control detects the yaw rate provided by the wind source and steers the rear axle towards the wind source to correct the yaw rate of the vehicle. The result from this control approach is the vehicle has a heading angle that is straighter than the other tested vehicles, as well as decreased side slip angles and decreased yaw rates.

These results demonstrate that the LQR controller not only assists with lateral vehicle dynamics, but by damping the yaw rate and lateral acceleration, rollover can be avoided. The external disturbance from a crosswind is also damped by the LQR controller which provides evidence for the LQR controller assisting in various environments.

CHAPTER 7
CONCLUSIONS & FUTURE WORK

The results presented in this thesis demonstrate the benefit to using controlled rear axle steering to improve the stability and maneuverability on an 8x8 combat vehicle. The controllers were designed with only rear axle steering in mind rather than steering the rear two axles as this is a design many companies are producing (Section **1.5**). The two control systems presented were the Zero Side Slip (ZSS) feed-forward controller, which provided responsiveness with a direct speed-based relationship for the rear axle steering from the front axle steering, and the Linear Quadratic Regulator (LQR) optimal controller which used the reference model from the conventional vehicle to achieve desired side slip angle and yaw rate. The results for the maneuvers deliver the best choices for controlled rear axle steering at different operating conditions. The ZSS performed best at low speeds, below 30 km/h, by increasing the maneuverability, requiring less steering input to achieve a similar radius turn, and increasing the rate which yaw rate is generated. The LQR controller performed best at speeds over 40 km/h, providing acceptable compromise of maneuverability while increasing the stability based on the reference model. The proposed controllers were simulated within TruckSim© using a validated vehicle model for the 8x8 combat vehicle in co-simulation with Simulink. The maneuvers used to test the control system methods for the RAS included a 15-meter slalom, 100-ft radius circle constant acceleration, modified J-Turn, FMVSS 126 ESC, and the NATO double lane change. The lower speed tests were performed over two road friction coefficients, μ=0.35 and 0.85.

The goals that were achieved include

- A feed-forward controller was designed based on the vehicle parameters with the intention of limiting the side-slip angle of the vehicle to reduce the turning radius of the vehicle.
- A feed-back controller was developed using the yaw rate and sideslip angle of the vehicle as a reference to increase the stability of the vehicle
- The proposed controllers were successfully implemented into MATLAB/Simulink for use in co-simulation with TruckSim©

- The vehicle-controller configurations were analyzed by performing simulations of standard test maneuvers

- The ZSS controller was determined to be successful at reducing the turning radius while maintaining controllability at speeds less than 30 km/h.

- The LQR controller was found to increase the vehicle stability at high speed as well as maintain acceptable lateral translation during a high-speed emergency maneuver

7.1 GENERAL CONCLUSIONS

Vehicle safety has been greatly improved over the years with the adoption of anti-lock braking systems, traction control systems and electronic stability control systems. The advancements of vehicle powertrain along side the advancement of computational power and control systems, more complex systems that can be integrated into one another can be introduced. The use of control systems increases the safety of vehicles by actively monitoring and adjusting the control of the vehicle. Control systems are often expanded off of systems that are already included in the vehicle package. (ie. ESC and ETC were expanded off of the system used for ABS) The introduction of rear axle steering as a method for reducing turning radius on these vehicles have offered another method of vehicle control. In this thesis the possibility of using the rear axle steering to control the yaw rate and sideslip angle have been explored.

The working foundations for vehicle dynamics and control theory were introduced to support the work in the sections of tire dynamics, lateral vehicle dynamics and control system fundamentals.

A literature review to support the direction of the body of work was conducted on lateral vehicle dynamics control, rear axle steering and the implementation on several types of vehicles including multi-axle vehicles. The focus of the literature review was on the methods and results of implementing rear axle steering as a method of linear vehicle dynamics control. The effectiveness of both feed-forward and certain feed-back control methods to improve the vehicle stabilization and performance was evident during this section. Zero side slip (ZSS) feed-forward control method was determined to be the most effective approach for decreasing the turning radius and increase the maneuverability of the

vehicle at low speeds. Since it is developed based on the vehicle parameters, it should provide a method for decreasing tire wear as well as best performance at specific speeds. Optimal control theory has been widely studied for vehicle control as the vehicle is a complex system. A linear quadratic regulator (LQR) controller is determined as a good method to use as it can be used in a reference tracking system that observes ideal behaviour based on the driver's input.

Vehicle models used to design the controllers and test the controlled vehicles were developed. To test the controlled vehicles, a previously validated TruckSim© full vehicle model was used. A linear 2 DOF plant model of the 8x8 vehicle with rear axle steering was derived based on the differential equations of lateral and yaw motion of the bicycle model to be used in the synthesis of the LQR controller. The reference signal for the desired yaw rate and side slip angle was developed using the linear steady state model of the conventional, fixed rear axle, vehicle in conjunction with a first order time delay based on the vehicle speed and road friction surface. The zero-sideslip (ZSS) method to control the rear axle was developed based on the rear axle steering bicycle model at steady state with zero sideslip angle.

The layout of the control strategy was presented focusing on the implementation of the LQR controller into the active yaw controller. The LQR theory was presented including the development of the LQR gain. The active yaw controller uses the reference yaw rate and sideslip angle to determine the output of the system. The feed-back signal is determined using the LQR feed-back gain which was optimized by configuring the performance index tuning. Using the maximum sideslip angle and the maximum yaw rate the performance index for the LQR optimal control theory cost function was defined.

Several simulations were performed to test the maneuverability of the vehicles. The 15-meter slalom was performed to asses the tight radius performance of the vehicles over high friction (μ=0.85) as well as low friction surfaces (μ=0.35). A 100-ft radius constant acceleration test was performed to see how the controllers transitioned from low to mid range speeds and he modified J-turn was performed to asses the mid-range (40 km/h) speed stability and maneuverability based on a fixed steering input. High speed simulations included the FMVSS 126 ESC to determine the performance and stability during an

125

emergency maneuver and the NATO double lane change to analyze the transient performance. These were both performed over the high friction surface at 60 and 80 km/h. The FMVSS 126 ESC was also performed over low friction surface.

The ZSS vehicle performed well at 20 km/h but did not perform well at above 30 km/h over the high friction surface. The LQR controller increased the stability of the vehicle but decreased the turning performance and required extra steering input to achieve the desired path results. The ZSS vehicle achieved the highest speed over low friction surface without losing control. All vehicle control configurations achieved high lateral accelerations around 0.6 g's during the modified J-turn maneuver, which is not ideal. However, the LQR controller reduced this slightly increasing the turning radius. In the final design of the controller, the question of whether maneuverability or stability at 40 km/h is more important will need to be answered. This will be dependent on the driver type and skill level.

During the 100-ft constant acceleration maneuver the ZSS performed the best at low speeds below 30 km/h by requiring the least steering input and the LQR performed the best when the vehicle reached steady state at around 50 km/h. The LQR vehicle was able to decrease the side slip angle significantly when the vehicle was travelling at 40 km/h and reaching steady state. This shows promise for the LQR during the transition zone from mid range speed to high speeds (45-50 km/h).

The LQR controlled vehicle performed most desirably in the high-speed maneuvers over both high and low friction surfaces. The LQR controlled vehicle was able to reduce the yaw rate, sideslip angle and duration of high lateral acceleration during all conditions of the FMVSS 126 ESC maneuver (60 km/h, 80 km/h over low friction and high friction surfaces). This was accomplished by decreasing the lateral displacement by an acceptable amount, especially when comparing to the ZSS controlled vehicle. The LQR controller brought the vehicle back to driving straight more quickly than the conventional vehicle and at a small increase compared to the ZSS controller. The ZSS lateral displacement was critically decreased compared to the LQR and conventional vehicles over the low friction surface which is one of the major considerations to dismiss this controller for use at higher speeds.

126

For the NATO double lane change the same trend was found. The ZSS vehicle required extra steering input to achieve the same path compared to the LQR and the conventional vehicle. The LQR minimizes the peak side slip angles, yaw rate and lateral accelerations during the double lane change at 60 km/h and 80 km/h when compared to the conventional vehicle and the ZSS vehicle. The LQR vehicle does increase the steering input required by the driver compared to the conventional vehicle, however this is expected when adjusting vehicle behaviour with a focus on safety.

It was proven that during a maneuver guaranteed to rollover the conventional vehicle at 60 km/h, both the ZSS and LQR vehicles prevented the rollover from occurring. The LQR controller minimized the sideslip angle, yaw rate and lateral acceleration compared to the ZSS controller during the recovery portion of the maneuver. Without directly monitoring the roll angle or the load transfer ratio from left side to right side, the controllers can decrease the risk of rollover.

Overall the ZSS vehicle performs best at low speeds with increased maneuverability and the LQR controlled vehicle performs best at higher speeds with better lateral stability and acceptable decrease in performance. This subject is impossible to look at equally from a performance standpoint and a safety standpoint and the discussion on what to compromise needs to be discussed with the users. The LQR controller at high speeds provides higher stability which is likely to be desired in military vehicles as safety is a primary objective. This controlled vehicle will require less training for high speed driving as the control system will add stability and may increase the safety of the vehicle. At low speeds, errors are generally easier to fix and do not occur in a quick period of time. This makes the ZSS controller desirable at low speeds as it increases the maneuverability, despite the increased yaw rate and lateral accelerations. The ZSS vehicle will likely not feel natural to the driver as the sideslip angles are opposite from the conventional vehicle at low speeds. However, the driver will be able to feel the increased maneuverability. Less driver training should be required as the vehicle is more maneuverable at low speeds using the ZSS controller and easier to maintain control at high speeds using the LQR controller.

7.2   FUTURE WORK

This thesis has explored the use of optimal control as a lower level control system in a complex vehicle. The LQR control system has potential to be implemented on the vehicle as a method to improve stability at high speeds and the ZSS has high potential to improve the maneuverability. In order to apply it on a vehicle, the activation speeds for each controller needs to be evaluated. The best method for determining this is through the use of the suggestions presented in this thesis as a starting point and finalize through driver-in-the-loop testing, either in simulation or on the physical vehicle.

This thesis uses exact values for the road friction coefficient, however this is currently not available or is not reliable on most vehicles. Using road condition ranges will allow the controller to use a single road coefficient value for each range. This method should be simulated to find the optimal average road friction coefficient setting to be used in the LQR control synthesis.

These 8x8 combat vehicles already require significant driver training. The LQR controller has high potential to increase the stability of the vehicle while respecting the performance of the conventional vehicle. Tuning the LQR controller for different level of driver skill should be investigated by limiting the maximum yaw rate to lower values. This could provide a training tool to the military and increased 'training-wheels' without the intrusive feeling of the braking system used in ESC.

For lower speeds the use of the ZSS vehicle model should be explored as a reference model for use in an LQR reference control system. This would allow for the vehicle to dampen external disturbances and operate closer to the zero side slip steady state vehicle model.

Finally, before the system should be introduced to the physical vehicle, hardware testing should be completed to investigate the physical and computational requirements of the system. A drive-hardware-in-the-loop setup will allow issues such as sensor noise and fault detection to be dealt with as well as the human interaction with the control system be monitored. Additionally, this would allow the hardware requirements to be tested to include fault detection and to address sensor noise.

REFERENCES

[1]   G. o. Canada. (2017, 2018-04-13). *Vehicles*. Available: http://www.army-armee.forces.gc.ca/en/vehicles/index.page

[2]   E. Besch, "Infantry Fighting Vehicles: Their Evolution and Significance," *Marine Corps Gazette,* vol. 67, no. 7, p. 50, 1983.

[3]   N. Logan, "CFB Wainwright accident: LAV III has a history of rollovers," in *Global News*, ed. Online: National Online Journalist/Global National Web Producer, 2014.

[4]   IIHS. (2016, June 03). *Stability control could prevent a third of fatal crashes*. Available: http://www.iihs.org/iihs/news/desktopnews/electronic-stability-control-could-prevent-nearly-one-third-of-all-fatal-crashes-and-reduce-rollover-risk-by-as-much-as-80-effect-is-found-on-single-and-multiple-vehicle-crashes

[5]   M. Blundell and D. Harty, *The Multibody Systems Approach to Vehicle Dynamics*. Coventry: Elsevier, 2015.

[6]   J. Y. Wong, *Theory of Ground Vehicles*. Hoboken: John Wiley & Sons, Inc., 2008.

[7]   Michelin, "The Tyre Grip," *Société de Technologie Michelin,* Presentation 2001.

[8]   S. Skogestad, I. Postlethwaite, and S. Skogestad, *Multivariable feedback control: Analysis and design*, 2 ed. United States: Wiley, John & Sons, 2005.

[9]   N. S. Nise, *Control systems engineering* (no. Book, Whole). Hoboken, NJ: John Wiley & Sons, Inc, 2015.

[10]   P. Duddu. (2013, 2018-04-05). *The world's 10 best armoured personel carriers*. Available: https://www.army-technology.com/features/featurethe-worlds-best-armoured-personnel-carriers-4142101/

[11]   A. Technology. (2017). *Piranha V Armoured Wheeled Vehicles*. Available: https://www.army-technology.com/projects/piranhav/

[12]   FNSS. *PARS III 8x8*. Available: http://www.fnss.com.tr/en/product/pars-8x8

[13]   Patria. (2018). *Patria AMVXP Armoured Wheeled Vehicle*. Available: https://www.patria.fi/sites/default/files/file_attachments/patria_amv_xp_brochure_lowres.pdf

[14]   E. Clifford-Marsh. (2008). *Sweden Ditches SEP Programme*. Available: https://www.army-technology.com/news/news3888-html/

[15]   U. Kiencke and L. Nielsen, *Automotive Control Systems: For Engine, Driveline and Vehicle*. Springer-Verlag New York, Inc., 2000, p. 422.

[16]   A. Lie, C. Tingvall, M. Krafft, and A. Kullgren, "The effectiveness of electronic stability control (ESC) in reducing real life crashes and injuries," *Traffic injury prevention,* vol. 7, no. 1, pp. 38-43, 2006.

[17]   (2017). *Regulations Amending the Motor Vehicle Safety Regulations (Electronic Stability Control Systems for Heavy Vehicles)*. Available: http://www.gazette.gc.ca/rp-pr/p2/2017/2017-06-14/html/sor-dors104-eng.html

[18]   D. Piyabongkarn, R. Rajamani, J. A. Grogg, and J. Y. Lew, "Development and experimental evaluation of a slip angle estimator for vehicle stability control," *IEEE Transactions on Control Systems Technology,* vol. 17, no. 1, pp. 78-88, 2009.

[19]   E. Liebemann, K. Meder, J. Schuh, and G. Nenninger, "Safety and performance enhancement: The Bosch electronic stability control (ESP)," *SAE Paper,* vol. 20004, no. 2004, pp. 21-0060, 2004.

[20]   R. Rajamani, *Vehicle dynamics and control*. Springer Science & Business Media, 2011.

[21] K. U. Sawase, Yuichi; Miura, Takami;, "Left-Right Torque Vectoring Technology as the Core of Super All Wheel Control (S-AWC)," *Mitsubishi Technical Review,* 2006.

[22] H. E. Tseng, B. Ashrafi, D. Madau, T. A. Brown, and D. Recker, "The development of vehicle stability control at Ford," *IEEE/ASME transactions on mechatronics,* vol. 4, no. 3, pp. 223-234, 1999.

[23] H. Tseng, D. Madau, B. Ashrafi, T. Brown, and D. Recker, "Technical challenges in the development of vehicle stability control system," in *Control Applications, 1999. Proceedings of the 1999 IEEE International Conference on*, 1999, vol. 2, pp. 1660-1666: IEEE.

[24] D. D. Hoffman and M. D. Rizzo, "Chevrolet C5 corvette vehicle dynamic control system," SAE Technical Paper0148-7191, 1998.

[25] J. Ahmadi, A. K. Sedigh, and M. Kabganian, "Adaptive vehicle lateral-plane motion control using optimal tire friction forces with saturation limits consideration," *IEEE Transactions on vehicular technology,* vol. 58, no. 8, pp. 4098-4107, 2009.

[26] R. Daily and D. M. Bevly, "The use of GPS for vehicle stability control systems," *IEEE Transactions on Industrial Electronics,* vol. 51, no. 2, pp. 270-277, 2004.

[27] K. S. Sawase, Yoshiaki, "Application of active yaw control to vehicle dynamics by utilizing driving/braking force," *JSAE Review,* vol. 20, pp. 289-295, 1999.

[28] *Electronic Stability Control Systems*, NHTSA–200727662, 2007.

[29] C. Ghike, T. Shim, and J. Asgari, "Integrated control of wheel drive--brake torque for vehicle-handling enhancement," *Proceedings of the Institution of Mechanical Engineers, Part D: Journal of Automobile Engineering,* vol. 223, no. 4, pp. 439-457, 2009.

[30] J Ackermann, Dr T B•unte, and D Odenthal, "Advantages of Actve Steering for Vehicle Dynamics Control," 1999.

[31] J. Ackermann and T. Bünte, "Yaw disturbance attenuation by robust decoupling of car steering," *Control Engineering Practice,* vol. 5, no. 8, pp. 1131-1136, 1997.

[32] R. Vigneshwaran, K. S. Chaithanyan, N. Sathish, S. Prashanth, and M. Parasaran, "Optimization of Four Wheel Steering," *Int. J. of Multidisciplinary and Current research,* vol. 6, 2018.

[33] S. Kharrazi, M. Lidberg, P. Lingman, J.-I. Svensson, and N. Dela, "The effectiveness of rear axle steering on the yaw stability and responsiveness of a heavy truck," *Vehicle System Dynamics,* vol. 46, no. S1, pp. 365-372, 2008.

[34] A. G. Nalecz and A. C. Bindemann, "Handling properties of four wheel steering vehicles," SAE Technical Paper0148-7191, 1989.

[35] M. Nagai and M. Ohki, "Theoretical study on active four–wheel–steering system by virtual vehicle model following control," *International Journal of Vehicle Design,* vol. 10, no. 1, pp. 16-33, 1989.

[36] Y. Furukawa, N. Yuhara, S. Sano, H. Takeda, and Y. Matsushita, "A review of four-wheel steering studies from the viewpoint of vehicle dynamics and control," *Vehicle System Dynamics,* vol. 18, no. 1-3, pp. 151-186, 1989.

[37] T. Eguchl, Y. Saklta, K. Kawagoe, S. Kaneko, K. Morl, and T. Matsumoto, "Development of "Super Hicas", a New Rear Wheel Steering System with Phasereversal Control," SAE Technical Paper0148-7191, 1989.

[38] T. Takiguchi, N. Yasuda, S. Furutani, H. Kanazawa, and H. Inoue, "Improvement of vehicle dynamics by vehicle-speed-sensing four-wheel steering system," SAE Technical Paper0148-7191, 1986.

[39]   D. R. Pillar, M. C. Wrege, and C. J. Kraning, "All-wheel steering systems," ed: Google Patents, 1995.

[40]   Y. Lin, "Improving vehicle handling performance by a closed-loop 4ws driving controller," SAE Technical Paper0148-7191, 1992.

[41]   G. F. Franklin, J. D. Powell, and M. L. Workman, *Digital control of dynamic systems*. Addison-wesley Menlo Park, CA, 1998.

[42]   H. Sato, A. Hirota, H. Yanagisawa, and T. Fukushima, "Dynamic characteristics of a whole wheel steering vehicle with yaw speed feedback rear wheel steering," in *Road Vehicle Handling, I Mech E Conference Publications 1983-5. Sponsored by Automobile Division of the Institution of Mechanical Engineers under patronage of Federation Internationale des Societes d'Ingenieurs des Techniques de l'Automobile (FISITA) he*, 1983, no. C124/83.

[43]   M. Yamamoto, "Active control strategy for improved handling and stability," SAE Technical Paper0148-7191, 1991.

[44]   J. C. Whitehead, "Four wheel steering: Maneuverability and high speed stabilization," SAE Technical Paper0148-7191, 1988.

[45]   M. Nagai, Y. Hirano, and S. Yamanaka, "Integrated control of active rear wheel steering and direct yaw moment control," *Vehicle System Dynamics,* vol. 27, no. 5-6, pp. 357-370, 1997.

[46]   T. Hiraoka, O. Nishihara, and H. Kumamoto, "Model-following sliding mode control for active four-wheel steering vehicle," *Review of Automotive Engineering,* vol. 25, no. 3, p. 305, 2004.

[47]   B. Friedland, *Control system design: an introduction to state-space methods*. Courier Corporation, 2012.

[48]   G. Mastinu and M. Ploechl, *Road and off-road vehicle system dynamics handbook*. CRC Press, 2014.

[49]   D. Odenthal, T. Bunte, and J. Ackermann, "Nonlinear steering and braking control for vehicle rollover avoidance," in *Control Conference (ECC), 1999 European*, 1999, pp. 598-603: IEEE.

[50]   B. Schofield, T. Hagglund, and A. Rantzer, "Vehicle dynamics control and controller allocation for rollover prevention," in *Computer Aided Control System Design, 2006 IEEE International Conference on Control Applications, 2006 IEEE International Symposium on Intelligent Control, 2006 IEEE*, 2006, pp. 149-154: IEEE.

[51]   C. R. Carlson and J. C. Gerdes, "Optimal rollover prevention with steer by wire and differential braking," in *Proceedings of IMECE*, 2003, vol. 3, pp. 16-21.

[52]   Y. Zhang, A. Khajepour, and X. Xie, "Rollover prevention for sport utility vehicles using a pulsed active rear-steering strategy," *Proceedings of the Institution of Mechanical Engineers, Part D: Journal of Automobile Engineering,* vol. 230, no. 9, pp. 1239-1253, 2016.

[53]   C. Harnisch, "Strategies of Intelligent Multi-Axle-Steering in Terrain," in *PROCEEDINGS OF THE INTERNATIONAL CONFERENCE-INTERNATIONAL SOCIETY FOR TERRAIN VEHICLE SYSTEMS*, 1999, vol. 2, pp. 827-836.

[54]   Avtoros. (2013, January 18). *Wamah Under the sign of Shaman*. Available: http://avtoros.info/upload/files/Shaman_2015_eng.pdf

[55]   K. Watanabe, J. Yamakawa, M. Tanaka, and T. Sasaki, "Turning characteristics of multi-axle vehicles," *Journal of Terramechanics,* vol. 44, no. 1, pp. 81-87, 2007.

[56]   K. Huh, J. Kim, and J. Hong, "Handling and driving characteristics for six-wheeled vehicles," *Proceedings of the Institution of Mechanical Engineers, Part D: Journal of Automobile Engineering,* vol. 214, no. 2, pp. 159-170, 2000.

[57] B. Chen, C. Yu, and W. Hsu, "Optimal steering control for six-wheeled vehicle," in *Proceeding of International Symposium on Advanced Vehicle Control*, 2006, pp. 605-610.

[58] S. An, H. Lee, W. Cho, G. Jung, K. Yi, and K. Lee, "Development of steering algorithm for 6WS military vehicle and verification by experiment using a scale-down vehicle," in *Proc. Int. Symp. Advanced Vehicle Control*, 2006, vol. 245250.

[59] S.-J. An, K. Yi, G. Jung, K. I. Lee, and Y.-W. Kim, "Desired yaw rate and steering control method during cornering for a six-wheeled vehicle," *International Journal of Automotive Technology,* journal article vol. 9, no. 2, pp. 173-181, 2008.

[60] U. Kiencke and A. Daiß, "Observation of lateral vehicle dynamics," *Control Engineering Practice,* vol. 5, no. 8, pp. 1145-1150, 1997.

[61] M. K. Salaani and G. J. Heydinger, "Model Validation of the 1997 Jeep Cherokee for the National Advanced Driving Simulator," SAE Technical Paper0148-7191, 2000.

[62] P. LeBlanc and M. El–Gindy, "Directional stability of a straight truck equipped with a self–steering axle," *International Journal of Vehicle Design,* vol. 13, no. 5-6, pp. 459-474, 1992.

[63] M. El–Gindy and E. Mikulcik, "Sensitivity of a vehicle's yaw rate response: application to a three–axle truck," *International Journal of Vehicle Design,* vol. 14, no. 4, pp. 325-352, 1993.

[64] H. Ragheb, "Torque Control Strategy for Off-Road Vehicle Mobility," Doctor of Philosophy (PhD), University of Ontario Institute of Technology, Oshawa, Canada, 2014.

[65] M. J. Hillegass, J. G. Faller, M. S. Bounds, M. El-Gindy, and A. S. Joshi, "Validating the directional performance of multi-wheeled combat vehicle computer simulation models," in *ASME 2004 International Mechanical Engineering Congress and Exposition*, 2004, pp. 781-789: American Society of Mechanical Engineers.

[66] M. J. Hillegass, J. G. Faller, M. S. Bounds, M. El-Gindy, and A. S. Joshi, "Validating the directional performance of multi-wheeled combat vehicle computer simulation models," in *ASME 2005 International Mechanical Engineering Congress and Exposition*, Florida, 2005: American Society of Mechanical Engineers.

[67] D. E. Williams, "Generalised multi-axle vehicle handling," *Vehicle System Dynamics,* vol. 50, no. 1, pp. 149-166, 2012.

[68] E. Esmailzadeh, A. Goodarzi, and G. R. Vossoughi, "Optimal yaw moment control law for improved vehicle handling," *Mechatronics,* vol. 13, no. 7, pp. 659-675, 2003.

[69] "<2009_-_F_Cheli_- Development and implementation of a tv algorithm for an innovative 4WD driveline for a high perf vehicle.pdf>."

[70] A. Odrigo, "Development of multi-wheel drivetrain control system for future electric combat vehicle," 2017.

[71] F. Cheli, S. Melzi, E. Sabbioni, and M. Vignati, "Torque vectoring control of a four independent wheel drive electric vehicle," in *ASME 2013 International Design Engineering Technical Conferences and Computers and Information in Engineering Conference*, 2013, pp. V001T01A003-V001T01A003: American Society of Mechanical Engineers.

[72] J. Edelmann, M. Plöchl, W. Reinalter, and W. Tieber, "A passenger car driver model for higher lateral accelerations," *Vehicle System Dynamics,* vol. 45, no. 12, pp. 1117-1129, 2007.

[73] A. Bryson and Y.-C. Ho, "Applied optimal control: Optimization, estimation, and control (revised edition)," *Levittown, Pennsylvania: Taylor & Francis,* 1975.

[74] S. B. D. Alves, "Helicopter flight modeling and robust autonomous control with uncertain dynamics," Universidade da Beira Interior, 2012.

[75]   A. E. Bryson and Y.-C. Ho, "Optimization, estimation and control," *Ginn and Company,* 1969.

[76]   W. W. Bylsma, J. Beno, D. Weeks, D. Bresie, and A. Guenin, "Electromechanical suspension performance testing," TEXAS UNIV AT AUSTIN CENTER FOR ELECTROMECHANICS2000.

[77]   G. J. Forkenbrock and D. Elsasser, "An assessment of human driver steering capability," *National Highway Traffic Safety Administration DOT HS,* vol. 809, p. 875, 2005.

[78]   N. H. T. S. Administration, "Laboratory test procedure for FMVSS 126, electronic stability control systems," 2007.

[79]   N. H. T. S. Administration, "PROPOSED FMVSS No. 126 Electronic Stability Control Systems," *Washington, DC: US Department of Transportation,* 2006.